**AWARD NUMBER: W81XWH-18-1-0624**

**TITLE: Improving Cardiorespiratory Performance in DMD via Combinatorial Dystrophin and Ribonucleotide Reductase Gene Therapy**

**PRINCIPAL INVESTIGATOR: Dr. Guy L. Odom**

**CONTRACTING ORGANIZATION: University of Washington**

**REPORT DATE: OCTOBER 2020**

**TYPE OF REPORT: Annual**

**PREPARED FOR:** U.S. Army Medical Research and Materiel Command
Fort Detrick, Maryland 21702-5012

# REPORT DOCUMENTATION PAGE

*Form Approved*
*OMB No. 0704-0188*



| 1. REPORT DATE | 2. REPORT TYPE | 3. DATES COVERED |
|---|---|---|
| October 2020 | Annual | 30SEPT2019 - 29SEPT2020 |

**4. TITLE AND SUBTITLE :**

Improving Cardiorespiratory Performance in DMD via Combinatorial Dystrophin and Ribonucleotide Reductase Gene Therapy

**5a. CONTRACT NUMBER**

**5b. GRANT NUMBER**
W81XWH-18-1-0624

**5c. PROGRAM ELEMENT NUMBER**

**6. AUTHOR(S)**
Guy L. Odom

E-Mail: godom@uw.edu

**5d. PROJECT NUMBER**

**5e. TASK NUMBER**

**5f. WORK UNIT NUMBER**

**7. PERFORMING ORGANIZATION NAME(S) AND ADDRESS(ES)**

University of Washington
Grant & Contracts Division
4333 Brooklyn Ave NE
Seattle WA 98195-0001

**8. PERFORMING ORGANIZATION REPORT NUMBER**
1

**9. SPONSORING / MONITORING AGENCY NAME(S) AND ADDRESS(ES)**

U.S. Army Medical Research and Development Command
Fort Detrick, Maryland 21702-5012

**10. SPONSOR/MONITOR'S ACRONYM(S)**

**11. SPONSOR/MONITOR'S REPORT NUMBER(S)**

**12. DISTRIBUTION / AVAILABILITY STATEMENT**

Approved for Public Release; Distribution Unlimited

**13. SUPPLEMENTARY NOTES**

**14. ABSTRACT** Duchenne muscular dystrophy (DMD) is caused by mutations in the gene encoding dystrophin, a structural protein that links the cytoplasmic contractile components of muscle cells to the extracellular matrix. Our dual target research strategy mediated by recombinant adeno-associated viral vectors (rAAV) utilizes dystrophin replacement (structural-based therapy) coupled with contractile performance enhancement via ribonucleotide reductase (RNR) expression (contractile augmentation therapy)). Therefore, we will address the underlying DMD structural deficit (lack of dystrophin), protecting muscle cells from further injury, while simultaneously improving cardiac muscle contractility & relaxation via a promising new nucleotide therapy. We recently published data (see appendix) demonstrating rAAV/RNR treatment improves cardiac performance of deteriorating or aged (22-24 month-old) hearts of *dmd* mice, and that improved performance was sustained long-term. In fulfillment of Aim-1 for this grant, following vector production/ purification (Oct-Nov, 2018), *dmd* mice were administered rAAV's (Dec-Jan 2018/19). Echocardiography has been performed on the majority of treated mice with end points forthcoming on the final 2-cohorts of animals over the coming weeks (Nov. 2019). End points for the 4-cohorts of treated mice for Aim-1/Phase-1 are currently in process (Oct-Nov 2019) where we have performed cardiac perfusion assays (baseline performance, pressure-volume relationships, & high-workload performance) in ~60% of the mice at the time of writing this report.

**15. SUBJECT TERMS**

NONE LISTED

| 16. SECURITY CLASSIFICATION OF: | | | 17. LIMITATION OF ABSTRACT | 18. NUMBER OF PAGES | 19a. NAME OF RESPONSIBLE PERSON |
|---|---|---|---|---|---|
| a. REPORT | b. ABSTRACT | c. THIS PAGE | | | USAMRMC |
| Unclassified | Unclassified | Unclassified | Unclassified | 56 | 19b. TELEPHONE NUMBER *(include area code)* |

## TABLE OF CONTENTS

1. **INTRODUCTION:** *Narrative that briefly (one paragraph) describes the subject, purpose and scope of the research.*

**Subject**: Dystrophin provides a structural link between the inside and outside of muscle cells to protect against damage during exercise. Duchenne muscular dystrophy (DMD) patients carrying mutations to the dystrophin gene gradually lose muscle function and ultimately die due to weakened heart and breathing muscles.
**Purpose**: Two current limitations of DMD cardiac gene therapy include: (1) overcoming the preexisting damage to muscles caused by disease progression that ultimately leads to cardiomyopathy-or worse (heart failure), and (2) the inability to restore lost function of those muscle cells that express a highly truncated dystrophin protein (i.e. micro-dystrophin, currently advancing in clinical trials). These challenges limit the effective response of strategies for sustained protective therapy.
**SCOPE**: To address these concerns, we propose a two-pronged approach: dystrophin replacement (structural-based therapy) coupled with contractile performance enhancement via ribonucleotide reductase (RNR) expression (contractile augmentation therapy). Cardiac muscle lacks the ability to regenerate, so endowing existing cardiomyocytes that actively contribute to rhythmic contractions with the ability for sustained increases in force production (via elevated RNR and dATP) represents a mechanistic based therapy at the level of the muscle contractile unit (sarcomere) that increases whole heart function. We have demonstrated that the contractile protein myosin can utilize dATP as a preferred energy that results in stronger, faster heart muscle cell contraction as well as faster relaxation to improve whole heart function for both systole and diastole. This RNR strategy may be even more effective when combined with dystrophin replacement strategies to improve the stability of muscle cell structure. Our DOD proposal is clearly focused on bringing successful cardiac gene therapies for DMD into clinical application in the next 3-5 years with the goal of making a significant clinical impact.

2. **KEYWORDS:** *Provide a brief list of keywords (limit to 20 words).*

Adenosine triphosphate
Deoxyadenosine triphospate
Becker muscular dystrophy
Dilated cardiomyopathy
Dystrophin Glycoprotein Complex
Duchenne muscular dystrophy
Dystrophin
Echocardiography
Heart failure
Muscle creatine kinase
recombinant Adeno-associated viral vector
Ribonucleotide reductase
Rate Pressure Product
Tissue Doppler Imaging
Micro-dystrophin

3. **ACCOMPLISHMENTS:** *The PI is reminded that the recipient organization is required to obtain prior written approval from the awarding agency grants official whenever there are significant changes in the project or its direction.*

**Task 1**: We will test the hypothesis that the treatment of dystrophic mice with AAV-mediated RNR can halt adverse cardiac remodeling progression, and increase cardiac contractile performance when combined with AAV-mediated μDys. These will be tested in *mdx*$^{4cv}$ dystrophic mice. (Mos 1-12)

**Task 2**: Investigate the hypothesis that AAV6-mediated μDys and RNR treatments will *rescue* function in a more progressive and severely affected model of DMD (Mos. 13-24). These *in vivo* studies will be tested in

*mdx/utrn*$^{+/-}$ dystrophic mice. (Mos 11-24) The *in vitro* studies that are part of RNAi knockdown experiments will commence in year-1 to potentially substantiate *in vivo* efforts of Aim-2 in year-2.

[*Note: Due to COVID19 impact on our laboratory & institute we have applied for (& received) extension-based funding. This funding is essential for initiation/completion of "Task 2" experiments given the timing of the pandemic & the long term animal studies which were to be initiated February/March of 2020. We are in the process of escalating breeding to accommodate the necessary animal numbers for these studies that will now take place 2021-2022 as reflected in the updated SOW (updated August 2020).*]

**Task 3**: These studies will test the hypothesis that AAV-mediated RNR expression can enhance the functional capacity of dystrophin gene editing in an advanced model of DMD. These *in vivo* studies will be tested in *mdx/utrn*$^{+/-}$ dystrophic mice. (Mos 22-36) As noted above, these studies are now scheduled for 2022 due to the COVID19 impact.

- **1a.** Echocardiography will be performed using a Visualsonics Vivo2100 and standard imaging planes: M-mode, conventional and Tissue Doppler imaging (TDI). Assayed parameters include stroke volume, cardiac output, LV end-systolic (LVESD) and end-diastolic (LVEDD), fractional shortening, LV wall mass MPI (Tei index, the proportion of systole that is isovolemic), and Ea/Aa (early/late diastolic wall-motion velocity ratio). These assays will continue throughout the project as part of the goals of each specific aim (Regnier & Odom Labs). (Mos. 1-36)

  **We have performed echocardiography imaging and analysis on the mice enrolled in Aim-1/Phase-1 of this project. In summary, conventional echocardiography showed no difference at baseline (BL) for HR, EF & FS. At end-point combinatorial (RNR+uDys) therapy showed increased FS & EF (right panel, A.). Dobutamine effectively ablated this difference by increasing wt, mdx4cv, & mdx4cv+ uDys levels (right panel, B.).**

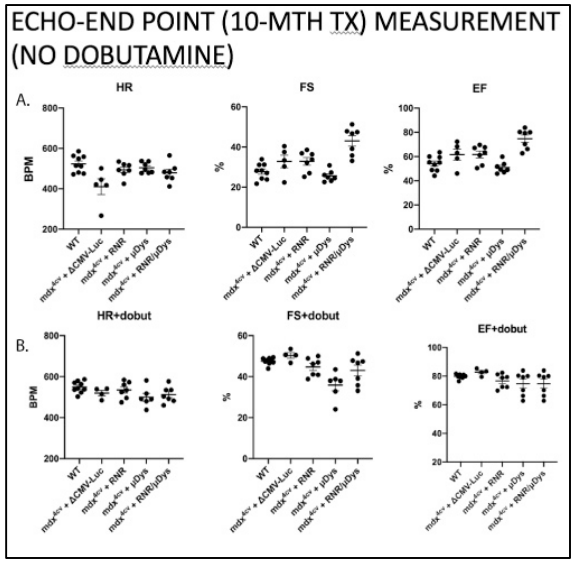


- **1b.** Langendorff perfusion assays will be performed to determine basal function & high workload challenge capacities in treated and control hearts. Hearts are perfused at a constant pressure of 80mmHg with a modified Krebs-Henseleit (KH) buffer supplemented with glucose and pyruvate. Left ventricular (LV) function is monitored during the experiment via a water-filled balloon inserted to the LV and connected to a pressure transducer. LV systolic pressure (LVSP), end diastolic pressure (EDP), heart rate (HR), and minimum and maximum rate of pressure change in the ventricle (± dP/dt) are obtained from the attached data acquisition system (PowerLab, ADInstruments, Colorado Springs, CO). Pressure-volume relationships (i.e., Frank-Starling curves) are assessed by gradually increasing the volume of the LV balloon. Following baseline measures, hearts are allowed to equilibrate for 5 minutes and then the perfusate will be changed to the same buffer as above except for the addition of 4.0 mmol/L $CaCl_2$ to simulate a high workload (HWL) challenge for 20 minutes (Regnier & Odom Labs). (Mos. 9-11; 21-23; 33-35)

  - **We have performed cardiac perfusion assays (Langendorff) & analysis of mice previously enrolled in Aim-1/Phase-1 of this project (see below, A-C). Langendorff end point data for LVdevP & RPP showed significance (Dunnetts T3) for each therapeutic treatment group (see below, D.).**

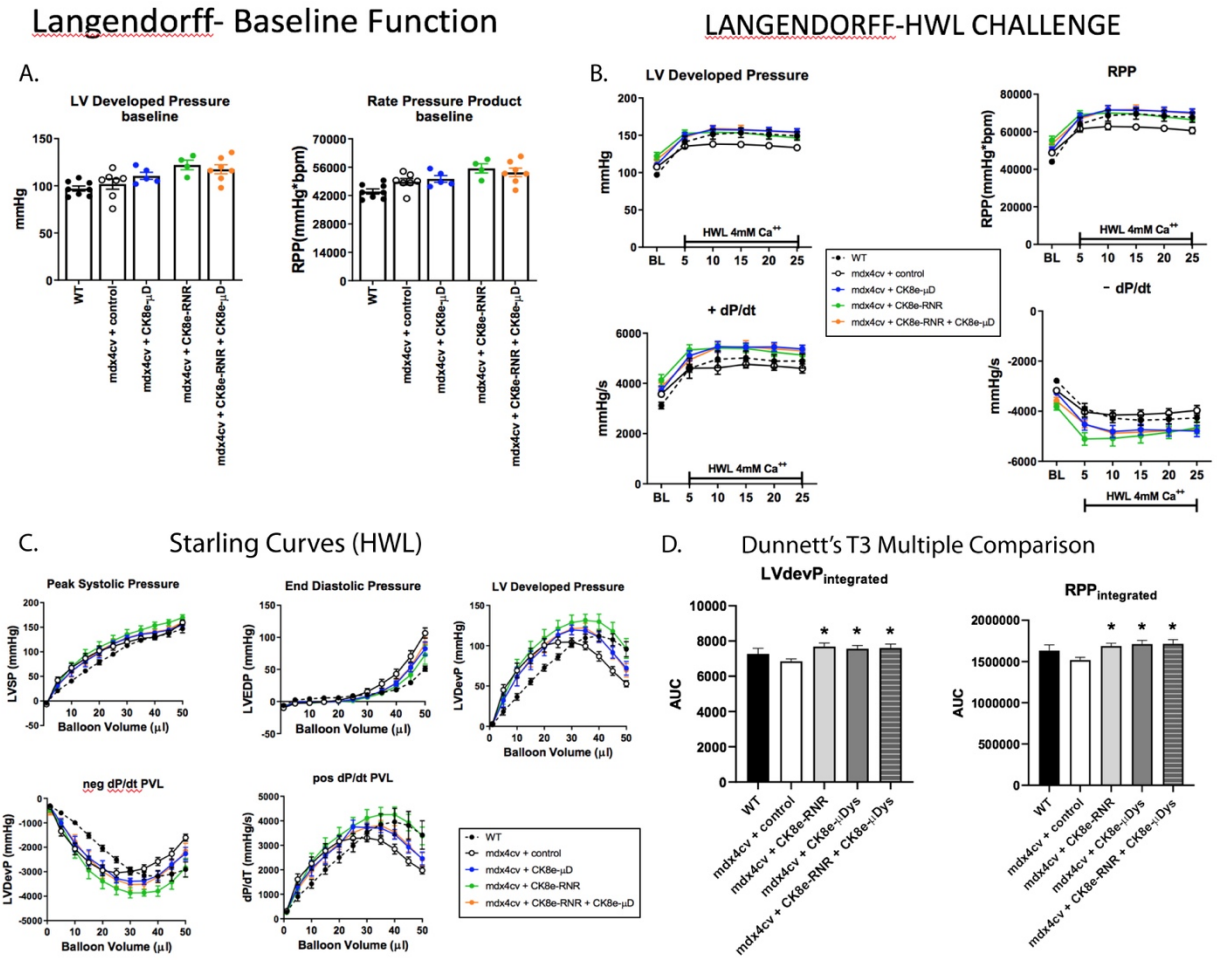


**1d.** Metabolic profiling will be performed using the Agilent 1260/AB-Sciex 5500 Qtrap LC-MS/MS instrument and HILIC (hydrophilic interaction chromatography) protocols developed previously by Dr. Raftery. The development of highly multiplexed targeted methods using advanced LC-MS/MS instruments provides fast data acquisition and reasonably tight quality control, resulting in reproducible measurement of more than 160 metabolites located in 25 different metabolic pathways (individual metabolite CVs = 5-30%). This system provides detailed information on metabolites involved in glycolysis, the TCA cycle, pentose phosphate shunt, as well as amino acid, fatty acid, and nucleic acid metabolism and other pathways (Regnier & Raftery labs). At right, is the multivariate scores plot for wt & mdx$^{4cv}$ clustering.

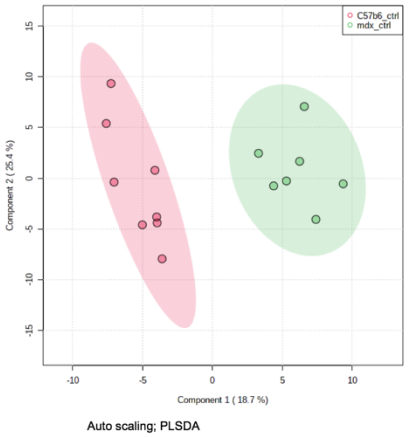


- The results of PLS-DA analysis of metabolite levels derived from MS are shown as score plots.
- Each red or green point in the score plot represents one mouse.
- In these plots, points (known as scores) for animals/mice that exhibit similar metabolite profiles will appear closer to each other and vice versa.
- Overall, the score plots show good clustering and separation of the cohorts presented.

- It is interesting that each group (cohort) of samples is distinctly different from one another, which indicates significant differences in metabolite profiles for each group.
- In turn, for the initial univariate analysis following, internal standard validation, normalization, etc., each experimental cohort is initially compared to controls (wt & mdx) with each metabolite (>200 total). Cohort data is grouped by average, >2-fold change, & P-value ($p<0.05$). As shown below with representative data sets, what is clear based on fold change & p-values, is that there are many metabolites that show significant difference between each pair of groups.

# Univariate Analysis (mdx comparison)

| mdx_RNR/mdx_ctrl | fold change |
|---|---|
| | |
| Mevalonate (147.0 / 59.0) | 3.01 |
| Shikimic Acid (173.0 / 93.0) | 2.03 |
| Mannitol (181.0 / 119.0) | 2.07 |
| Cholecalciferol (385.0 / 91.0) | 2.33 |
| Serotonin (160.0 / 115.0) | 0.48 |
| isovalerylcarnitine (246.0 / 85.0) | 2.59 |
| DL DOPA (198.0 / 152.0) | 2.1 |
| Malondialdehyde (71.0 / 41.0) | 3.22 |

| mdx_uDys/mdx_ctrl | fold change |
|---|---|
| | |
| Tetrahydrobiopterin (240.0 / 59.0) | 0.486 |
| UDP-Glucose (565.0 / 323.0) | 0.484 |
| Ergocalciferol (397.0 / 91.0) | 0.215 |

| mdx_RNR+uDys/mdx_ctrl | Fold change |
|---|---|
| | |
| F16BP/F26BP/G16BP (339.0 / 79.0) | 2.3 |
| 2'-deoxycytidine (228.0 / 112.0) | 2.24 |
| Serotonin (160.0 / 115.0) | 0.42 |
| Malondialdehyde (71.0 / 41.0) | 2.92 |

# Univariate Analysis- Tx cohort comparison

| mdx_uDys/mdx_RNR | | | mdx_RNR+uDys/mdx_uDys | | | mdx_RNR+uDys/mdx_RNR | |
|---|---|---|---|---|---|---|---|
| | | | | | | | |
| Shikimic Acid (173.0 / 93.0) | 0.3 | | F16BP/F26BP/G16BP (339.0 / 79.0) | 2.24 | | Shikimic Acid (173.0 / 93.0) | 0.44 |
| Tetrahydrobiopterin (240.0 / 59.0) | 0.344 | | 2'-deoxycytidine (228.0 / 112.0) | 2.47 | | Tetrahydrobiopterin (240.0 / 59.0) | 0.438 |
| NADH (666.0 / 649.0) | 0.364 | | Malondialdehyde (71.0 / 41.0) | 3.3 | | n-isobutyrylglycine (144.0 / 74.0) | 0.398 |
| Ergocalciferol (397.0 / 91.0) | 0.246 | | n-isobutyrylglycine (144.0 / 74.0) | 0.283 | | Aspartic Acid (134.0 / 74.0) | 0.465 |
| DL DOPA (198.0 / 152.0) | 0.455 | | | | | Adenine (134.0 / 107.0) | 0.488 |
| isovalerylcarnitine (246.0 / 85.0) | 0.43 | | | | | isovalerylcarnitine (246.0 / 85.0) | 0.468 |
| Mevalonate (147.0 / 59.0) | 0.32 | | | | | Mevalonate (147.0 / 59.0) | 0.42 |
| Cholecalciferol (385.0 / 91.0) | 0.417 | | | | | | |
| UDP-Glucose (565.0 / 323.0) | 0.388 | | | | | | |
| Malondialdehyde (71.0 / 41.0) | 0.274 | | | | | | |
| 3-Indoxyl Sulfate (212.1 / 80.0) | 2.11 | | | | | | |
| Hippuric Acid (178.0 / 134.0) | 2.12 | | | | | | |

- Following the univariate analysis, a multivariate analysis was performed using partial least squares discriminate analysis (PLS-DA). A summary of the cohort clustering is presented below. Importantly, the results are in accordance with the results obtained by univariate analysis.

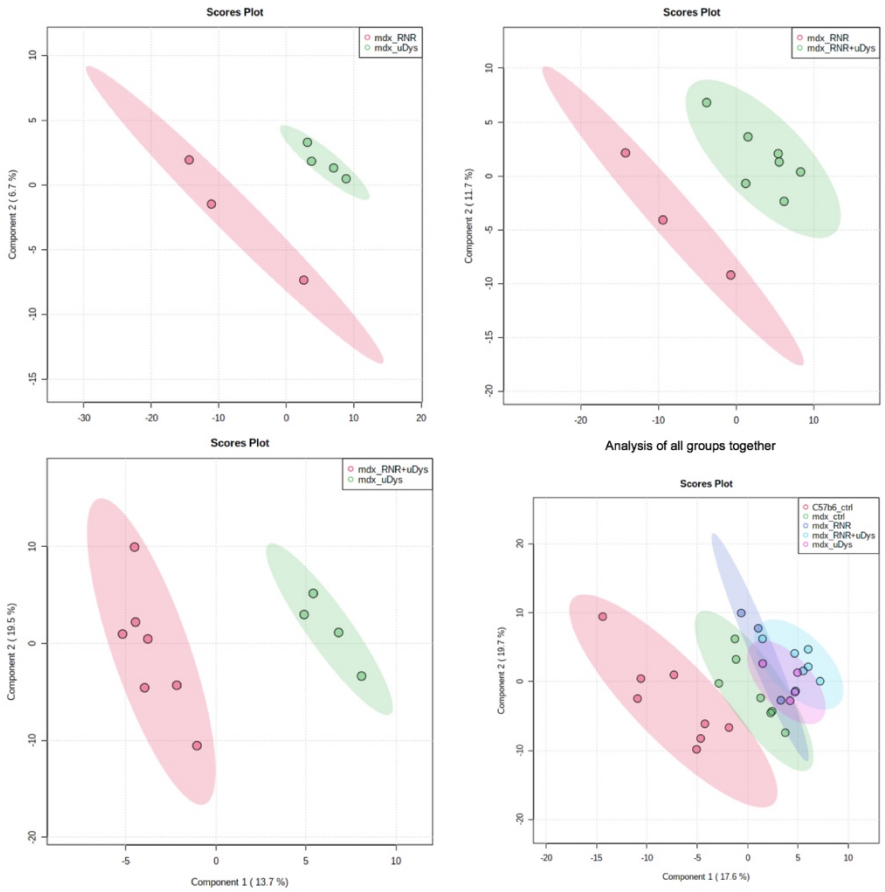

We then performed pathway analysis (64 pathways) on cardiac tissue. When comparing wt:mdx$^{4cv}$ the vast majority of significant differences in pathways implicated amino acid metabolism (below, A.). Additional pathways with significance are the pentose phosphate pathway and glyoxylate metabolism. This is in contrast to mdx4cv:mdx4cv+RNR which displayed more weighted differences in fatty acid metabolism in addition to TCA cycle and glycolysis/gluconeogenesis (below, B.). Similarly alpha-lineolic acid metabolism (long chain fatty acid biosynthesis) was shown significant in the cohort of mdx$^{4cv}$ mice treated with micro-dystrophin (below, C.). The comparison of pathways for mdx$^{4cv}$+RNR:mdx$^{4cv}$+uDys revealed significance in pyrimidine metabolism, folate synthesis, steroid hormone biosynthesis, and arginine biosynthesis (below, D.). Pathways implicated for mdx$^{4cv}$+RNR:mdx$^{4cv}$+RNR & uDys included folate biosynthesis, the TCA cycle, histidine metabolism, phenylalanine metabolism, & arginine biosynthesis (below, E.). Lastly, mdx$^{4cv}$+RNR:mdx$^{4cv}$ +RNR & uDys demonstrated significance for alpha-LNA metabolism, arachidonic acid metabolism, and a collection of amino acid metabolic pathways (below, F.).

A.

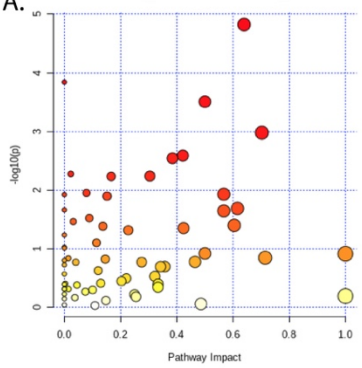


Total 64 pathways mapped  Pathway with FDR corrected p <0.05

| Pathway Name | Match Status | p | -log(p) | Holm p | FDR | Impact |
|---|---|---|---|---|---|---|
| Histidine metabolism | 7/16 | 1.5009E-5 | 4.8236 | 9.606E-4 | 9.606E-4 | 0.63933 |
| Valine, leucine and isoleucine biosynthesis | 4/8 | 1.4442E-4 | 3.8404 | 0.0090985 | 0.0046215 | 0.0 |
| Riboflavin metabolism | 2/4 | 3.1136E-4 | 3.5067 | 0.019304 | 0.0066423 | 0.5 |
| Glycine, serine and threonine metabolism | 13/34 | 0.0010531 | 2.9775 | 0.064241 | 0.01685 | 0.70251 |
| Arginine biosynthesis | 7/14 | 0.0025913 | 2.5865 | 0.15548 | 0.030725 | 0.42132 |
| Purine metabolism | 18/66 | 0.0028805 | 2.5405 | 0.16995 | 0.030725 | 0.3845 |
| Valine, leucine and isoleucine degradation | 3/40 | 0.0053399 | 2.2725 | 0.30971 | 0.041756 | 0.02264 |

B.

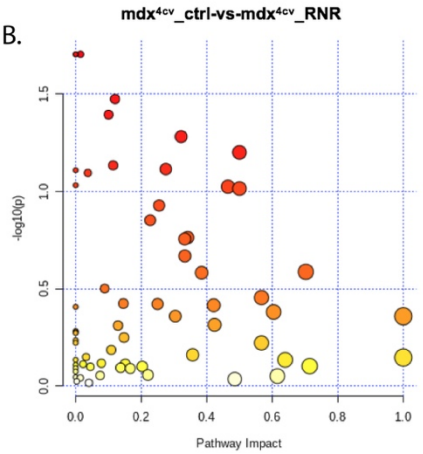


FDR corrected p <0.05: None

| Pathway Name | Match Status | p | -log(p) | Holm p | FDR | Impact | Details |
|---|---|---|---|---|---|---|---|
| Fatty acid biosynthesis | 1/47 | 0.019717 | 1.7052 | 1.0 | 0.42063 | 0.01473 | KEGG SMP |
| Fatty acid elongation | 1/39 | 0.019717 | 1.7052 | 1.0 | 0.42063 | 0.0 | KEGG SMP |
| Fatty acid degradation | 1/39 | 0.019717 | 1.7052 | 1.0 | 0.42063 | 0.0 | KEGG SMP |
| Citrate cycle (TCA cycle) | 3/20 | 0.033486 | 1.4751 | 1.0 | 0.44166 | 0.12027 | KEGG |
| Glycolysis / Gluconeogenesis | 2/26 | 0.040298 | 1.3947 | 1.0 | 0.44166 | 0.10044 | KEGG SMP SMP |

C.

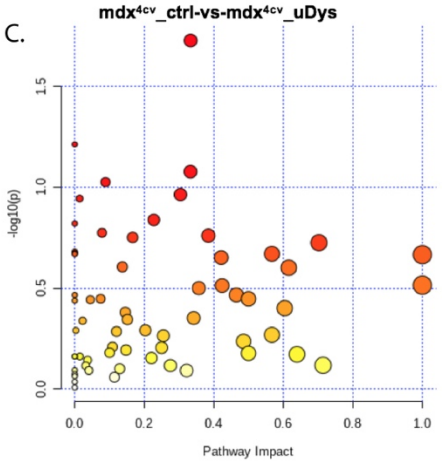


FDR corrected p <0.05: None

| Pathway Name | Match Status | p | -log(p) | Holm p | FDR | Impact | Details |
|---|---|---|---|---|---|---|---|
| alpha-Linolenic acid metabolism | 1/13 | 0.018774 | 1.7264 | 1.0 | 0.75209 | 0.33333 | KEGG |

D.

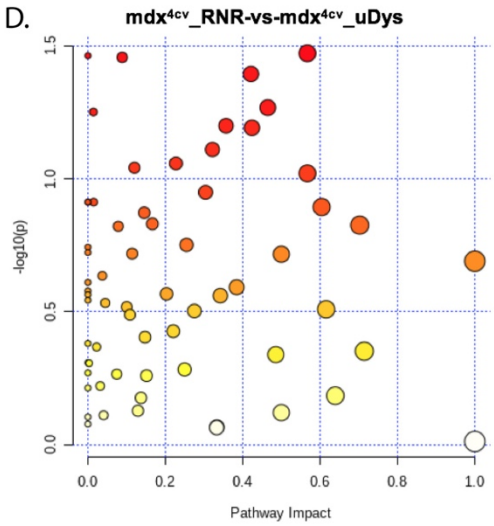


FDR corrected p <0.05: None

| Pathway Name | Match Status | p | -log(p) | Holm p | FDR | Impact | Details |
|---|---|---|---|---|---|---|---|
| Pyrimidine metabolism | 16/39 | 0.033752 | 1.4717 | 1.0 | 0.45961 | 0.56714 | KEGG SMP |
| Steroid hormone biosynthesis | 1/77 | 0.034487 | 1.4623 | 1.0 | 0.45961 | 0.0 | KEGG |
| Folate biosynthesis | 1/27 | 0.034977 | 1.4562 | 1.0 | 0.45961 | 0.08868 | KEGG |
| Arginine biosynthesis | 7/14 | 0.040369 | 1.394 | 1.0 | 0.45961 | 0.42132 | KEGG |

E.

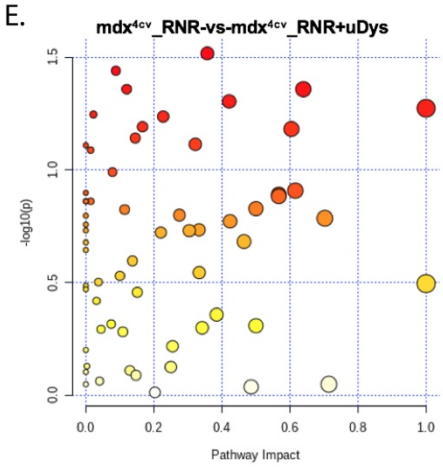


FDR corrected p <0.05: None

| Pathway Name | Match Status | p | -log(p) | Holm p | FDR | Impact | Details |
|---|---|---|---|---|---|---|---|
| Phenylalanine metabolism | 3/12 | 0.030414 | 1.5169 | 1.0 | 0.35727 | 0.35714 | KEGG SMP |
| Folate biosynthesis | 1/27 | 0.036325 | 1.4398 | 1.0 | 0.35727 | 0.08868 | KEGG |
| Histidine metabolism | 7/16 | 0.043845 | 1.3581 | 1.0 | 0.35727 | 0.63933 | KEGG SMP |
| Citrate cycle (TCA cycle) | 3/20 | 0.043863 | 1.3579 | 1.0 | 0.35727 | 0.12027 | KEGG |
| Arginine biosynthesis | 7/14 | 0.049668 | 1.3039 | 1.0 | 0.35727 | 0.42132 | KEGG |

F.

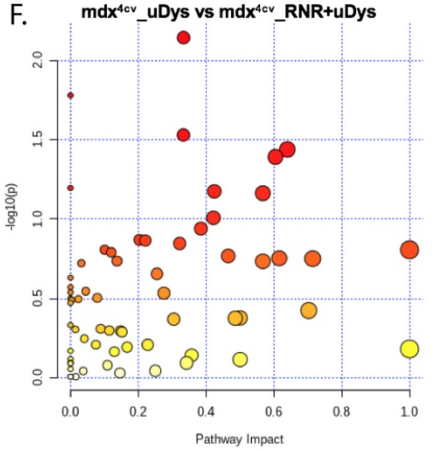


FDR corrected p <0.05: None

| Pathway Name | Match Status | p | -log(p) | Holm p | FDR | Impact | Details |
|---|---|---|---|---|---|---|---|
| alpha-Linolenic acid metabolism | 1/13 | 0.007217 | 2.1416 | 0.46189 | 0.46189 | 0.33333 | KEGG |
| Biosynthesis of unsaturated fatty acids | 4/36 | 0.01668 | 1.7778 | 1.0 | 0.52053 | 0.0 | KEGG |
| Arachidonic acid metabolism | 1/36 | 0.029572 | 1.5291 | 1.0 | 0.52053 | 0.33292 | KEGG SMP |
| Histidine metabolism | 7/16 | 0.03647 | 1.4381 | 1.0 | 0.52053 | 0.63933 | KEGG SMP |
| Alanine, aspartate and glutamate metabolism | 12/28 | 0.040666 | 1.3908 | 1.0 | 0.52053 | 0.60416 | KEGG SMP |

- Hearts were additionally analyzed by Oxygraph (O2K) via the CTMR, to gain overall insight with regard toward treatment affects on mitochondrial respiration complexes. Indeed, mitochondria are akin to a energy bank for the cell through numerous biochemical pathways that breakdown glucose & result in the generation of ATP. Briefly, the O2K is a modular system for high-resolution respirometry (HRR) for mitochondria and cell research. HRR is the basis for combined measurement of respiration & ROS production, mitochondrial membrane potential, ATP production, Ca2+, or pH. An additional advantage as it relates to these studies is it enables use of small amounts of biological samples for bioenergetic and oxidative phosphorylation analysis. The heart apex was used for all samples, while the remainder ventricular portion went toward patch-clamp freezing for metabolomics.

- **In regards to the O2K data there are several considerations that should be noted:**

1. Capacity values are the maximum respiration values for the tissues, so non-adjusted for mito content.
2. Normalized values have been adjusted to mito content by citrate synthase.
3. "Leak state" is with the addition of malate, pyruvate, and glutamate without any other substrates.
4. State 3 complex I values is after addition of saturating ADP.
5. State 3 complex I max is after addition of cytochrome C. This acts as a quality control in case the mitochondria have been damaged during preparation. A large bump from state 3 complex I indicates a poor prep.
6. State 3 is with the addition of succinate. This is *typically where you will see the greatest respiration* as complexes I and II are both chugging along at max capacity.
7. Complex II is measurement of only complex II following the inhibition of complex I by rotenone.
8. Complex IV is a measurement of only complex IV as the previous complex activity has been inhibited by antimycin A.

## Heart Capacity

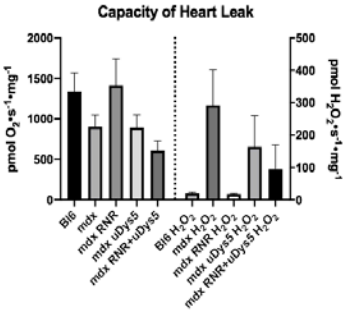


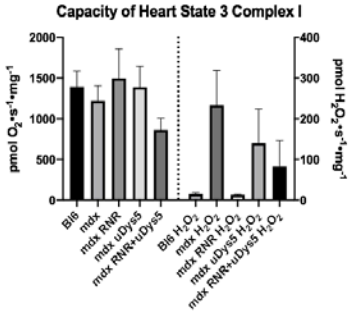


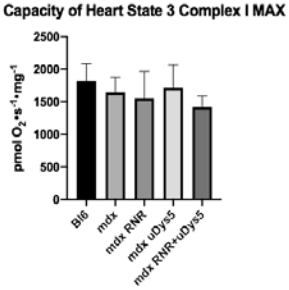


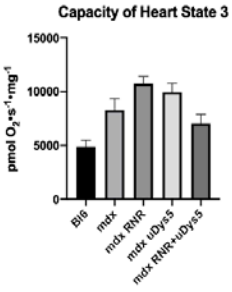


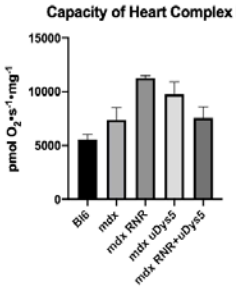


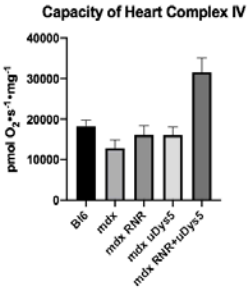


## Heart Normalized

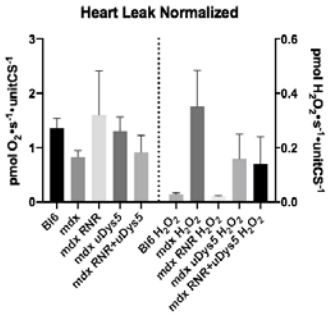


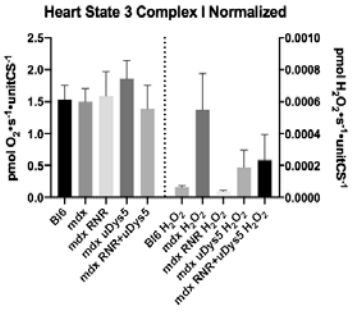


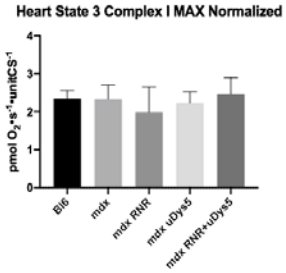


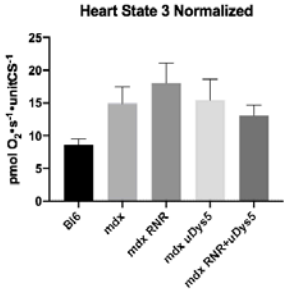


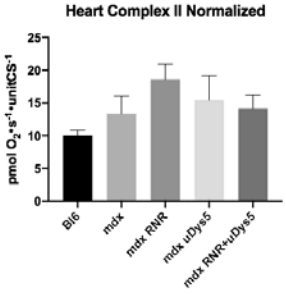


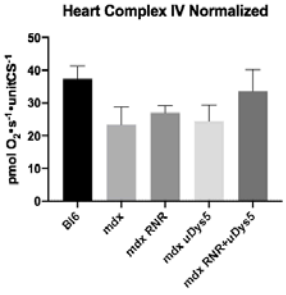

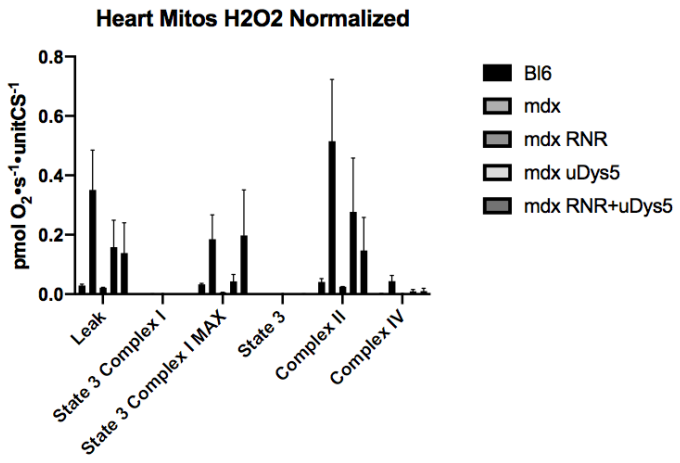


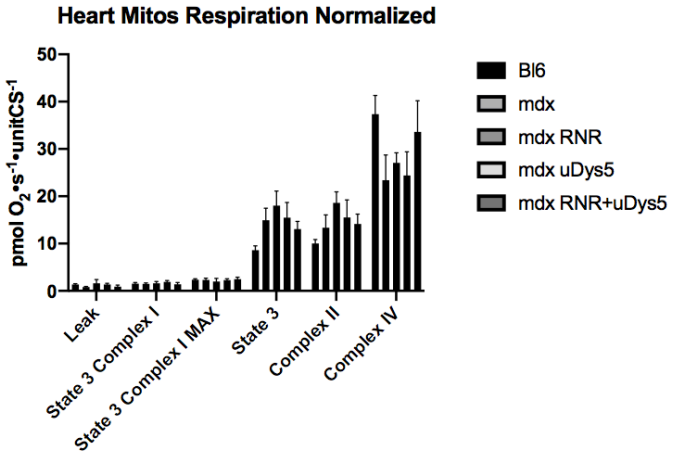


**O2K Data Insights:**

- **The *mdx*-RNR mice seem to have lower overall oxidant production. This does come with the big grain of salt given this group only contains 3 animals.**
- **The expression of uDys may boost mitochondrial content in the *mdx* mice, especially in skeletal muscle. Increasing power would help answer this.**
- **There does appear like some of the respiratory states show trends of rescue of the *mdx* mice when RNR & uDys5 are expressed together. Again, animals number caveats apply.**

**What opportunities for training and professional development has the project provided?**

**As it relates to the funding of this project, 3 conferences (#4-6) have been attended over the past fiscal year, listed below.**

1. Kolwicz SC, Hall JK, Murry J, Moussavi-Harami F, Flint G, Chen X, Hauschka SD, Chamberlain JS, Regnier M, and **Odom GL.** A cardiac function-enhancing gene therapy approach via deoxy-ATP elevation rescues cardiac dysfunction in a DMD cardiomyopathy mouse model. Parent Project for Muscular Dystrophy Annual Conference, Orlando FL, June 27-30, 2019.
2. Banks GB, Chamberlain JS, and **Odom GL**. Microutrophin expression in dystrophic mice displays myofiber type differences in therapeutic effects. PLOS Genetics, Nov 16(11):e1009179 epub, 2020. (PMID: 33175853)
3. Robeson-KZ, Moussavi-Harami F, Davis J, **Odom GL**, Regnier M. New Promoters to Improve the Efficiency of Cardiac Gene Therapies Using 2 Deoxy-ATP. BCVS, July 29-Aug 1, 2019.
4. Ravneet R, **Odom GL**, Chamberlain JS, and Lee D Magnetic resonance biomarkers for dystrophic striated muscles treated with recombinant adeno-associated viral vector mediated micro-dystrophin. MDA Clinical & Scientific Conference, Orlando FL, March 21-25, 2020.
5. Vohra R, **Odom G**L, Chamberlain JS and Donghoon Lee: Monitoring micro-dystrophin treatment effects in *mdx*$^{4cv}$ mice using magnetic resonance imaging and spectroscopy. ISMRM annual meeting, Paris, FR. August 8-13 2020.
6. Vohra R, **Odom GL**, Chamberlain JS and Donghoon Lee: MR detects improvement in cardiac function and fibrosis after micro-dystrophin treatment in dystrophic mice. ISMRM annual meeting, Paris, FR. August 8-13 2020.

Additionally, The UW Center for Translational Muscle Research Annual Symposium was attended. Briefly, the symposium featured talks by CTMR pilot grant awardees and investigators from our group; panel discussions with clinicians and leaders from centers and institutes supporting research and development. Efforts are being made to reschedule a metablomics educational series through the CTMR that unfortunately were previously cancelled due to COVID19.

**How were the results disseminated to communities of interest?**

Recent published work is available on the Journal of the American College of Cardiology:Basic to Translational Science website, scheduled to be published in the November issue.

http://basictranslational.onlinejacc.org/content/early/2019/09/25/j.jacbts.2019.06.006

Most recently, published work can be found on the PLOS Genetics website as well as being listed on Pubmed.

**https://journals.plos.org/plosgenetics/article?id=10.1371/journal.pgen.1009179**

**https://pubmed.ncbi.nlm.nih.gov/33175853/**

Additionally, we submitted a manuscript last month, currently under review with the Journal of Clinical Investigation entitled "A new mouse model for evaluating micro-dystrophin gene therapy prevention of heart failure in Duchenne muscular dystrophy cardiomyopathy".

**What do you plan to do during the next reporting period to accomplish the goals?**

During the next reporting period we will be continuing the efforts of Aim-2 within this DMDRP-IIRA that have been delayed as a primary result of the COVID19 pandemic. Currently, our goal is to administer vector to mice for Aim-2 in the winter of 2021. The animals will be followed to endpoint, which is anticipated to occur in the fall of 2021. Vector production for Aim-3 is projected to be initiated late summer 2021, with administration late 2021/early 2022.

4. **IMPACT:**

**What was the impact on the development of the principal discipline(s) of the project?**

Nothing to Report.

**What was the impact on other disciplines?**

Nothing to Report.

**What was the impact on technology transfer?**

Nothing to Report.

**What was the impact on society beyond science and technology?**

Nothing to Report.

5. **CHANGES/PROBLEMS:**

**Changes in approach and reasons for change**

With the exception of implementation of COVID-19 institutional (laboratory) protocols-Nothing to Report.

**Actual or anticipated problems or delays and actions or plans to resolve them**

As a result of COVID-19, we applied for & received support from DOD to extend our research calendar an additional 12-months to enable completion of the proposed research.

**Changes that had a significant impact on expenditures**

Nothing to Report.

**Significant changes in use or care of human subjects, vertebrate animals, biohazards, and/or select agents**

*Nothing to Report.*

**Significant changes in use or care of human subjects**

Nothing to Report.

**Significant changes in use or care of vertebrate animals**

Nothing to Report.

**Significant changes in use of biohazards and/or select agents**

Nothing to Report.

**6. PRODUCTS:**

Kolwicz SC, Flint GV, Hall JK, Moussavi-Harami F, Chen X, Hauschka SD, Regnier M, and **Odom GL**. Gene Therapy Rescues Cardiac Dysfunction in Duchenne Muscular Dystrophy Mice by Elevating Cardiomyocyte Deoxy-Adenosine Triphosphate. JACC Basic to Translation Research, November 2019.

Banks GB, Chamberlain JS, and **Odom GL**. Microutrophin expression in dystrophic mice displays myofiber type differences in therapeutic effects. PLOS Genetics, November 2020.

**Books or other non-periodical, one-time publications.**

Nothing to Report.

**Other publications, conference papers and presentations**.

Nothing to Report.

**Website(s) or other Internet site(s)**

Nothing to Report.

**Technologies or techniques**

Nothing to Report.

- **Inventions, patent applications, and/or licenses**
  *Identify inventions, patent applications with date, and/or licenses that have resulted from the research. Submission of this information as part of an interim research performance progress report is not a substitute for any other invention reporting required under the terms and conditions of an award.*

  **US Provisional Patent filed-June 25th 2019.**

**Title: Use of ribonucleotide reductase alone or in combination with micro-dystrophin to treat Duchenne muscular dystrophy striated muscle disease.**

- **Other Products**

  **Nothing to Report.**

## 7. PARTICIPANTS & OTHER COLLABORATING ORGANIZATIONS

**What individuals have worked on the project?**

| | |
|---|---|
| *Name:* | *Guy L. Odom* |
| *Project Role:* | *PI* |
| | *No Change* |
| *Name:* | *Michael Regnier* |
| *Project Role:* | *Collaborator* |
| | *No Change* |
| *Name:* | *Stephen D. Hauschka* |
| *Project Role:* | *Co-Investigator* |
| | *No Change* |
| *Name:* | *Niclas Bengtsson* |
| *Project Role:* | *Co-Investigator* |
| | *No Change* |
| *Name:* | *Galina Flint* |
| *Project Role:* | *Research Scientist* |
| | *No Change* |
| *Name:* | *Quynh Nyugen* |
| *Project Role:* | *Research Scientist* |
| | *No Change* |
| *Name:* | *Xiolan Chen* |
| *Project Role:* | *Research Scientist* |
| | *No Change* |
| *Name:* | *James Moore* |
| *Project Role:* | *Research Scientist* |
| | *No Change* |

**Has there been a change in the active other support of the PD/PI(s) or senior/key personnel since the last reporting period?**

Guy L. Odom (PI)- Nothing to Report.

Niclas Bengtsson (Co-I)- Nothing to Report.

Stephen D. Hauschka (Co-I)- Nothing to Report.

Michael Regnier (OMC)-

COMPLETED

1 R56 AG 055594-01 (M. Regnier, PI)
**Title:** Myocardial Infarct in Aging Animals and dATP Therapy
**Time commitment:** 1.8 calendar months (15% effort)
**Supporting agency:** NIH
**Funding agency contact:**
Program Official: Dr. Candace L. Kerr
National Institute on Aging
301-496-6402
candace.kerr@nih.gov
**Performance period:** 9/30/17-8/31/18
**Level of funding:**
**Goal:** The goal of this project is two-fold 1) to determine how age compounds the effect of myocardial infarct (MI) on heart function and how this affects skeletal muscle function and exercise tolerance; and 2) to determine the ability of 2 deoxy-ATP (dATP) to affect heart and skeletal muscle performance, metabolism and exercise tolerance in age and MI induced heart failure.
**Specific aims:**
Aim 1. To determine how aging influences the effect of MI on the contractile function of cardiac and skeletal muscle and exercise capacity.
Aim 2. To determine how RNR over-expression and elevated dATP can restore contractile function of cardiac and skeletal muscle, and exercise capacity of aging rodents both before and after MI. We have previously studied the effect of cardiac-specific elevation of dATP on young post-MI heart and cardiac muscle performance.
Aim 3. To determine how RNR over-expression and elevated dATP affect the metabolism of cardiac and skeletal muscle from aging and infarcted rodents.
**Overlap:** There is no scientific or budgetary overlap.

4 R01 HD 048895-11 (M. Bamshad, PI)
**Title:** Genetic and Molecular Basis of Congenital Contractures
**Role:** Co-Investigator
**Time commitment:** 0.96 calendar months (8% effort)
**Supporting agency:** NIH
**Funding agency contact:**
Program Official: Dr. Reiko Toyama
National Institute of Child Health & Human Development
301-435-2723
toyamar@mail.nih.gov
**Performance period:** 7/1/12-6/30/18
**Level of funding:**
**Goal:** The goal of this project is to study myosin and thin filament regulatory proteins associated with human distal arthrogryposis, and the dysfunction of skeletal muscle contraction. Feasibility of novel gene therapies will also be studied.
**Specific aims:**
Aim 1: Discover genes for both well-known and novel forms of Distal Arthrogryposis.
Aim 2: Determine the mechanisms of contractile apparatus dysfunction caused by DA-associated mutations of myofilament proteins.
**Overlap:** There is no scientific or budgetary overlap.

NSF CBET-1509106 (N. Sniadecki, PI)

**Title:** Development of a Micropost Approach for the Contractile Maturation of iPS-Derived Cardiomyocytes
**Role:** Co-Investigator
**Time commitment:** 0.18 calendar months (1.5% effort)
**Supporting agency:** NSF
**Funding agency contact:**
Program Manager: Michele Grimm
CBET Div Of Chem, Bioeng, Env, & Transp Sys
ENG Directorate for Engineering
703-292-4641
mgrimm@nsf.gov
**Performance period:** 6/1/15-5/31/19
**Level of funding:**
**Goal:** The goal of this project is to develop technologies that enhance the maturation of patient derived iPS muscle cells *in vitro* with the capability to longitudinally assess mechanical performance.

NEW

**NIH P30 AR074990-01 (Michael Regnier, Daniel Raftery, Thomas Daniel, Multi-PI)**
**Title:** UW Center for Translational Muscle Research
**Time commitment:** 1.56 calendar months (13% effort)
**Supporting agency:** NIH/NIAMS
**Grants Officer:** Teresa Do, Grants Management Specialist, NIH/NIAMS, 6701 Democracy Blvd., Democracy I, Suite 800, Bethesda, MD 20892-4872, 301-594-3512, Teresa.Do@nih.gov.
**Performance period:** 04/05/19-02/29/24
**Level of funding:**
**Goals:** The goal of this center is to provide a unifying resource and state of the art approaches to enhance skeletal muscle research at the UW and to recruit new investigators into the field. The proposed Center will offer tools, facilities and expertise in a combination available only at the UW to facilitate novel insights to muscle pathologies and move new therapeutics towards the clinic and the marketplace.
**Specific aims:**
The UW CTMR will:
(1) Provide leadership and training that promotes novel interdisciplinary research and fosters new collaborations in translational muscle research locally and at other US and international institutions.
(2) Provide services and scientific resources to accelerate progress on existing projects and facilitate development of novel high risk, high reward projects that can lead to significant advances and follow-on funding. (3) Become a centralizing agent that coordinates research efforts, provides multi-project data analysis and mining, and multi-scale mechanistic interpretations with predictive power.
(4) Develop state of the art and novel approaches that drivemuscle disease and treatment research forward.
(5) Provide outreach activities to A) recruit new scientists and clinician investigators into muscle research and B) disseminate important research findings to the scientific community and the public.
**Overlap:** There is no scientific or budgetary overlap.

**NIH RM1 (James Spudich, Daniel Bernstein, Multi-PI)**
**Role:** University of Washington sub-award PI
**Title:** A Multiscale hiPSC Platform to Solve the Genotype-Phenotype Conundrum in Inherited Disease
**Time commitment:** 2.88 calendar months (24% effort)
**Supporting agency:** NIH/NIGMS
**Grants Officer:** Jessica Dean, Grants Management Specialist, NIH/NIGMS, Room 2AN32F, 45 Center Drive MSC 6200, Bethesda, MD, 20892-6200, 301-451-2447, deanje@mail.nih.gov.
**Performance period:** 04/01/19-03/31/24
**Level of funding:**

**Goals:** The overarching goal of our interdisciplinary team is to understand how changes in intrinsic force generation and the mechanical environment affect the structure and function of striated muscle.
**Specific aims:**
(1) Determine how structural changes in myosin affect the chemo-mechanical properties of the myosin-actin interaction for individual and small assemblies of motor proteins.
(2) Determine how changes in myosin kinetics and force production influence the growth, maturation, and function of single hiPSC-CMs and multicellular tissue constructs.
(3) Determine how changes in myosin kinetics and force production influence the growth, maturation, and function of engineered hiPSC skeletal myotubes/myocytes.
UW will perform mechanical assessments of hiPSC-CMs (Aim 2) and hiPSC-SMs (Aim 3) containing myosin mutations that will be provided by the Stanford group. We will also perform molecular dynamics simulations of myosin and model sarcomere function for these mutations. Measurements will be made for single cells and individual myofibrils isolated from cells. We will identify magnitude and kinetic parameters that correlate with measures of myosin motors mechanics and actin motility (Aim 1).

**What other organizations were involved as partners?**

**Nothing to Report.**

## 8. SPECIAL REPORTING REQUIREMENTS

**COLLABORATIVE AWARDS:**

***Not Applicable***

**QUAD CHARTS:**
***Not Applicable***

## 9. APPENDICES:

*See below.*

JACC: BASIC TO TRANSLATIONAL SCIENCE VOL. 4, NO. 7, 2019


PRECLINICAL RESEARCH

# Gene Therapy Rescues Cardiac Dysfunction in Duchenne Muscular Dystrophy Mice by Elevating Cardiomyocyte Deoxy-Adenosine Triphosphate

Stephen C. Kolwicz, Jr, PhD,[a] John K. Hall, PhD,[b] Farid Moussavi-Harami, MD,[c] Xiolan Chen, PhD,[d,e] Stephen D. Hauschka, PhD,[d,e] Jeffrey S. Chamberlain, PhD,[b,d,e] Michael Regnier, PhD,[e,f,g,*] Guy L. Odom, PhD[b,e,g,*]

## VISUAL ABSTRACT

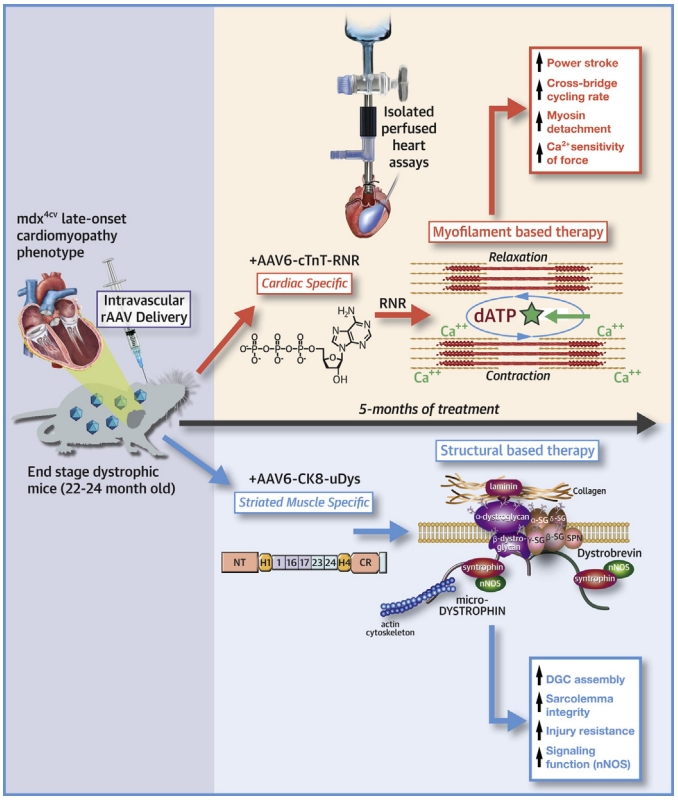


Kolwicz, S.C. Jr. et al. J Am Coll Cardiol Basic Trans Science. 2019;4(7):778-91.

## HIGHLIGHTS

- **rAAV vectors increase cardiac-specific expression of RNR and elevate cardiomyocyte 2-dATP levels.**
- **Elevated myocardial RNR and subsequent increase in 2-dATP rescues the performance of failing myocardium, an effect that persists long term.**

ISSN 2452-302X https://doi.org/10.1016/j.jacbts.2019.06.006

- **We show the ability to increase both cardiac baseline function and high workload contractile performance in aged (22- to 24-month old) mdx4cv mice, by high-level muscle-specific expression of either microdystrophin or RNR.**
- **Five months post-treatment, mice systemically injected with rAAV6 vector carrying a striated muscle-specific regulatory cassette driving expression of microdystrophin in both skeletal and cardiac muscle, exhibited the greatest effect on systolic function. In comparison, mice treated with rAAV6 vector carrying RNR that expresses exclusively in cardiac muscle not only exhibited greatly improved baseline systolic function but also improved diastolic function.**
- **Importantly, vector-directed overexpression of RNR did not impair cardiac reserve during increased physiological demand in aged mdx4cv hearts.**

**ABBREVIATIONS AND ACRONYMS**

**μDys** = microdystrophin

**CK8** = miniaturized murine creatine kinase regulatory cassette

**CMV** = cytomegalovirus

**cTnT** = cardiac troponin T

**dADP** = deoxy-adenosine diphosphate

**dATP** = deoxy-adenosine triphosphate

**DMD** = Duchenne muscular dystrophy

***mdx*** = mouse muscular dystrophy model

**rAAV** = recombinant adeno-associated viral vector

**RNR** = ribonucleotide reductase

## SUMMARY

Mutations in the gene encoding for dystrophin leads to structural and functional deterioration of cardiomyocytes and is a hallmark of cardiomyopathy in Duchenne muscular dystrophy (DMD) patients. Administration of recombinant adeno-associated viral vectors delivering microdystrophin or ribonucleotide reductase (RNR), under muscle-specific regulatory control, rescues both baseline and high workload-challenged hearts in an aged, DMD mouse model. However, only RNR treatments improved both systolic and diastolic function under those conditions. Cardiac-specific recombinant adeno-associated viral treatment of RNR holds therapeutic promise for improvement of cardiomyopathy in DMD patients. (J Am Coll Cardiol Basic Trans Science 2019;4:778–91)


Duchenne muscular dystrophy (DMD) and its milder and allelic form, Becker muscular dystrophy (BMD), are the most frequent muscular dystrophies, occurring once in ~5,000 male births, and are due to mutations in the dystrophin gene (1). DMD patients typically die due to cardiac and respiratory muscle failure; thus, maintenance of adequate function in both cardiac and skeletal muscle is critical for optimal DMD therapy. The primary function of dystrophin is to provide a structural role by mechanically linking the subsarcolemmal cytoskeleton to the extracellular matrix through the dystrophin-glycoprotein complex (DGC) (2). This linkage transmits the forces of contraction to the extracellular matrix and protects muscles from contraction-induced injury (3–7). In addition to a structural or mechanical role, the DGC also serves as a scaffold for cytoplasmic and membrane-associated signaling proteins and ion channels (8–11). The complete absence of dystrophin results in drastic reductions of all DGC components (12–14). Together, an absence of dystrophin and reduction in the DGC components causes membrane destabilization and permeability defects that lead to myofiber degeneration, repeated cycles of degeneration/regeneration, and the gradual replacement of muscle fibers with fibrotic, connective, and adipose tissue.

In contrast, some in-frame deletions, truncations, and missense mutations lead to reduced dystrophin expression associated with milder phenotypes. These

From the [a]Mitochondria and Metabolism Center, University of Washington, Seattle, Washington; [b]Department of Neurology, University of Washington, Seattle, Washington; [c]Division of Cardiology, Department of Medicine, University of Washington, Seattle, Washington; [d]Department of Biochemistry, University of Washington, Seattle, Washington; [e]Wellstone Muscular Dystrophy Specialized Research Center, University of Washington, Seattle, Washington; [f]Department of Bioengineering, University of Washington, Seattle, Washington; and the [g]Center for Cardiovascular Biology, University of Washington, Seattle, Washington. *Drs. Regnier and Odom contributed equally to this work and are joint senior authors.
This work was supported by grants from the National Institutes of Health (NIH): R01 HL111197 (to Dr. Regnier and Hauschka), R01 HD048895, K08 HL128826 (to Dr. Moussavi-Harami) and R01 HL128368 (to Dr. Regnier) and 1U54AR065139-01A1 (to Drs. Hauschka, Chamberlain, Regnier, and Odom). Dr. Kolwicz was funded by the American Heart Association 14SDG18590020. Dr. Chamberlain has received personal fees from Solid Biosciences, SAB. All other authors have reported that they have no relationships relevant to the contents of this paper to disclose.
The authors attest they are in compliance with human studies committees and animal welfare regulations of the authors' institutions and US Food and Drug Administration guidelines, including patient consent where appropriate. For more information, visit the *JACC: Basic to Translational Science* author instructions page.

Manuscript received February 27, 2019; revised manuscript received June 20, 2019, accepted June 20, 2019.

pathologies are largely curtailed in mouse (*mdx*) and canine (*cxmd*) models of DMD following the vector-mediated delivery of muscle-specific expression of highly functional miniaturized versions of dystrophin, microdystrophin (μDys) (15-24). In *mdx* mice, muscle pathology is milder than in humans, with the exception of the diaphragm; however, the dystrophic phenotype worsens with increasing age including the development of cardiac dysfunction (25-32). Administration of recombinant adeno-associated viral (rAAV)-mediated μDys therapy in *mdx* mice preceding the onset of cardiomyopathy is highly cardioprotective (33-35). However, when *mdx* mice are treated with μDys at a late stage of cardiomyopathy, such as would be the case for a number of DMD patients, a full rescue of the dysfunctional cardiac phenotype is not achieved (30,35-37).

SEE PAGE 792

We have developed a cardiac function-enhancing gene therapy approach that targets myosin in contractile filaments by overexpressing the enzyme ribonucleotide reductase (RNR). RNR converts adenosine diphosphate (ADP) to deoxy-ADP (dADP), which is rapidly converted to deoxy-adenosine triphosphate (dATP) in cells. In numerous in vitro studies, we have shown that dATP increases cross-bridge binding and cycling, resulting in stronger, faster contraction and faster relaxation (38-45). We have also reported that dATP improves contractile properties of myocardium from end-stage human heart failure (HF) in vitro (42) and dogs with end-stage idiopathic dilated cardiomyopathy (46). In normal rodent muscle, we reported that increases in cardiomyocytes and cardiac function occur with as little as ~1% of the ATP pool in the dATP form (40,47). Similarly, rAAV-mediated delivery of RNR under cardiac-specific regulatory control resulted in enzyme overexpression exclusively in cardiomyocytes and significantly improved left ventricular function without adverse cardiac remodeling in normal and infarcted rodent hearts (48). Our data indicated that dATP could rescue the preload responsiveness of failing hearts, suggesting restoration of the abnormal Frank-Starling Law of the Heart that often occurs in HF.

In the current study, we compare the relative therapeutic capacity of CK8-driven μDys or cardiac troponin T (cTnT)-driven RNR, via intravenously administered rAAV vectors in an advanced-age, DMD cardiomyopathy mouse model. We show a restoration of myocardial workload as indicated by rate pressure product (RPP) for baseline function in $mdx^{4cv}$ mice treated with RNR. This outcome was primarily attributed to the normalization of left ventricular developed pressure (LVDevP). Although $mdx^{4cv}$ mice treated with μDys appeared to normalize LVDevP, this did not result in a significant increase in RPP. Upon further evaluation of cardiac function, the pressure-volume relationship revealed that systolic pressure response with increased preload was significantly improved with the treatment of either RNR or μDys. However, only RNR treatment resulted in significant improvements in diastolic functional parameters, returning them to values that were similar to wild-type (WT) control hearts. As a further assessment of cardiac function, we tested hearts using a high workload challenge protocol. Both RNR and μDys treatments improved systolic function in $mdx^{4cv}$ hearts without compromising cardiac reserve. These positive results suggest that targeted expression of RNR within the myocardium can significantly improve contractile performance in an advanced-age model of DMD cardiomyopathy and may have therapeutic implications for DMD patients.

## METHODS

**ANIMAL EXPERIMENTS.** Male WT C57Bl/6J (The Jackson Laboratory, Bar Harbor, Maine) and $mdx^{4cv}$ (generated in-house) mice were used for these studies (17). All animals were experimentally manipulated in accordance with the Institutional Animal Care and Use Committee of the University of Washington. Experimental mice were administered vector at 22 to 24 months of age via the retro-orbital sinus with a 200-μl bolus injection in Hanks balanced saline solution at a dose of $2 \times 10^{14}$ vg/kg. All mice were housed in a specific-pathogen free animal care facility using a 12-h light/12-h dark cycle with access to food and water ad libitum.

**VECTOR PRODUCTION.** rAAV genomes containing the CK8 regulatory cassette (expressed exclusively in skeletal and cardiac muscle) and the human codon optimized (GenScript) μDys (ΔR2-15/ΔR18-22/ΔCT) (24), followed by the rabbit beta-globin poly-adenylation (pA) signal, were generated using standard cloning techniques. The rAAV genomes containing the cardiac muscle-specific cTnT455 regulatory cassette, the codon optimized human RNR transgene flanked by 100-bp untranslated regions, and the rabbit beta-globin pA were generated as previously described (48). The "dead" rAAV genomes or promoter-less firefly luciferase followed by the human growth hormone (hGH) pA (kindly provided by J.S.C., University of Washington, Seattle, Washington) were used to generate the control rAAV genomes. The resulting constructs were cotransfected with the pDG6 packaging plasmid into HEK293 cells to

generate rAAV vectors carrying serotype 6 capsids, which were harvested, enriched, and quantitated as previously described (49).

**VECTOR GENOME QUANTIFICATION.** Total DNA was extracted from flash-frozen tissue samples with Tri-Reagent (MRC Inc., Cincinnati, Ohio), according to manufacturer's instructions. All real-time polymerase chain reaction (PCR) reactions were performed on a QuantStudio 3 Real Time PCR System (Applied Biosystems, Foster City, California) in a total volume of 15 μl, consisting of 5 μl sample DNA, 10.0 μl TaqMan Universal PCR Master Mix (Applied Biosystems), 0.2 μM of each primer, and 0.1 μM TaqMan custom probe (Applied Biosystems). Reaction conditions were 50° C for 2 min, 95° C for 10 min, and 40 cycles of [95° C for 15 s followed by 60° C for 1 min]. Each sample was analyzed in triplicate for concentration of total murine genomes and of total vector genomes. For vector genome detection by quantitative PCR, the primers used to amplify either the rAAV6-cTnT455-RNR or rAAV6-CK8-μDys, or rAAV6-Δcytomegalovirus(CMV)-Luc (control vector) were unique to each vector. For the RNR vector, the amplicon spanned from the distal region of the cTnT promoter, continuing into the proximal RNR1 subunit. For the μDys vector, the amplicon was contained within the CK8 regulatory cassette, whereas the amplicon for the control vector resided within the hGH pA. hGH primers included: 5′-CACAATCTTGGCTCACTGCAA-3′, 5′-GGAGGCTGAG GCAGGAGAA-3′; TaqMan probe: 5′-6FAM- CTCCGCC TCCTGGGTTCAAGCG-MBGNQ-3′; CK8 RC primers: 5′-CCCGAGATGCCTGGTTATAATT-3′, 5′- CGGGAACAT GGCATGCA-3′; TaqMan probe: 5′-6FAM-CCCCCCAAC ACCTGCTGCCTCT-MBGNQ-3′; cTnT455-RNR1 primers: 5′-CCCAGTCCCCGCTGAGA-3′, 5′-AGGTTCCAGGCGCT GCT-3′; and TaqMan probe: 5′-6FAM-ACTCATCAATG TATCTTATCATG-MBGNQ-3′. Results were presented relative to DNA content in each 5-μl DNA tissue sample to determine vector genomes per ng DNA.

**TISSUE PROCESSING AND IMAGING ANALYSIS.** Tissues were collected and analyzed 5 months post-administration of vectors and compared with age-matched male control vector (rAAV6-ΔCMV-Luc) injected *mdx*$^{4cv}$ and WT mice. Hearts were either snap frozen in liquid nitrogen or were embedded in optimal cutting temperature compound (VWR International, Bridgeport, New Jersey) and flash frozen in liquid nitrogen cooled isopentane for histochemical or immunofluorescence analysis. The snap frozen samples were further processed by grinding to a powder under liquid nitrogen in a mortar kept on dry ice for subsequent extraction of nucleic acid and protein.

Heart cross-sections (10 μm) were co-stained with antibodies raised against alpha 2-laminin (Sigma, St. Louis, Missouri; rat monoclonal, 1:200), the hinge-1 domain of dystrophin (alexa488 conjugated MANEX1011b, Developmental Studies Hybridoma Bank, University of Iowa, mouse monoclonal, 1:200), the human RRM1 (Abcam, Cambridge, United Kingdom; rabbit monoclonal, 1:200), and the human RRM2 (Abcam, rabbit monoclonal, 1:200). Conjugated secondary antibodies (Jackson Immuno, Goat anti-Rabbit) were used at a 1:500 dilution. Slides were mounted using ProLong Gold with DAPI (Thermo Fisher Scientific) and imaged via a Leica SPV confocal microscope. Confocal micrographs covering a majority of the heart left ventricular muscle sections were acquired and montaged via the Fiji toolset (ImageJ) and InDesign (Adobe, San Jose, California). For histology, Masson's trichrome staining was used to examine heart cross-sections. Briefly, 10-μm muscle cryosections were sequentially stained in Wiegerts' iron hematoxylin (10 min), 1% Ponceau-acetic acid (5 min), and 1% aniline blue (5 s).

**WESTERN BLOTTING.** Radioimmunoprecipitation analysis buffer supplemented with 5 mM ethylenediaminetetraacetic acid and 3% protease inhibitor cocktail (Sigma, Cat# P8340), was used to extract muscle proteins for 0.5 h on ice with gentle agitation every 10 min. Total protein concentration was determined using Pierce BCA assay kit (Fisher Scientific, Kent, Washington). Muscle lysates from WT, control *mdx*$^{4cv}$, and treated *mdx*$^{4cv}$ (30 μg) mice were denatured at 99°C for 10 min, quenched on ice, and separated via gel electrophoresis after loading onto Criterion 4-12% Bis-Tris polyacrylamide gels (BioRad). Overnight protein transfer to 0.45 mm polyvinylidene difluoride membranes was performed at constant 43 volts at 4°C in Towbin's buffer containing 20% methanol. Blots were blocked for 1 h at room temperature in 5% non-fat dry milk for 1 h before overnight incubation with antibodies raised against the hinge-1 region of dystrophin (Developmental Studies Hybridoma Bank, University of Iowa, 1:300), anti-RRM1 (Abcam, rabbit monoclonal, 1:1,000), anti-RRM2 (Abcam, rabbit monoclonal 1:1,000), and anti-GAPDH (Sigma, Rabbit polyclonal, 1:50,000). Horseradish-peroxidase conjugated secondary antibody staining (1:50,000) was performed for 1 h at room temperature before signal development using Clarity Western ECL substrate (BioRad) and visualization using a Chemidoc MP imaging system (BioRad).

**QUANTIFICATION OF CARDIAC dATP.** Approximately 25 μg of flash frozen, freshly ground ventricle

cardiac tissue was used for direct quantification of intracellular dATP using the high-performance liquid chromatography (HPLC)-with tandem mass spectrometry (MS/MS) method previously described (50). Briefly, samples were extracted 1 to 3 days before measurement using a 50% methanol solution. The supernatant was stored at -20°C until ready for injection into the HPLC-MS/MS system. A Water's Xevo-TQ-S mass spectrometer coupled with a Water's Acquity I-Class HPLC was used for the analysis (Milford, Massachusetts). Monitoring in negative mode via electrospray ionization was used to acquire MS/MS ions. dATP concentrations were quantified with standards and normalized to tissue weight.

**LANGENDORFF ISOLATED PERFUSED HEART EXPERIMENTS.** Ex vivo cardiac function was assessed in Langendorff isolated heart preparations as previously described (47,48,51). Hearts were perfused at a constant pressure of 80 mm Hg with a modified Krebs-Henseleit buffer supplemented with glucose and pyruvate. The perfusate contained (mmol/l): 118 NaCl, 25 $NaHCO_3$, 5.3 KCl, 2.0 $CaCl_2$, 1.2 $MgSO_4$, 0.5 ethylenediaminetetraacetic acid, 10.0 glucose, and 0.5 pyruvate, equilibrated with 95% $O_2$ and 5% $CO_2$ (pH 7.4). Temperature was maintained at 37.5°C throughout the protocol. Left ventricular (LV) function was monitored via a water-filled balloon inserted into the LV and connected to a pressure transducer. LV systolic pressure (LVSP), end diastolic pressure, heart rate (HR), and minimum and maximum rate of pressure change in the ventricle (±dP/dt) were obtained from the attached data acquisition system (PowerLab, ADInstruments, Colorado Springs, Colorado). After 5 min of stabilization, hearts were equilibrated for 10 min at spontaneous HRs and then fixed at a HR of ~450 beats/min with an electrical stimulator (Grass Technologies, Warwick, Rhode Island). Pressure-volume relationships (i.e., Frank-Starling curves) were assessed by gradually increasing the volume of the LV balloon. After a 5-min recovery period, the perfusate was changed to an identical buffer as above except for the addition of 4.0 mmol/l $CaCl_2$ to simulate a high workload challenge for 20 min.

**STATISTICAL ANALYSIS.** All values are reported as means\ ± SEM. Starling curves and high workload function were analyzed by 2-way repeated measures analysis of variance followed by pairwise comparisons using Tukey's alpha adjustment method. Other endpoint data were analyzed via 1-way analysis of variance or Student's *t*-tests as appropriate. Kaplan-Meier methods were used to analyze survival curves and compared using the log-rank test. Statistical significance was tested at the $p < 0.05$ level. Statistical analyses were completed using Prism 7.0 (GraphPad Software, San Diego, California).

## RESULTS

**IMPROVEMENTS IN BASELINE CARDIAC FUNCTION IN VECTOR-TREATED MDX$^{4CV}$ HEARTS.** As depicted in **Figure 1**, 22- to 24-month-old *mdx*$^{4cv}$ mice were administered 1 of 3 treatments: rAAV6-cTnT455- RNR (referred to as *mdx*$^{4cv}$+RNR); rAAV6-CK8- μDys (referred to as *mdx*$^{4cv}$+ μDys), or rAAV6-ΔCMV-Firefly Luciferase control vector (referred to as*mdx*$^{4cv}$) at a dose of $2 \times 10^{14}$ vg/kg. By the end of the 20-week treatment period, both *mdx*$^{4cv}$+RNR and *mdx*$^{4cv}$+ μDys mice showed improvements in survival rates compared to *mdx*$^{4cv}$ mice, although this did not reach statistical significance (Supplemental Figure 1). At the end of 5 months, an extensive evaluation of ex vivo cardiac function using the Langendorff isolated heart preparation was performed. The isolated heart technique allows for the direct assessment of inherent myocardial function without the confounding effects of neuro-humoral or other systemic variables. An additional cohort of age-matched, untreated C57BL6 mice (WT) was used as comparison control. At baseline, RPP was significantly decreased in *mdx*$^{4cv}$ hearts due to an approximate 20% decrease in LVDevP (Supplemental Figures 1A and 1B). RNR-treated *mdx*$^{4cv}$ mice exhibited a restoration of RPP ($p = 0.056$) primarily due to a normalization of LVDevP (Supplemental Figures 2A and 2B). Although μDys-treated *mdx*$^{4cv}$ hearts appeared to normalize LVDevP, this did not lead to a significant improvement in RPP (Supplemental Figures 2A and 2B). Both +dP/dt and -dP/dt, an index of ventricular contractility and relaxation, respectively, were decreased 30% in *mdx*$^{4cv}$ hearts ($p = 0.061$). The +dP/dt was similar to control in both RNR-treated *mdx*$^{4cv}$ and μDys-treated *mdx*$^{4cv}$ hearts. However, only RNR-treated *mdx*$^{4cv}$ hearts showed -dP/dt values similar to control levels (Supplemental Figures 2C and 2D).

**POSITIVE CHANGES IN FRANK-STARLING MECHANICS IN VECTOR-TREATED MDX$^{4CV}$ HEARTS.** To evaluate further systolic and diastolic function in vector-treated *mdx*$^{4cv}$ hearts, we examined the pressure-volume relationship (i.e., Frank-Starling mechanism) in the isolated perfused heart preparation. The LVSP response to increased preload was significantly improved in both in *mdx*$^{4cv}$+RNR and *mdx*$^{4cv}$+μDys hearts compared to *mdx*$^{4cv}$ (**Figure 2A**). However, only RNR treatment improved the diastolic response in *mdx*$^{4cv}$ hearts, to levels similar to WT (**Figure 2B**). Both contractility and relaxation (i.e., +dP/dt and

**FIGURE 1 Overview of Experimental Design for the Treatment of Aged (22-24 Month) *mdx*$^{4cv}$ Mice**

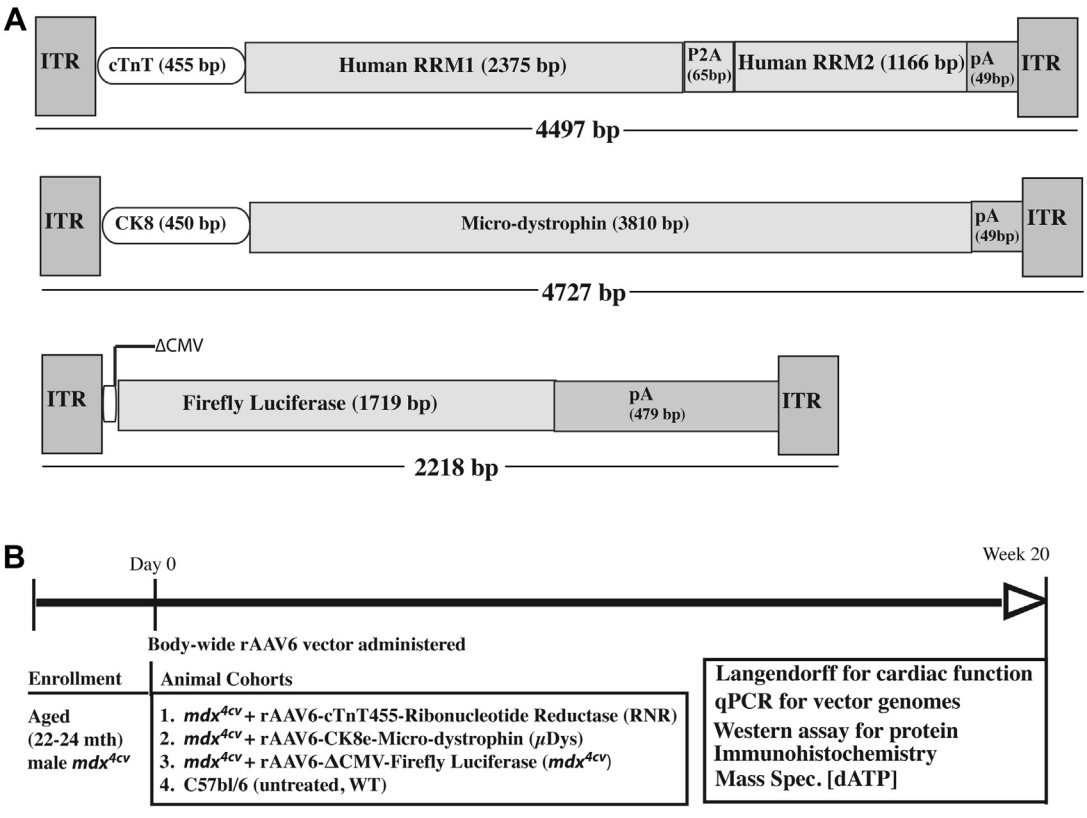


**(A)** Graphic representation of rAAV6 vectors used in the present study. The ribonucleotide reductase vector contains the human cDNA for the RRM1 and RRM2 subunits whose expression is driven by the cardiac specific (cTnT455) regulatory cassette (RC). The human microdystrophin (ΔR2-R15/ΔR18-R22/ΔCT) vector has expression driven by the CK8 muscle-specific RC. The control vector used in the present study carries the firefly luciferase transgene whose CMV early promoter/enhancer RC has been deleted. **(B)** Outline of animal enrollment, vector administration, and experimental protocols implemented following a treatment period of 5 months. cDNA = complementary DNA; CMV = cytomegalovirus; ITR = inverted terminal repeat; dATP = deoxy-adenosine triphosphate; p2A = porcine teschovirus-1 2A; pA = poly-adenylation; qPCR = quantitative polymerase chain reaction; rAAV6 = recombinant adeno-associated viral vector 6; RC = regulatory cassette; WT = wild-type.

-dP/dt, respectively) were impaired in *mdx*$^{4cv}$ compared to age-matched control subjects (Figures 2D and 2E). Both *mdx*$^{4cv}$+ RNR and *mdx*$^{4cv}$+ μDys hearts had significantly elevated +dP/dt values above *mdx*$^{4cv}$ (Figure 2D). Interestingly, treatment of *mdx*$^{4cv}$ hearts with RNR also significantly improved -dP/dt values (Figure 2E). All told, these data suggest that both RNR and μDys treatment can improve systolic function in *mdx*$^{4cv}$ hearts. However, only the RNR treatment corrected diastolic dysfunction in *mdx*$^{4cv}$ hearts.

**AUGMENTED RESPONSE TO INCREASED CARDIAC WORKLOAD IN TREATED MDX$^{4CV}$ HEARTS.** We previously reported that RNR overexpression in transgenic or vector-treated mouse hearts elevated baseline function but did not impair the response to a short-term physiologic increase in cardiac work (47,48). To verify that the improved systolic and diastolic function in RNR-treated *mdx*$^{4cv}$ hearts at baseline was not associated with an inability to respond to an increased energetic demand, we stressed hearts with a combination of high calcium and elevated heart rates, via pacing stimulation. As shown in Figures 3A and 3B, *mdx*$^{4cv}$ hearts had a blunted response to the increased workload as both LVDevP and RPP were ~25% to 30% lower than WT hearts. In addition, both +dP/dt and -dP/dt were impaired in *mdx*$^{4cv}$ relative to WT hearts (Figures 3C and 3D). Systolic parameters in *mdx*$^{4cv}$+μDys hearts were effectively improved and similar to age-matched WT hearts for the entire duration of the workload challenge

**FIGURE 2 Pressure-Volume Relationships in Isolated Perfused Hearts From Vector-Treated *mdx*$^{4cv}$ Mice**

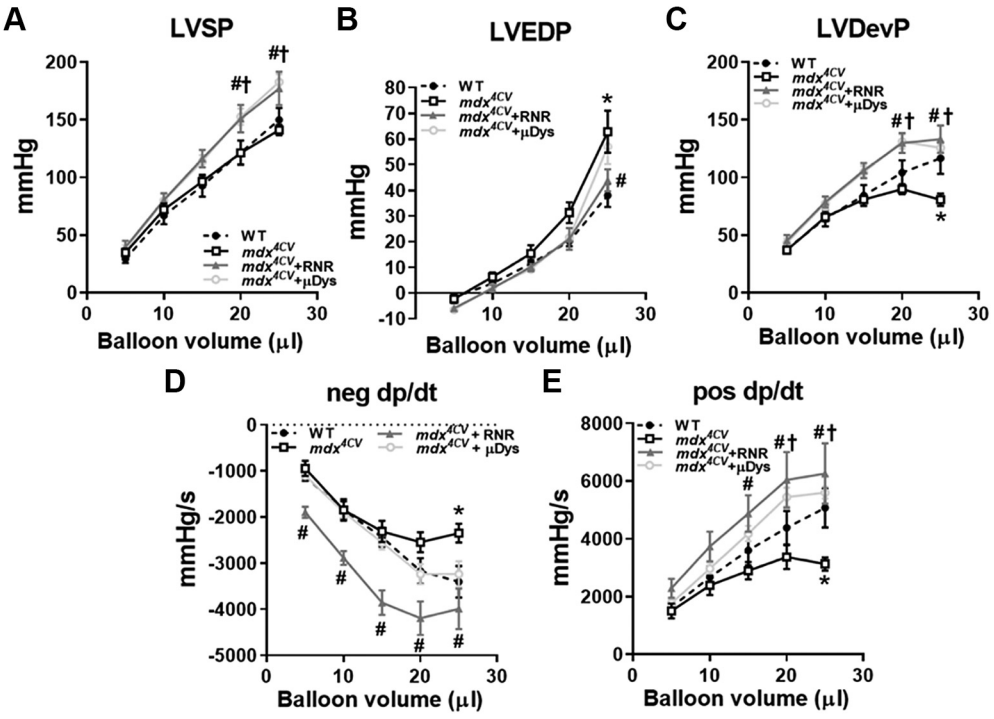


Hearts were isolated from *mdx*$^{4cv}$ mice treated with control vector (*mdx*$^{4cv}$, n = 6), ribonucleotide reductase (*mdx*$^{4cv}$+ RNR, n = 6), or microdystrophin (*mdx*$^{4cv}$+ μDys, n = 5). Age-matched, nondiseased, nontreated wild-type (WT) mice were used as control subjects (n = 8). The pressure-volume relationship (i.e., Frank-Starling mechanism) was evaluated by gradually increasing the volume of the left ventricular (LV) balloon. Hearts were paced at 450 beats/min throughout the protocol. **(A)** Left ventricular systolic pressure (LVSP). **(B)** LV end-diastolic pressure (LVEDP). **(C)** LV developed pressure (LVDevP, the difference between systolic and diastolic pressures). **(D)** Positive (pos) rate of pressure change was calculated by the first derivative of the ascending LV pressure wave (+dP/dt), and is used as an index of ventricular contractility. **(E)** Negative (neg) rate of pressure change calculated by the first derivative of the descending LV pressure wave (–dP/dt), and is used as an index of ventricular relaxation. * $p < 0.05$ *mdx*$^{4cv}$ versus WT; # $p < 0.05$ *mdx*$^{4cv}$+ RNR versus *mdx*$^{4cv}$; † $p < 0.05$ *mdx*$^{4cv}$+ μDys versus *mdx*$^{4cv}$.

(Figures 3A to 3C). Measures of systolic function significantly increased in *mdx*$^{4cv}$+ RNR hearts during the initial half of the high workload protocol and remained ~15% higher than *mdx*$^{4cv}$ (Figures 3A to 3C). Interestingly, -dP/dt values tended to be elevated only in *mdx*$^{4cv}$+ RNR hearts during the physiologic challenge (Figure 3D). These data show that both RNR and μDys treatments improve systolic function in *mdx*$^{4cv}$ hearts without compromising cardiac reserve. Combined with the baseline and pressure-volume relationship assessments, our data show that, in addition to the systolic enhancements, RNR has an added benefit of improving diastolic function.

**RNR AND μDys TRANSDUCTION, EXPRESSION, AND CARDIOMYOCYTE LOCALIZATION.** To evaluate the localization of RNR and μDys protein within the hearts of mice, we performed immunofluorescence imaging. As shown in Figure 4, the RNR subunit (Rrm1) was robustly expressed in ventricles of RNR-treated mice. The expression of μDys appeared to be saturated relative to full-length dystrophin levels, with both being properly localized to the sarcolemma of cardiomyocytes. We also evaluated general muscle histopathology and potential differences in myocardial fibrosis by Masson trichrome staining, and observed no discernable difference between treated or untreated *mdx*$^{4cv}$ mice (Figure 5). In addition, neither RNR nor μDys treatment significantly altered body weight, heart weight, or the heart weight-to-body weight ratio (Supplemental Figure 3). Western blotting was performed to determine the extent of rAAV vector 6-mediated RNR and μDys protein expression profiles in ventricular tissue (Figure 6). We observed μDys protein expression in ventricular tissue that approached levels similar to WT mice, whereas both human RNR subunits were found to be elevated to comparable levels within ventricular tissue (Figure 6A). To evaluate the relative proportions of

**FIGURE 3** The Response of Vector-Treated $mdx^{4cv}$ Mice to High Workload Challenge in Langendorff Isolated Heart Preparations

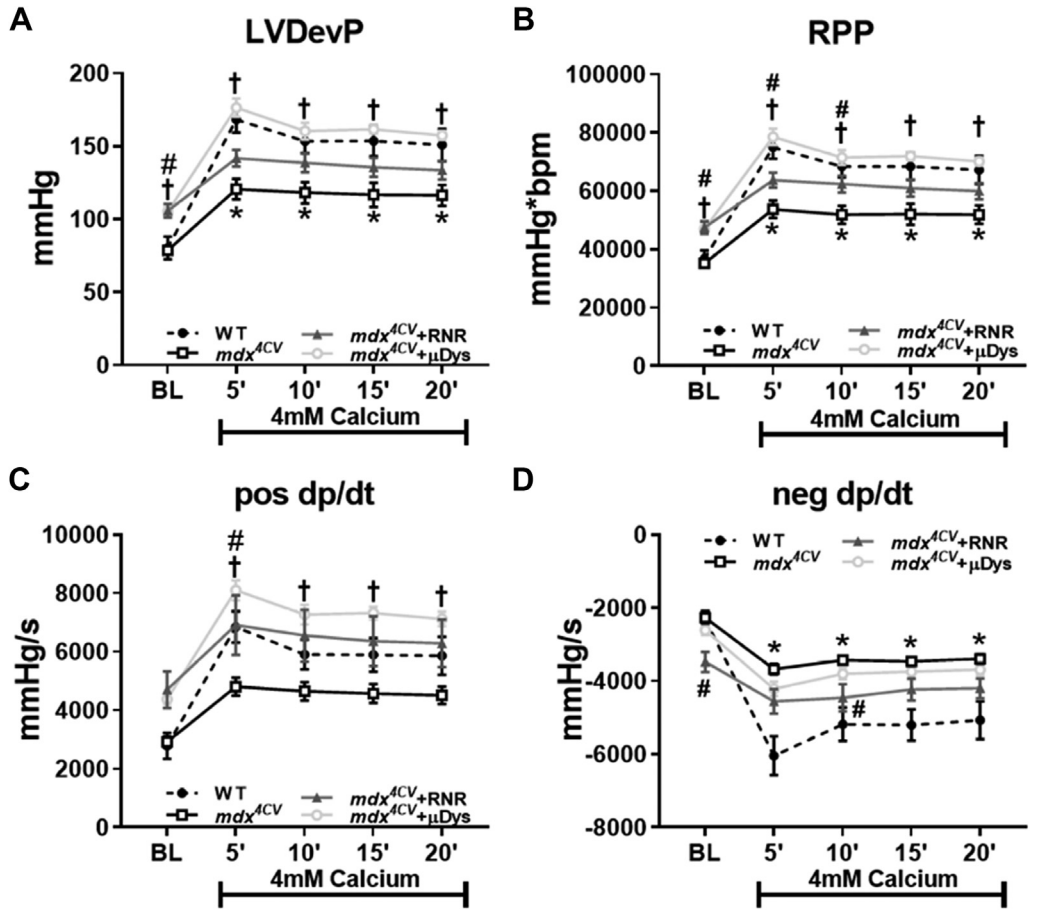


Hearts were isolated from $mdx^{4cv}$ mice treated with control vector ($mdx^{4cv}$, n = 6), ribonucleotide reductase ($mdx^{4cv}$+ RNR, n = 6), or microdystrophin ($mdx^{4cv}$+ µDys, n = 5). Age-matched, nondiseased, nontreated wild-type (WT) mice were used as control subjects (n = 4). All hearts were perfused with a glucose-pyruvate buffer containing high calcium (4.0 mmol/l) to simulate a high workload challenge for 20 min. Hearts were paced at 450 beats per minute throughout the protocol. **(A)** LVDevP (the difference between systolic and diastolic pressures). **(B)** Rate pressure product (RPP, the product of LVDevP and HR). **(C)** Positive rate of pressure change calculated by the first derivative of the ascending LV pressure wave (+dP/dt), is used as an index of ventricular contractility. **(D)** Negative rate of pressure change calculated by the first derivative of the descending LV pressure wave (-dP/dt), is used as an index of ventricular relaxation. * $p < 0.05$ $mdx^{4cv}$ versus WT; # $p < 0.05$ $mdx^{4cv}$+ RNR versus $mdx^{4cv}$; † $p < 0.05$ $mdx^{4cv}$+ µDys versus $mdx^{4cv}$. Abbreviations as in Figures 1 and 2.

dATP concentrations within ventricular tissue, we performed HPLC-MS/MS analysis on ground ventricular tissue from $mdx^{4cv}$ and $mdx^{4cv}$+ RNR mice. The concentration of dATP within the ventricular tissue obtained from $mdx^{4cv}$ mice treated with RNR (0.57 ± 0.22 pmol dATP/mg) was approximately 10-fold higher relative to $mdx^{4cv}$ control subjects (0.05 ± 0.02 pmol dATP/mg) (Figure 6B). For adult WT, we previously reported an average dATP value of 0.02 pmol/mg tissue with a SD of 0.01 (50). Additionally, cardiac vector genome data was comparable relative to the vector dose administered (Figure 6C).

## DISCUSSION

In the present study, we used a novel gene therapy approach that targets myosin in the contractile filaments of cardiomyocytes via overexpression of the RNR enzyme to rescue cardiomyopathy in a DMD mouse model. RNR overexpression results in elevated dATP, which can be used by cardiac myosin (in place of ATP), and increases cross-bridge binding and cycling, resulting in stronger, faster contraction and faster relaxation (38–45,52). We developed an rAAV vector that over-expresses RNR selectively in heart

**FIGURE 4 Cardiac Transduction Following Intravenous Delivery of Ribonucleotide Reductase or Microdystrophin**

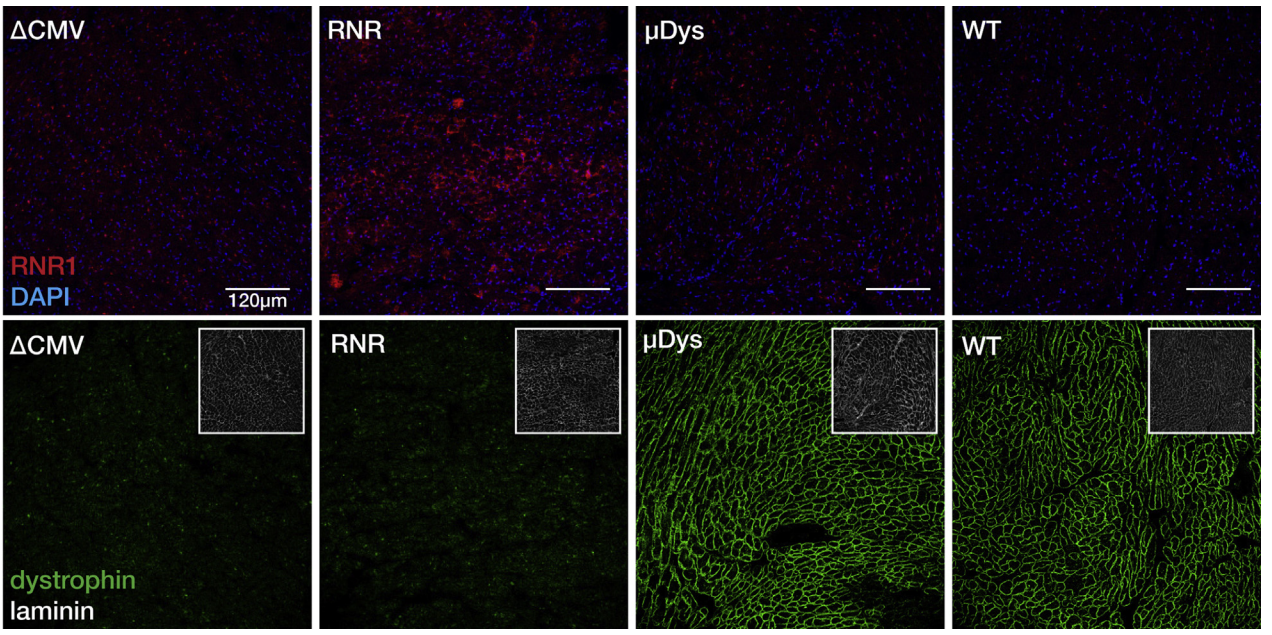


At 5 months after vector administration, cryosections were prepared and immunostained with antisera against dystrophin or ribonucleotide reductase. A considerable level of protein is detected for each ribonucleotide reductase subunit-1 (human specific) as indicated by immunofluorescent staining **(red)** localized primarily within the cytoplasm of cardiomyocytes with occasional perinuclear accumulation **(upper panel)**. On the lower panel, the robust level of expression for dystrophin in WT and in aged *mdx*$^{4cv}$ mice treated with AAV6-CK8-μDys (laminin staining, **inset image**). Abbreviations as in Figures 1 and 2.

muscle via inclusion of a modified cardiac-specific enhancer/promoter derived from the human cTnT gene, which facilitates increases in myocyte contraction and cardiac performance in normal rodent hearts as well as in infarcted rodents and pig hearts (48,53). Importantly, we previously showed that dATP-producing cells deliver it to surrounding myocardium by diffusion through gap junctions (54), such that only a minority of cardiomyocytes needs to be transduced to have global benefits within the heart. We now show that using this vector technology leads to a clear benefit of improving cardiac function in an advanced-age model of DMD cardiomyopathy.

Early manifestations of impaired cardiac dysfunction in *mdx* mice are generally not reported. Khairallah et al.(55) observed a decline in LV function in isolated perfused hearts that coincided with decreased fatty acid oxidation and increased glucose oxidation. However, perfused heart function in *mdx* mice was maintained at 8 months, despite significant reductions in phosphocreatine levels and free energy availability from ATP hydrolysis (56). The authors surmised that young adult *mdx* hearts, akin to DMD patient hearts, experience right ventricular dilation, LV diastolic deficits, and abnormal energy metabolism. More recently, a declination in cardiac function was not observed until 12 months of age (57) and abnormal in vivo pressure-volume dynamics were observed in 22-month-old *mdx* mice (58). Treatment of young male *mdx* mice with rAAV6 vector delivering cytomegalovirus (CMV) promoter/enhancer driven microdystrophin did not correct the impairments in +dP/dt, -dP/dt, or LV systolic pressure when assessed at 5 months of age via hemodynamic analysis (35). However, an improvement was noted for the preload recruited stroke work in *mdx* mice treated with μDys compared to untreated *mdx* or WT control subjects (35).

In our current study, 27-month to 29-month-old mice were subjected to ex vivo assessment of cardiac function using the Langendorff isolated heart preparation, which is a century-old methodology with several advantages and limitations (59). The perfusate used is similar to, but not the same as blood, and situations of physiologic challenge (e.g., Frank-Starling and high calcium) may exaggerate the in vivo situation. However, the procedure remains a simple and reproducible experiment that allows for interrogation of cardiac physiology in the absence of confounding systemic variables and serves as a viable

**FIGURE 5** Heart Histologic Staining of $mdx^{4cv}$ Mice Suggests No Morphologic Alterations From RNR Therapy

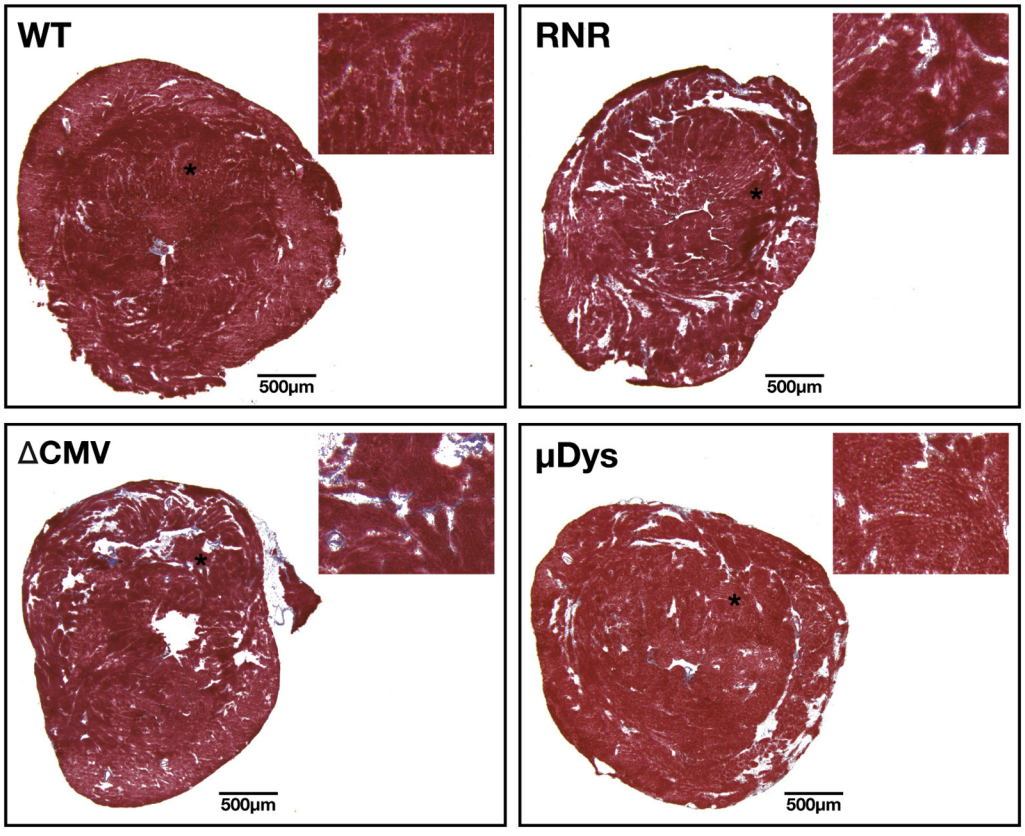


Representative full-view photomicrographs of Masson trichrome staining of the hearts from $mdx^{4cv}$ mice displaying control vector (ΔCMV), and rAAV6-treated with either RNR or μDys from mdx4cv mice. Similarly, a 20× enlarged view of the corresponding images **(*)** is shown. Abbreviations as in **Figures 1 and 2**.

tool to perform cardiac phenotyping in preclinical studies (60). Under baseline conditions and at spontaneous heart rates, we observed a significant reduction in RPP in $mdx^{4cv}$ hearts. Decreased systolic and diastolic performance in $mdx^{4cv}$ hearts also existed while examining the length-tension relationship (i.e., Frank-Starling mechanism). Treatment of $mdx^{4cv}$ mice with either the RNR or the μDys vector restored systolic pressure development without affecting spontaneous HRs at baseline. Both of the treatments restored the disrupted Frank-Starling response, particularly for systolic function. The RNR treatment also had beneficial effects on the diastolic properties of the $mdx^{4cv}$ myocardium. This strongly supports our previous studies where we observed a tendency for overexpression of RNR to improve myocardial diastolic response in young, healthy, transgenic mice (47), mice treated with AAV (48), and in a porcine HF model (53).

In addition to the evaluation of basal cardiac performance, we tested cardiac reserve with a combination of high calcium plus elevated HRs and confirmed a significantly blunted response in 27-month to 29-month-old $mdx^{4cv}$ hearts. Consistent with a previous report in young *mdx* mice (35), expressing μDys in aged $mdx^{4cv}$ hearts significantly improved systolic performance during increased physiologic demand to a level similar to age-matched healthy control subjects. We previously reported that transgenic or vector-directed overexpression of RNR did not impair cardiac reserve during increased physiologic demand in young healthy hearts (47,48). Herein, we report that RNR over-expression in $mdx^{4cv}$ hearts normalizes both the systolic and diastolic response to an increased cardiac challenge.

Approximately two-thirds of DMD mutations are deletions that span 1 or more exons, often leading to large deletions clustering around 2 mutational

**FIGURE 6 Protein Expression Levels for μDys, RNR, and Resultant Vector Genomes Due to rAAV6-Mediated Gene Transfer**

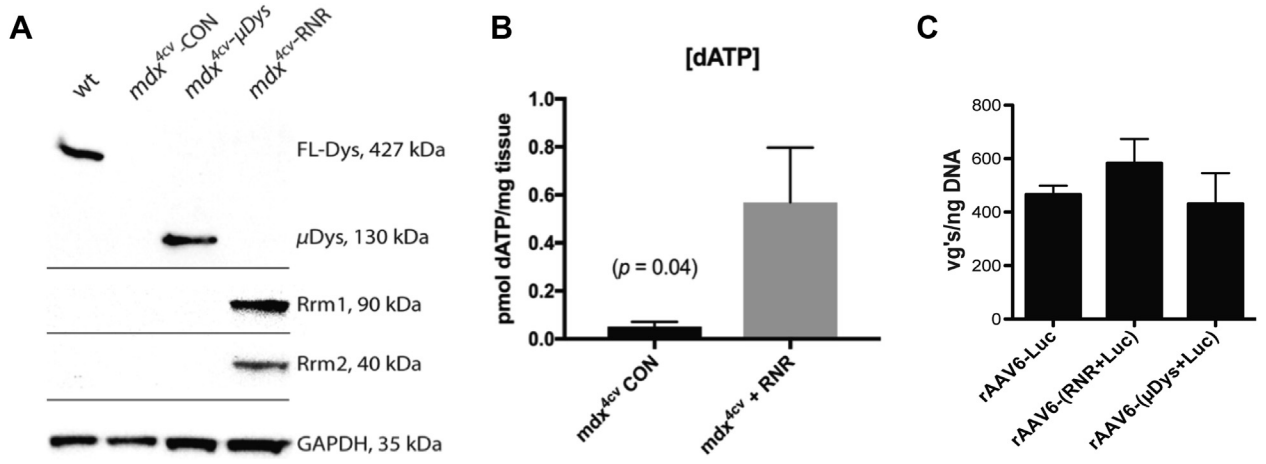


**(A)** RNR and μDys protein expression detection as revealed by immunoblotting of cardiac whole tissue lysates using either RRM1, RRM2, or antidystrophin antibody. **(B)** HPLC-MS/MS intracellular [dNTP] quantification from methanol extracted cardiac tissue. **(C)** qPCR analysis of vector genomes from cardiac tissue revealed similar vector genomes being represented for all treated cohorts. dNTP = deoxynucleotide triphosphate; HPLC-MS/MS = high-performance liquid chromatography–tandem mass spectrometry; qPCR = quantitative polymerase chain reaction; other abbreviations as in Figures 1 and 2.

hotspots; the most common spanning from exons 45-55 resulting in removal of a central portion of the rod domain inclusive of disrupting the neuronal nitric oxide synthase (nNOS) localization domain. The second most common hotspot spans from exons 3-19, and removes the majority of the amino-terminal actin-binding domain 1 which is essential for dystrophin function. When such deletions interrupt the reading frame, the resultant mutated protein usually expresses at extremely low levels and associates with the loss of ambulation at or before 12 years of age. Even when such deletions produce an in-frame partially functional truncated protein, such as occurs in BMD, dramatic phenotype diversity can occur. For example, in a previous study, BMD subjects whose out-of-phase deletions, toward the alignment of adjoining spectrin-like repeats, developed dilated cardiomyopathy at nearly a decade earlier than in patients with in-phase deletions (61). In contrast to large deletion mutations, there are reported cases where individual missense mutations lead to X-linked dilated cardiomyopathy (62-64). In one case, a novel missense mutation within exon 9 at nucleotide 1043 resulted in a T279A amino acid change in a highly conserved position of mutation. This mutation resulted in a substitution of a beta-sheet for alpha-helical structure, destabilizing the protein, and leading to the cardiac specific phenotype described by the authors (63).

DMD-related cardiomyopathy usually occurs during middle to late adolescence, but the clinical presentation is deceptive, as patients are wheelchair-bound and are not required to perform increased cardiac workload. The diversity of cardiac phenotype in DMD suggests many levels of pathogenic mechanisms. The pathologic heterogeneity of the DMD ventricular myocardium is a consequential result of myocardial atrophy (65,66), compensatory mechanisms leading to cardiac remodeling with ensuing ventricular dilation and fibrosis (67,68). Absence of clear genotype-phenotype correlation in DMD probably results from at least 4 secondary cellular processes including aberrant intracellular $Ca^{2+}$ homeostasis, decreased nitric oxide–cyclic guanosine monophosphate pathways, mitochondrial dysfunction, and increased reactive oxygen species, which individually or collectively influence the clinical phenotype (69). As an indication of the progressive nature of DMD cardiomyopathy, the estimated overall incidence of latent DCM is 25% by 6 years of age and 59% by 10 years of age in DMD patients (70). As such, further evidence suggests latency in cardiac dysfunction at basal levels that becomes more pronounced with an induction of increased physiological demand. Consistent with these observations, an impaired response to beta-adrenergic stimulation by either dobutamine or isoproterenol can be detected in *mdx* mice at 3 to 4 months of age (35,71). Exercise can

potentially be a double-edged sword for DMD, where the enthusiasm for potential skeletal muscle benefits can be dampened by the insidious cardiotoxicity from training (72–74). With gene replacement therapy via rAAV-mediated μDys in current ongoing clinical trials, it will be of interest to assess cardiac function to determine whether additional therapeutic support in the form of increased contractility will be beneficial.

Relative expression assays by immunofluorescence and Western blotting indicate robust expression levels for the RNR subunits (RRM1 and RRM2) and μDys in the vast majority of cardiomyocytes. However, intracellular variability in RNR protein detection (via immunostaining) was observed for both RRM1 and RRM2, indicating that not all cardiomyocytes were effectively transduced. Nevertheless, we previously have shown that gap junction transport of dATP from transduced cardiomyocytes to adjacent cardiomyocytes occurs (54), which likely accounted for the consistently elevated LV function of mice treated with the rAAV vector that over-expresses RNR. This is in contrast to the anchored sarcolemma localization of μDys, which would occur only in transduced muscle cells. Additionally, because muscle-specific regulatory cassettes were used for expression of therapeutic proteins, we can surmise that <1% of protein expression would be generated from non-muscle cell types present in the heart, suggesting that the functional benefit was truly caused by cardiomyocyte transduction. As previously stated, the cTnT regulatory cassette drives RNR expression only in heart muscle, whereas the CK8 regulatory cassette drives μDys expression no selectively in both cardiac and skeletal muscle cells, but at only very low background levels in other tissues. This raises the possibility that the functional benefit of expressing μDys in skeletal muscles might increase energetic demands on the heart, thereby partially masking some of the μDys-derived cardiac functional benefits (37). Because RNR delivery to DMD mice of advanced age increased cardiac function in the absence of RNR expression in skeletal muscle, and because over-expression of endogenous RNR should be nonimmunogenic, supplemental RNR therapy in conjunction with μDys therapy might be beneficial for DMD patients. Future studies are aimed at determining the extent of functional restoration by combining both RNR- and μDys-based therapies.

**ACKNOWLEDGMENTS** The authors thank James Allen and Christine Halbert (Wellstone Muscular Dystrophy Specialized Research Center, University of Washington, Seattle, Washington) for assistance with vector production, purification, and quality assessment.

**ADDRESS FOR CORRESPONDENCE:** Dr. Guy L. Odom, Department of Neurology, University of Washington, 850 Republican Street, S248, Box 358055, Seattle, Washington 98109. E-mail: godom@uw.edu. OR Dr. Michael Regnier, Department of Bioengineering, University of Washington, 850 Republican Street, S180, Seattle, Washington 98109. E-mail: mregnier@uw.edu.

## PERSPECTIVES

**COMPETENCY IN MEDICAL KNOWLEDGE:** RNR over-expression represents an emerging therapy for improving cardiac dysfunction via cardiac myosin activation in a variety of clinical situations. Currently, there are 3 ongoing clinical trials using rAAV-mediated variants of μDys that have shown broad promise in terms of safety, and in biomarker indicators suggesting pathologic improvements. If cardiac dysfunction is detected in the patients from these clinical studies, our studies in aged, *mdx* mice suggest that combinatorial RNR therapy may be beneficial.

**TRANSLATIONAL OUTLOOK:** Our novel strategy of vector-mediated, cardiac-specific over-expression of RNR shows promising potential for rescuing both systolic and diastolic function in aged, DMD mice even in the absence of addressing the underlying dystrophin deficiency. Future studies investigating the combined effects of μDys and RNR may disclose an improved therapeutic strategy to provide structural and functional improvement of DMD patient hearts.

## REFERENCES

**1.** Emery AE, Muntoni F. Duchenne Muscular Dystrophy. 3rd ed. Oxford, United Kingdom: Oxford University Press, 2003:270.

**2.** Ervasti JM. Structure and function of the dystrophin-glycoprotein complex. In: Winder SJ, editor. Molecular Mechanisms of Muscular Dystrophies. Georgetown, Texas: Landes Biosciences, 2006:1–13.

**3.** Cox GA, Phelps SF, Chapman VM, Chamberlain JS. New *mdx* mutation disrupts expression of muscle and nonmuscle isoforms of dystrophin. Nature Genet 1993;4:87–93.

**4.** Brooks SV, Faulkner JA. Contractile properties of skeletal muscles from young, adult and aged mice. J Physiol (London) 1988;404:71–82.

**5.** Campbell KP. Three muscular dystrophies: loss of cytoskeleton-extracellular matrix linkage. Cell 1995;80:675–9.

**6.** Petrof BJ, Shrager JB, Stedman HH, Kelly AM, Sweeney HL. Dystrophin protects the sarcolemma from stresses developed during muscle contraction. Proc Natl Acad Sci U S A 1993;90:3710–4.

**7.** Ramaswamy KS, Palmer ML, van der Meulen JH, et al. Lateral transmission of force is impaired in skeletal muscles of dystrophic mice and very old rats. J Physiol 2011;589 Pt 5:1195–208.

**8.** Chao DS, Gorospe JR, Brenman JE, et al. Selective loss of sarcolemmal nitric oxide synthase in Becker muscular dystrophy. J Exp Med 1996;184:609–18.

**9.** Froehner SC. Just say NO to muscle degeneration? Trends Mol Med 2002;8:51–3.

**10.** Grady RM, Grange RW, Lau KS, et al. Role for alpha-dystrobrevin in the pathogenesis of dystrophin-dependent muscular dystrophies. Nat Cell Biol 1999;1:215–20.

**11.** Lapidos KA, Kakkar R, McNally EM. The dystrophin glycoprotein complex: signaling strength and integrity for the sarcolemma. Circ Res 2004;94:1023–31.

**12.** Ervasti JM, Campbell KP. A role for the dystrophin-glycoprotein complex as a transmembrane linker between laminin and actin. J Cell Biol 1993;122:809–23.

**13.** Ibraghimov-Beskrovnaya O, Ervasti JM, Leveille CJ, et al. Primary structure of dystrophin-associated glycoproteins linking dystrophin to the extracellular matrix. Nature 1992;355:696–702.

**14.** Yoshida M, Ozawa E. Glycoprotein complex anchoring dystrophin to sarcolemma. J Biochem (Tokyo) 1990;108:748–52.

**15.** England SB, Nicholson LV, Johnson MA, et al. Very mild muscular dystrophy associated with the deletion of 46% of dystrophin. Nature 1990;343:180–2.

**16.** Valentine BA, Winand NJ, Pradhan D, et al. Canine X-linked muscular dystrophy as an animal model of Duchenne muscular dystrophy: a review. Am J Med Genet 1992;42:352–6.

**17.** Im WB, Phelps SF, Copen EH, et al. Differential expression of dystrophin isoforms in strains of mdx mice with different mutations. Hum Mol Genet 1996;5:1149–53.

**18.** Phelps SF, Hauser MA, Cole NM, et al. Expression of full-length and truncated dystrophin mini-genes in transgenic *mdx* mice. Hum Mol Genet 1995;4:1251–8.

**19.** Crawford GE, Faulkner JA, Crosbie RH, et al. Assembly of the dystrophin-associated protein complex does not require the dystrophin COOH-terminal domain. J Cell Biol 2000;150:1399–410.

**20.** Harper SQ, Hauser MA, DelloRusso C, et al. Modular flexibility of dystrophin: implications for gene therapy of Duchenne muscular dystrophy. Nat Med 2002;8:253–61.

**21.** Wang B, Li J, Xiao X. Adeno-associated virus vector carrying human minidystrophin genes effectively ameliorates muscular dystrophy in mdx mouse model. Proc Natl Acad Sci U S A 2000;97:13714–9.

**22.** Sakamoto M, Yuasa K, Yoshimura M, et al. Micro-dystrophin cDNA ameliorates dystrophic phenotypes when introduced into mdx mice as a transgene. Biochem Biophys Res Commun 2002;293:1265–72.

**23.** Chamberlain JS. Gene therapy of muscular dystrophy. Hum Mol Genet 2002;11:2355–62.

**24.** Hakim CH, Wasala NB, Pan X, et al. A five-repeat micro-dystrophin gene ameliorated dystrophic phenotype in the severe DBA/2J-mdx model of Duchenne muscular dystrophy. Mol Ther Methods Clin Dev 2017;6:216–30.

**25.** Cox GA, Cole NM, Matsumura K, et al. Overexpression of dystrophin in transgenic mdx mice eliminates dystrophic symptoms without toxicity [see comments]. Nature 1993;364:725–9.

**26.** Stedman HH, Sweeney HL, Shrager JB, et al. The mdx mouse diaphragm reproduces the degenerative changes of Duchenne muscular dystrophy. Nature 1991;352:536–9.

**27.** Brooks SV, Faulkner JA. Skeletal muscle weakness in old age: underlying mechanisms. Med Sci Sports Exerc 1994;26:432–9.

**28.** DelloRusso C, Crawford R, Chamberlain J, Brooks S. Tibialis anterior muscles of *mdx* mice are highly susceptible to contraction-induced injury. J Muscle Res Cell Motility 2001;22:467–75.

**29.** Lynch GS, Hinkle RT, Chamberlain JS, Brooks SV, Faulkner JA. Force and power output of fast and slow skeletal muscles from mdx mice 6-28 months old. J Physiol 2001;535 Pt 2:591–600.

**30.** Bostick B, Shin JH, Yue Y, et al. AAV microdystrophin gene therapy alleviates stress-induced cardiac death but not myocardial fibrosis in >21-m-old mdx mice, an end-stage model of Duchenne muscular dystrophy cardiomyopathy. J Mol Cell Cardiol 2012;53:217–22.

**31.** Gregorevic P, Blankinship MJ, Allen JM, Chamberlain JS. Systemic microdystrophin gene delivery improves skeletal muscle structure and function in old dystrophic mdx mice. Mol Ther 2008;16:657–64.

**32.** Quinlan JG, Hahn HS, Wong BL, et al. Evolution of the mdx mouse cardiomyopathy: physiological and morphological findings. Neuromuscul Disord 2004;14:491–6.

**33.** Gregorevic P, Allen JM, Minami E, et al. rAAV6-microdystrophin preserves muscle function and extends lifespan in severely dystrophic mice. Nat Med 2006;12:787–9.

**34.** Shin JH, Nitahara-Kasahara Y, Hayashita-Kinoh H, et al. Improvement of cardiac fibrosis in dystrophic mice by rAAV9-mediated microdystrophin transduction. Gene Ther 2011;18:910–9.

**35.** Townsend D, Blankinship MJ, Allen JM, et al. Systemic administration of micro-dystrophin restores cardiac geometry and prevents dobutamine-induced cardiac pump failure. Mol Ther 2007;15:1086–92.

**36.** Bostick B, Shin JH, Yue Y, Duan D. AAV-microdystrophin therapy improves cardiac performance in aged female mdx mice. Mol Ther 2011;19:1826–32.

**37.** Townsend D, Yasuda S, Chamberlain J, Metzger JM. Cardiac consequences to skeletal muscle-centric therapeutics for Duchenne muscular dystrophy. Trends Cardiovasc Med 2009;19:50–5.

**38.** Adhikari BB, Regnier M, Rivera AJ, Kreutziger KL, Martyn DA. Cardiac length dependence of force and force development kinetics with altered cross-bridge cycling. Biophysical J 2004;87:1784–94.

**39.** Clemmens EW, Entezari M, Martyn DA, Regnier M. Different effects of cardiac versus skeletal muscle regulatory proteins on in vitro measures of actin filament speed and force. J Physiol 2005;566 Pt 3:737–46.

**40.** Korte FS, Dai J, Buckley K, et al. Upregulation of cardiomyocyte ribonucleotide reductase increases intracellular 2 deoxy-ATP, contractility, and relaxation. J Mol Cell Cardiol 2011;51:894–901.

**41.** Kreutziger KL, Piroddi N, McMichael JT, Poggesi C, Tesi C, Regnier M. Cooperative activation and tension kinetics in cardiac muscle are strongly modulated by calcium binding kinetics of troponin C. J Mol Cell Cardiol 2011;50:165–74.

**42.** Moussavi-Harami F, Razumova MV, Racca AW, et al. 2-deoxy adenosine triphosphate improves contraction in human end-stage heart failure. J Mol Cell Cardiol 2015;79:256–63.

**43.** Regnier M, Lee DM, Homsher E. ATP analogs and muscle contraction: mechanics and kinetics of nucleoside triphosphate binding and hydrolysis. Biophys J 1998;74:3044–58.

**44.** Regnier M, Martin H, Barsotti RJ, et al. Cross-bridge versus thin filament contributions to the level and rate of force development in cardiac muscle. Biophys J 2004;87:1815–24.

**45.** Regnier M, Rivera AJ, Chen Y, Chase PB. 2-deoxy-ATP enhances contractility of rat cardiac muscle. Circ Res 2000;86:1211–7.

**46.** Cheng Y, Hogarth KA, O'Sullivan ML, Regnier M, Pyle WG. 2-deoxyadenosine triphosphate restores the contractile function of cardiac myofibril from adult dogs with naturally occurring dilated cardiomyopathy. Am J Physiol Heart Circ Physiol 2016;310:H80–91.

**47.** Nowakowski SG, Kolwicz SC, Korte FS, et al. Transgenic overexpression of ribonucleotide reductase improves cardiac performance. Proc Natl Acad Sci U S A 2013;110:6187–92.

**48.** Kolwicz SC Jr., Odom GL, Nowakowski SG, et al. AAV6-mediated cardiac-specific overexpression of ribonucleotide reductase enhances myocardial contractility. Mol Ther 2016;24:240–50.

**49.** Halbert CL, Allen JM, Chamberlain JS. AAV6 vector production and purification for muscle gene therapy. Methods Mol Biol 2018;1687:257–66.

**50.** Olafsson S, Whittington D, Murray J, Regnier M, Moussavi-Harami F. Fast and sensitive HPLC-MS/MS method for direct quantification of intracellular deoxyribonucleoside triphosphates from tissue and cells. J Chromatogr B Analyt Technol Biomed Life Sci 2017;1068-1069:90–7.

**51.** Kolwicz SC Jr., Tian R. Assessment of cardiac function and energetics in isolated mouse hearts using 31P NMR spectroscopy. J Vis Exp 2010;42:e2069.

**52.** Kreutziger KL, Piroddi N, Belus A, Poggesi C, Regnier M. $Ca^{2+}$-binding kinetics of troponin C influence force generation kinetics in cardiac muscle. Biophysical J 2007;92:477a.

**53.** Kadota S, Carey J, Reinecke H, et al. Ribonucleotide reductase-mediated increase in dATP

improves cardiac performance via myosin activation in a large animal model of heart failure. Eur J Heart Fail 2015;17:772–81.

**54.** Lundy SD, Murphy SA, Dupras SK, et al. Cell-based delivery of dATP via gap junctions enhances cardiac contractility. J Mol Cell Cardiol 2014;72:350–9.

**55.** Khairallah M, Khairallah R, Young ME, et al. Metabolic and signaling alterations in dystrophin-deficient hearts precede overt cardiomyopathy. J Mol Cell Cardiol 2007;43:119–29.

**56.** Zhang W, ten Hove M, Schneider JE, et al. Abnormal cardiac morphology, function and energy metabolism in the dystrophic mdx mouse: an MRI and MRS study. J Mol Cell Cardiol 2008;45:754–60.

**57.** Stuckey DJ, Carr CA, Camelliti P, et al. In vivo MRI characterization of progressive cardiac dysfunction in the mdx mouse model of muscular dystrophy. PLoS One 2012;7:e28569.

**58.** Bostick B, Yue Y, Duan D. Gender influences cardiac function in the mdx model of Duchenne cardiomyopathy. Muscle Nerve 2010;42:600–3.

**59.** Bell RM, Mocanu MM, Yellon DM. Retrograde heart perfusion: the Langendorff technique of isolated heart perfusion. J Mol Cell Cardiol 2011;50:940–50.

**60.** Liao R, Podesser BK, Lim CC. The continuing evolution of the Langendorff and ejecting murine heart: new advances in cardiac phenotyping. Am J Physiol Heart Circ Physiol 2012;303:H156–67.

**61.** Kaspar RW, Allen HD, Ray WC, et al. Analysis of dystrophin deletion mutations predicts age of cardiomyopathy onset in becker muscular dystrophy. Circ Cardiovasc Genet 2009;2:544–51.

**62.** Feng J, Yan J, Buzin CH, Towbin JA, Sommer SS. Mutations in the dystrophin gene are associated with sporadic dilated cardiomyopathy. Mol Genet Metab 2002;77:119–26.

**63.** Ortiz-Lopez R, Li H, Su J, Goytia V, Towbin JA. Evidence for a dystrophin missense mutation as a cause of X-linked dilated cardiomyopathy. Circulation 1997;95:2434–40.

**64.** Singh SM, Bandi S, Shah DD, Armstrong G, Mallela KM. Missense mutation Lys18Asn in dystrophin that triggers X-linked dilated cardiomyopathy decreases protein stability, increases protein unfolding, and perturbs protein structure, but does not affect protein function. PLoS One 2014;9:e110439.

**65.** Lee TH, Eun LY, Choi JY, et al. Myocardial atrophy in children with mitochondrial disease and Duchenne muscular dystrophy. Korean J Pediatr 2014;57:232–9.

**66.** Matsuoka S, Ii K, Akita H, et al. Clinical features and cardiopulmonary function of patients with atrophic heart in Duchenne muscular dystrophy. Jpn Heart J 1987;28:687–94.

**67.** Konstam MA, Kramer DG, Patel AR, Maron MS, Udelson JE. Left ventricular remodeling in heart failure: current concepts in clinical significance and assessment. J Am Coll Cardiol Img 2011;4:98–108.

**68.** Silva MC, Meira ZM, Gurgel Giannetti J, et al. Myocardial delayed enhancement by magnetic resonance imaging in patients with muscular dystrophy. J Am Coll Cardiol 2007;49:1874–9.

**69.** Shirokova N, Niggli E. Cardiac phenotype of Duchenne muscular dystrophy: insights from cellular studies. J Mol Cell Cardiol 2013;58:217–24.

**70.** Nigro G, LComi LI, Politano L, Bain RJ. The incidence and evolution of cardiomyopathy in Duchenne muscular dystrophy. Int J Cardiol 1990;26:271–7.

**71.** Li Y, Zhang S, Zhang X, et al. Blunted cardiac beta-adrenergic response as an early indication of cardiac dysfunction in Duchenne muscular dystrophy. Cardiovasc Res 2014;103:60–71.

**72.** Barbin IC, Pereira JA, Bersan Rovere M, et al. Diaphragm degeneration and cardiac structure in mdx mouse: potential clinical implications for Duchenne muscular dystrophy. J Anat 2016;228:784–91.

**73.** Costas JM, Nye DJ, Henley JB, Plochocki JH. Voluntary exercise induces structural remodeling in the hearts of dystrophin-deficient mice. Muscle Nerve 2010;42:881–5.

**74.** Nakamura A, Yoshida K, Takeda S, Dohi N, Ikeda S. Progression of dystrophic features and activation of mitogen-activated protein kinases and calcineurin by physical exercise, in hearts of mdx mice. FEBS Lett 2002;520:18–24.

**KEY WORDS** cardiomyopathy, diastolic dysfunction, dystrophin, ribonucleotide reductase, recombinant adeno-associated virus vectors

**APPENDIX** For supplemental figures, please see the online version of this paper.

PLOS GENETICS

RESEARCH ARTICLE

# Microutrophin expression in dystrophic mice displays myofiber type differences in therapeutic effects

**Glen B. Banks**[1,2,3], **Jeffrey S. Chamberlain**[1,2,3,4], **Guy L. Odom**[1,2,3]*

**1** Department of Neurology, University of Washington, Seattle, Washington, United States of America, **2** Department of Medicine, University of Washington, Seattle, Washington, United States of America, **3** Wellstone Muscular Dystrophy Specialized Research Center, University of Washington, Seattle, Washington, United States of America, **4** Department of BioChemistry, University of Washington, Seattle, Washington, United States of America

* godom@uw.edu





**Citation:** Banks GB, Chamberlain JS, Odom GL (2020) Microutrophin expression in dystrophic mice displays myofiber type differences in therapeutic effects. PLoS Genet 16(11): e1009179. https://doi.org/10.1371/journal.pgen.1009179

**Editor:** Gregory A. Cox, The Jackson Laboratory, UNITED STATES

**Received:** July 1, 2020

**Accepted:** October 6, 2020

**Published:** November 11, 2020



**Data Availability Statement:** All relevant data are within the manuscript and its Supporting Information files.

**Funding:** GBB was supported by grants from the Muscular Dystrophy Association (MDA) and the American Heart Association. GLO was supported by a T32 National Research Service Award and by a grant from the muscular dystrophy association (MDA) USA. The studies were additionally supported by a NIH grant AR40864 (to JSC). AAV vectors were produced by the Viral Vector Core lab of the Seattle Wellstone Muscular Dystrophy

## Abstract

Gene therapy approaches for DMD using recombinant adeno-associated viral (rAAV) vectors to deliver miniaturized (or micro) dystrophin genes to striated muscles have shown significant progress. However, concerns remain about the potential for immune responses against dystrophin in some patients. Utrophin, a developmental paralogue of dystrophin, may provide a viable treatment option. Here we examine the functional capacity of an rAAV-mediated microutrophin (μUtrn) therapy in the *mdx*$^{4cv}$ mouse model of DMD. We found that rAAV-μUtrn led to improvement in dystrophic histopathology & mostly restored the architecture of the neuromuscular and myotendinous junctions. Physiological studies of tibialis anterior muscles indicated peak force maintenance, with partial improvement of specific force. A fundamental question for μUtrn therapeutics is not only can it replace critical functions of dystrophin, but whether full-length utrophin impacts the therapeutic efficacy of the smaller, highly expressed μUtrn. As such, we found that μUtrn significantly reduced the spacing of the costameric lattice relative to full-length utrophin. Further, immunostaining suggested the improvement in dystrophic pathophysiology was largely influenced by favored correction of fast 2b fibers. However, unlike μUtrn, μdystrophin (μDys) expression did not show this fiber type preference. Interestingly, μUtrn was better able to protect 2a and 2d fibers in *mdx*:utrn$^{-/-}$ mice than in *mdx*$^{4cv}$ mice where the endogenous full-length utrophin was most prevalent. Altogether, these data are consistent with the role of steric hindrance between full-length utrophin & μUtrn within the sarcolemma. Understanding the stoichiometry of this effect may be important for predicting clinical efficacy.

## Author summary

Duchenne muscular dystrophy (DMD) is a severe muscle wasting disorder caused by mutations in the dystrophin gene. Utrophin is structurally similar to dystrophin and can potentially be utilized to prevent muscle necrosis in preclinical models of DMD.

Specialized research Center (NIH grant P50 AR065139) (www.mda.org). The funders had no role in study design, data collection and analysis, decision to publish, or preparation of the manuscript.

**Competing interests:** The authors have declared that no competing interests exist.

Consequently, utrophin-mediated therapies are a primary target for treating DMD, particularly as it may circumvent immune responses to dystrophin-mediated therapies. One promising therapeutic option is to utilize recombinant adeno-associated viral vectors (rAAV) to deliver a rationally designed miniaturized utrophin (μUtrn) to striated muscles to prevent necrosis. Here, we found that rAAV-μUtrn can profoundly prevent skeletal muscle necrosis in the *mdx*$^{4cv}$ mouse model of DMD. μUtrn was also able to replace many functions of dystrophin at the neuromuscular synapse and myotendinous junctions. However, we provide several lines of *in vivo* evidence that steric hindrance between μUtrn and the endogenous full-length utrophin on the sarcolemma impacts the longevity of the therapy in a muscle fiber-type selective manner. Understanding the stoichiometry of this effect may be important for predicting clinical efficacy.

## Introduction

Duchenne muscular dystrophy (DMD) is a severe muscle wasting disorder caused by mutations in the dystrophin gene [1, 2]. Mechanically, dystrophin functions in muscle akin to a large molecular spring that connects the cytoskeleton via actin to the dystrophin-glycoprotein complex (DGC) within the sarcolemma [3–8]. As such, muscle membranes in DMD are highly susceptible to contraction-induced injury and hypoxic stress after mild exercise [9–17]. Furthermore, the neuromuscular junctions in the *mdx* mouse model of DMD fragment upon skeletal muscle necrosis, and have fewer and shallower postsynaptic folds than wild-type muscles [18–20]. The folding is also reduced at the myotendinous junctions, which is a prominent site for force transfer and injury in some DMD patients [21–26]. The dystrophin protein contains an N-terminal actin binding domain, a large central rod domain, a cysteine rich region critical for the association with β-dystroglycan[27], and a C-terminal domain [28, 29] (**Fig 1A**). The large central rod domain includes 24 spectrin-like repeats that interact with the membrane [30], F-actin [31], localize nNOS to the sarcolemma [32, 33], and guide peripheral microtubules [34]. The central rod domain also includes 4 hinge regions that contain high concentrations of proline residues [8]. As an X-linked disorder, DMD is potentially amenable to

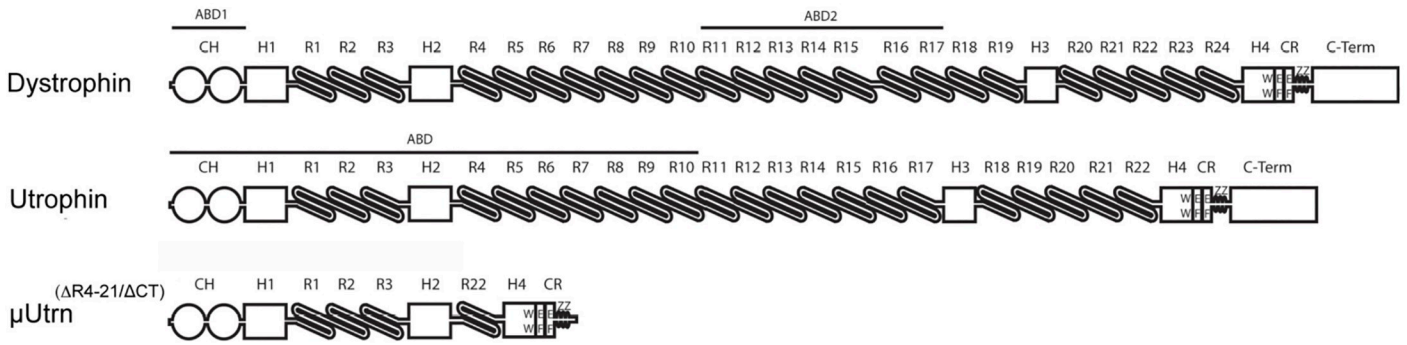


**Fig 1. Domain structure of dystrophin, utrophin and μUtrn.** Shown is an illustration depicting the major functional domains of full-length, (427 kDa) dystrophin, (400 kDa) utrophin, and (130 kDa) microutrophin (μUtrn). Dystrophin contains two actin-binding domains [ABD1, which has 2 calponin-homology domains (CH), and ABD2), while the single ABD of utrophin is continuous through spectrin-like repeat 10. The central rod domain of dystrophin is composed of 24 spectrin-like triple-helical elements or repeats (R) while utrophin contains 22 repeats, both proteins carry 4 hinge (H) domains. Toward the carboxy-terminus a WW domain within hinge 4 together with a cysteine rich (CR) domain composed of 2 EF-hands, and a Zinc finger domain (ZZ), form a binding domain for beta-dystroglycan. The Carboxyl-terminal domain (C-term) provides binding sites for the syntrophins and dystrobrevins. Micro-utrophin lacks repeats 4–22 as well as the CT domain (Odom, 2010).

https://doi.org/10.1371/journal.pgen.1009179.g001

dystrophin replacement gene therapies [35, 36]. In fact, rational design of miniaturized dystrophins for gene therapy using rAAV has proven affective at mitigating the dystrophic pathophysiology in various mammalian models of DMD [29, 32, 37–41]. Clinical trials that utilize different forms of μDys have reported varied success at an early stage of treatment, but none are anticipated to fully restore normal muscle function[42]. One concern regarding DMD clinical therapeutic development is the possibility that dystrophin may be recognized by the immune system as a neo-antigen in some DMD patients [43–46]. As such, we are also interested in the therapeutic capacity of the dystrophin paralogue, utrophin [44, 47].

Utrophin is structurally similar to dystrophin in that it contains an N-terminal actin-binding domain, a large central rod domain containing 22 spectrin-like repeats with 4 hinges, a cysteine rich region and a C-terminal domain [28] (Fig 1). Despite the structural similarities, utrophin differs from dystrophin in a variety ways, such as having a single actin-binding domain that extends from the N-terminus through to spectrin-like repeat 10; in contrast dystrophin has a secondary actin binding domain (ABD2, Fig 1) [48]. Interestingly, utrophin also displays differing molecular contact responses to actin relative to dystrophin, affecting rotational dynamics, resulting in increased actin resilience [48, 49]. Indeed, it has been hypothesized that one continuous actin binding site may display less elasticity toward contractile responses via the actin-utrophin-sarcolemma linkage to muscle stretches relative to dystrophin[50]. Whether this could be exacerbated *in vivo* considering the structure of micro-utrophin$^{(\Delta R4\text{-}R21/\Delta CT)}$ (μUtrn), having a continuous ABD that constitutes for ~65% of the entire micro-protein, is not known. To this end, it has also been found that μUtrn is as effective *in vitro* at regulating actin dynamics as full-length dystrophin as determined by time-resolved phosphorescence anisotropy[51]. A further contrast from dystrophin in the central rod domain has been demonstrated downstream of the dystrophin ABD2, where utrophin lacks the binding domains associated with nNOS restoration to the sarcolemma or the ability to guide microtubules[34, 52]. Despite these differences, transgenic expression of full-length utrophin can prevent muscle necrosis in sedentary *mdx* mice, thus making it a promising candidate for treating DMD patients, independent of the type or placement of the dystrophin mutation [44, 53]. The μUtrn construct contains essential functional elements of the native utrophin, namely N-terminal actin-binding domain, four spectrin-like triple helices of the central rod domain (R1-R3 + R22), two hinges (H2 & H4), and the CR domain enabling binding to beta-dystroglycan[27](i.e. ΔR4-R21/ΔCT), enabling DGC assembly for localization at the sarcolemma [7, 9, 54–56]. Indeed, repeat administration of TAT-μUtrn has been shown to mitigate the pathophysiology of *mdx* and *mdx*:*utrn*$^{-/-}$ double knockout (*dko*) mice [57, 58]. Similarly, rAAV-mediated delivery of uUtrn prolongs the lifespan and mitigates the skeletal muscle dystrophic pathophysiology of *dko* mice [47] and in the canine model of DMD[46]. Although μUtrn therapy for *dko* mice clearly provided a benefit with improvement and stabilization of the histopathology with improved functional capacity, and lifespan extension; animals were not "cured" per se as a result of the treatment. Importantly, in a recent study utilizing rAAV9-mediated μUtrn delivery to severely affected *D2/mdx* mice, a demonstrated benefit of the cardiac phenotype was reported using cine-MRI for indices such as stroke volume and ejection fraction, providing the first evidence of a functional cardiac benefit with μUtrn upregulation [59].

A potential compounding issue with a μUtrn therapeutic for DMD is whether endogenous utrophin could influence the expression, localization, and inherent functional capacity of μUtrn, with utrophin being generally present at low levels on the sarcolemma and also highly concentrated within the neuromuscular and myotendinous junctions [60–62]. The design of μUtrn was based on the first generation μDys$^{(\Delta R4\text{-}R23/\Delta CT)}$ capable of being packaged within AAV, where the μDys cDNA contained the N-terminal actin binding domain, a small

central rod domain containing hinges 1, 2, and 4, with four spectrin-like repeats, and the cysteine rich region [47, 63] (Fig 1A). Of note, μUtrn also includes a conserved polyproline site within hinge 2, that when present in μDys$^{(\Delta R4\text{-}R23/\Delta CT)}$, led to myotendinous strain injury, ringed myofiber formation, fragmentation of the neuromuscular synapses, and elongation of the synaptic folds in a subset of muscles in *mdx* mice [19, 26, 39]. Similar deleterious effects might be caused by the inclusion of hinge 2 in μUtrn. Therefore, in addition to histopathological and physiological assessment, this study was further aimed at evaluating neuromuscular and myotendinous junctions in *mdx*$^{4cv}$ mice treated with AAV-mediated delivery of μUtrn.

## Results

Fig 1 shows the domain structure of the μUtrn$^{(\Delta R4\text{-}R21/\Delta CT)}$ protein used in this study as well as the structures of full-length dystrophin and utrophin [63]. The 1,160 residue, 130 kDa μUtrn has an analogous structure to a highly functional first-generation μDys$^{(\Delta R4\text{-}R23/\Delta CT)}$ we described previously [47, 63], currently being tested in phase 1/2 clinical trials (NCT03375164). Both micro-proteins carry 4 spectrin-like repeats in the central rod domain, but contain the entire N-terminal actin-binding and the cysteine-rich (CR) dystroglycan-binding domains, enabling essential binding to F-actin, beta-dystroglycan, and assembly of the dystrophin-glycoprotein complex (DGC) at the sarcolemma (except for nNOS) [7, 9, 52, 54–56, 64]. The μUtrn protein also lacks the C-terminal (CT) domain, which can be deleted from utrophin or dystrophin with minimal impact on function [47, 63, 65]. The absence of the CT domain also enables endogenous Utrn to be distinguished from μUtrn using antibodies that recognize the CT domain. Both proteins are detected with antibodies against the N-terminal domain of Utrophin A. In some studies we added a N-terminal flag epitope for exclusive detection of μUtrn. Expression vectors for μUtrn were prepared in rAAV6 as previously described [37, 47, 66].

### Histopathlogy of mdx$^{4cv}$ muscles treated with μUtrn

Utrophin is expressed in new and maturing skeletal muscles during embryonic development in humans, and in mice this extends to ~2-weeks postnatal. As the muscle matures, utrophin expression is reduced and is ultimately replaced by dystrophin on the sarcolemma of normal muscles, but remains concentrated at the neuromuscular and myotendinous junctions. In the absence of dystrophin in DMD, utrophin appears to maintain this cadence where the expression is reduced as the muscle matures. However, without dystrophin expression to replace utrophin, the muscles become highly susceptible to contraction-induced injury. Muscle necrosis and the resulting inflammatory response activates resident satellite cells to regenerate myofibers leading to the re-establishment of utrophin at the sarcolemma of the maturing fibers. This cycle of utrophin expression continues for as long as the satellite cells are capable of replacing the lost muscle and leads to a patchwork of utrophin expression in the *mdx* muscles that are reflective of the stage of regeneration and maturation (Fig 2A). It is well known that slower muscle fiber types have higher levels of residual utrophin on the sarcolemma in DMD and are more resistant to the dystrophic pathophysiology[67–69]. To examine the effects of expressing human μUtrn in dystrophic mice, rAAV6-CMV-μUtrn ($2x10^{10}$ vector genomes (vg) was injected into the right gastrocnemius and tibialis anterior (TA) muscles of 1 week old *mdx*$^{4cv}$ mice, with the sham-injected contralateral muscles as controls. At 3 months post-injection the tissues were harvested, and adjacent cryosections were immunostained with N-terminal utrophin antibodies to detect both μUtrn and endogenous full-length utrophin (FL-Utrn), and with C-terminal utrophin antibodies to exclusively detect FL-Utrn. Sections were also

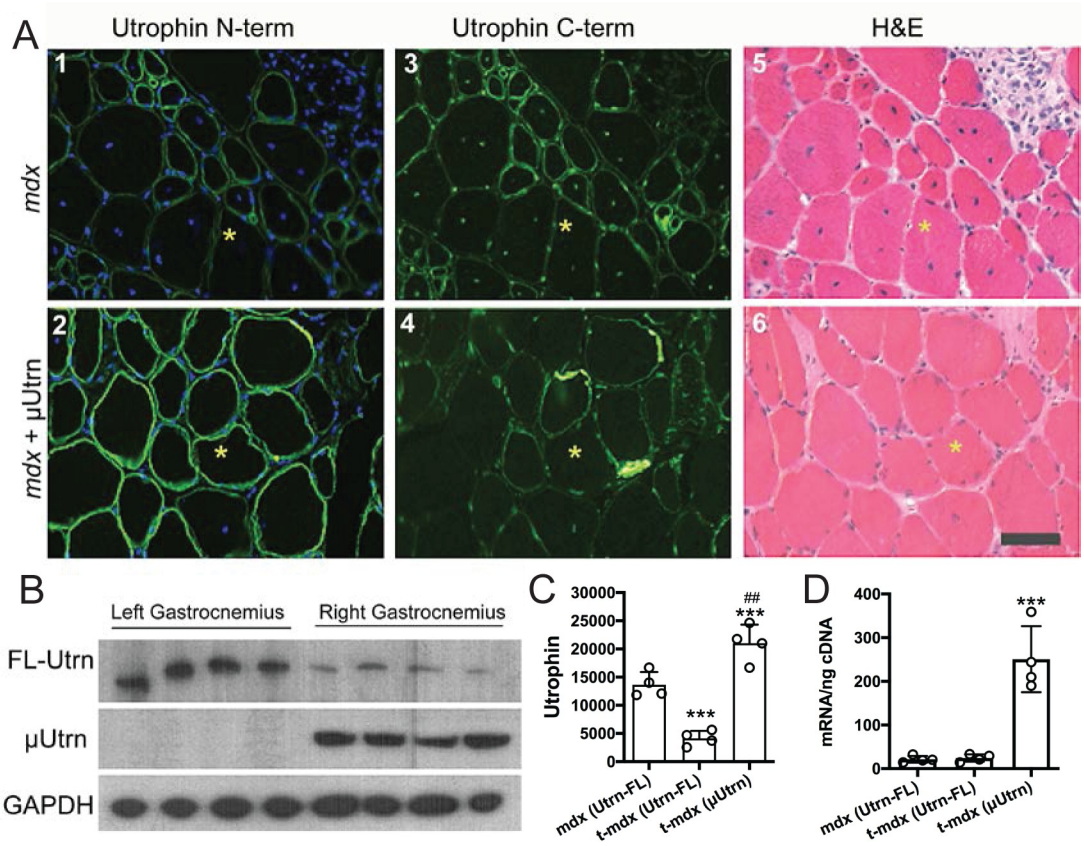


**Fig 2. µUtrn expression mitigates dystrophic pathology.** (A.) Adjacent sections of *mdx*$^{4cv}$ muscles and *mdx*$^{4cv}$ muscles directly injected with rAAV6-CK8-µUtrn. Scale bar = 50 µm. (B.) Western blot showing full length utrophin and µUtrn in untreated (left) and treated (right) gastrocnemius muscles (n = 4). GAPDH is the loading control. (C.) Quantitation of utrophin signal intensity from the Western blots. $^{***}P < 0.001$ compared to utrophin full-length in the treated muscles. (D.) Quantitation of full length utrophin and micro-utrophin mRNA by qRT-PCR. $^{***}P < 0.001$ compared to utrophin full-length in treated and untreated muscles.

https://doi.org/10.1371/journal.pgen.1009179.g002

stained with hematoxylin and eosin to detect inflammatory pathology and centrally-nucleated myofibers, a hallmark of muscle regeneration (Fig 2A, panels 5, 6; S1 Fig).

Consistent with previous studies [70], upregulated FL-Utrn was detectable in most myofibers within the dystrophic environment of untreated *mdx*$^{4cv}$ mouse gastrocnemius muscles (Fig 2A, panels 1, 3). Approximately 76% of the myofibers in untreated *mdx*$^{4cv}$ gastrocnemius muscles exhibited central nuclei (a marker of muscle regeneration, S1A Fig) and extensive areas of mononuclear cell infiltrates (Fig 2A, panel 5). Intense N-terminal immunostaining of Utrn was observed in the rAAV6-CMV-µUtrn-treated gastrocnemius muscles. Only ~3% of the Utrn-positive myofibers in treated muscles displayed centrally-located nuclei (S1 Fig). Importantly, the muscle fibers expressing uUtrn also contained low levels of FL-Utrn as demonstrated by the antibody that recognizes the C-terminus of FL-Utrn and is absent in the uUtrn.

µUtrn-treated gastrocnemius muscles also displayed an improved morphological appearance and significantly fewer regenerating myofibers, as assessed by immunostaining for "developmental" (embryonic or neonatal) myosin heavy chain (18% positive myofibers compared with 67% for controls; (Fig 2A, panels 5 and 6; S1 Fig). This reduction in myofiber

regeneration presumably accounts for the reduced full-length (FL) utrophin expression observed by both western analysis and immunostaining (Fig 2B and 2C), as regenerating myofibers have been shown to express elevated utrophin levels [71]. In contrast to the reduction in protein levels in treated mice, we found no difference in FL-Utrn mRNA levels between treated and untreated *mdx*$^{4cv}$ gastrocnemius muscles (Fig 2D). As anticipated, the mRNA levels of CMV-driven μUtrn were found to be much higher than the full-length transcripts in treated muscles ($P < 0.001$; Fig 2D). Expression of μUtrn in *mdx*$^{4cv}$ gastrocnemius muscles is thus sufficient to substantially ameliorate the dystrophic pathology.

## Physiological performance of mdx$^{4cv}$ muscles treated with μUtrn

To assess the functional capacity of μUtrn to ameliorate physiological deficits in *mdx*$^{4cv}$ muscles, we analyzed contractile properties of the treated TA muscles *in situ*, followed by assessment of morphology and utrophin expression.

We examined several physiological parameters known to be altered in *mdx*$^{4cv}$ TA muscles: *(1) Muscle Mass*: As previously reported muscle mass increases significantly in *mdx* mice and this is thought to be partially responsible for maintaining peak force production of *mdx* muscles [72, 73]. We confirmed the mass increase of *mdx*$^{4cv}$ TA muscles, and found that μUtrn expression partially reduced this increase (Fig 3A). *(2) Peak Force Production*: The increased muscle mass maintains peak force production in *mdx*$^{4cv}$ mice at this age, and was also unchanged in limbs treated with uUtrn. (Fig 3B). *(3) Specific Force Production*: This parameter is typically reduced in *mdx* muscles [37, 73], and we found it to be reduced by about 35% in *mdx*$^{4cv}$ TA muscles; μUtrn-treatment restored about 60% of this deficit ($P<0.05$; Fig 3C). *(4) Susceptibility to Eccentric Contraction-Induced Injury*: Since *mdx*$^{4cv}$ muscles are known to be susceptible to contraction-induced injury [37, 73], we used an *in situ* strain protocol to determine whether μUtrn treatment would ameliorate this damage. When subjected to increased strain, peak tetanic force production of *mdx*$^{4cv}$ TA muscles decreased significantly compared to the smaller decrease in wild type TAs. In contrast, μUtrn-treated dystrophic muscles exhibited significant protection against this perturbation (Fig 3D), albeit to a degree notably less than in wild type muscles or in previous studies with micro-dystrophin ([26], & S3 Fig).

Immunostained cryosections of TA muscles at 3 months post-injection revealed that ~60% of the total myofibers were μUtrn-positive, based on their much more intense N-terminal Utrn immunostaining (see Fig 2A, panel #2 vs. #1). The physiological data we measured thus represents the combined attributes of about 40% of the total fibers that contain little to no μUtrn (but variable levels of endogenous utrophin), and about 60% of the total fibers that contain variable μUtrn levels due to differences in fiber-to-fiber transduction.

## Myofiber type differences in μUtrn expression

A fundamental question of this study is whether expression of full-length utrophin functions synergistically with the highly truncated uUtrn or whether there is a potential for steric hindrance. Considering full-length utrophin is expressed at higher levels in type 1a, 2a and 2d fibers when compared to type 2b fiber types we examined whether there is a fiber-type expression pattern of μUtrn in treated muscles. μUtrn was more favorably expressed in the fast 2b fiber types (79% μUtrn-positive) when compared with Ia (25% positive), 2a (38% positive) and 2d (43% positive) fibers at 3 months post-injection (Fig 4A–4C). Interestingly, μUtrn-positive myofibers displayed a further increase in cross-sectional area beyond that observed in *mdx*$^{4cv}$ TA muscle, regardless of fiber type (Fig 4D).

To explore whether the μUtrn fiber-type expression differences may have resulted from properties of the CMV promoter/enhancer elements, we tested a vector carrying the muscle-

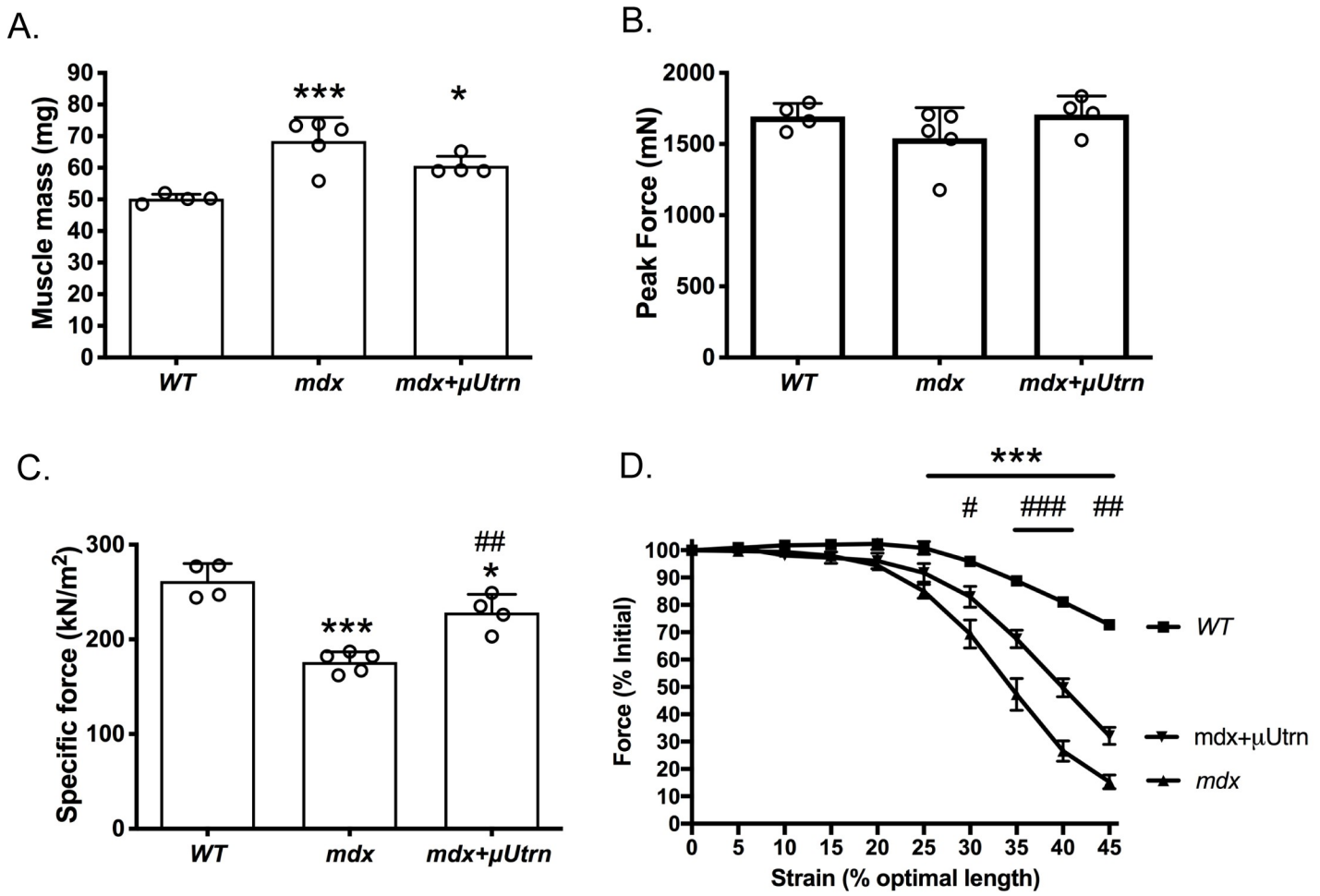


**Fig 3. *In situ* physiological assessment of tibialis anterior muscles following vector treatment.** (A.) Mean +/- S.D. tibialis anterior muscle mass. (B.) Mean +/- S.D. peak tetanic force production. (C.) Mean +/- S.D. specific force production. (D.) Peak tetanic force production after increasing strain. $^{*}P < 0.05$ and $^{***}P < 0.001$ compared to wild-type. $^{\#}P < 0.05$, $^{\#\#}P < 0.01$ and $^{\#\#\#}P < 0.001$ compared to $mdx^{4cv}$.

https://doi.org/10.1371/journal.pgen.1009179.g003

specific regulatory cassette CK8e (kindly provided by Dr. Stephen D. Hauschka). Initially, 2 week-old $mdx^{4cv}$ mice were intravenously (IV) infused with $2x10^{14}$ vg/kg of rAAV6-CK8e-Flag-μUtrn and muscles were examined 2 weeks post-injection (at 1-month of age). This experimental design focused on early stages of transgene expression, and the onset of $mdx^{4cv}$ mouse muscle pathology [74]. As revealed by immunostaining against the N-terminal FLAG epitope, μUtrn was found on the sarcolemma of approximately 88% of all muscle fiber types (S2A–S2C Fig; gastrocnemius muscle shown). This finding suggested that rAAV6-CK8e driven expression of μUtrn has a similar tropism for all four myofiber types. A second cohort of mice intravenously infused with rAAV6-CK8e-Flag-μUtrn was examined at a later time point (3 months of age). If uUtrn is not protecting the skeletal muscle, the muscle fibers deteriorate and regenerate leading to loss of the therapeutic cDNA and newly formed uUtrn negative myofibers. Similar to the earlier study with IM injection of rAAV6-CMV-μUtrn, we found that with IV delivery, μUtrn was expressed within a significantly greater number of type 2b myofibers compared with type 1, 2a and 2d fibers ($P < 0.001$; S2D–S2F Fig). Thus, the preferential expression of μUtrn in the fast 2b fibers at later time points was similar whether the CK8e (S2D–S2F Fig) or the CMV (S2G–S2I Fig) regulatory cassettes were used. Importantly,

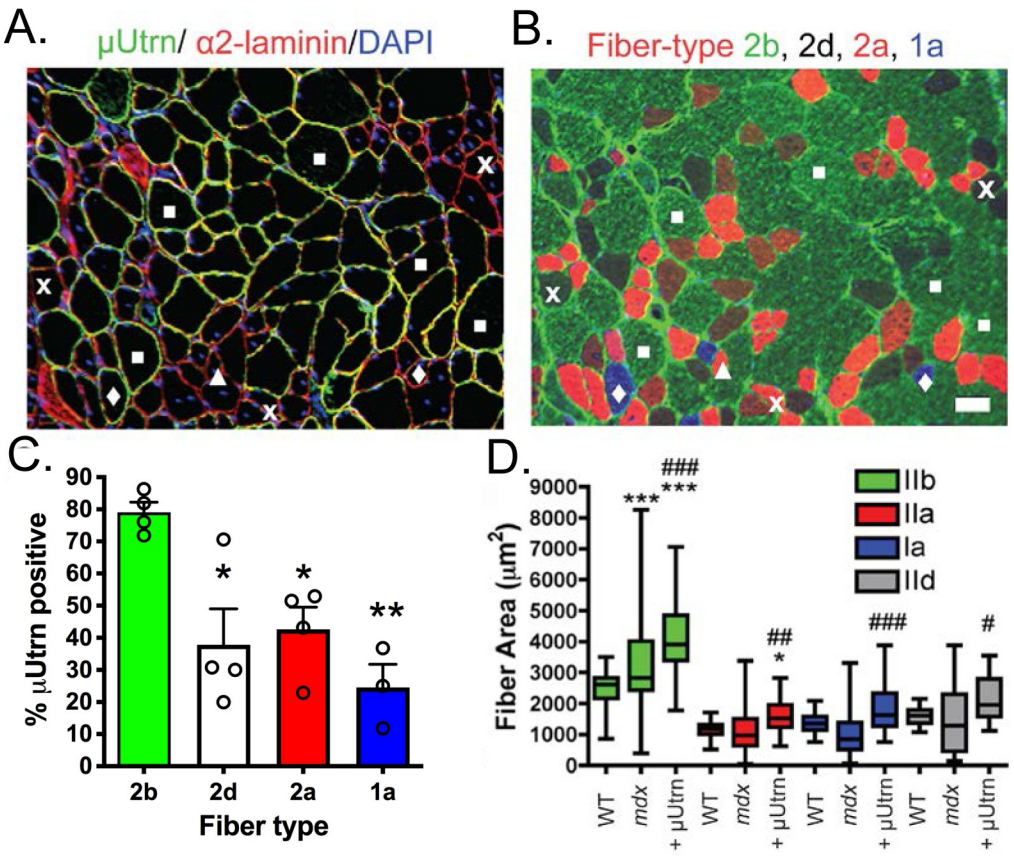


**Fig 4. μUtrn expression mitigates dystrophic pathology and demonstrates fiber-type preferences in gastrocnemius muscles.** (A) Immunostaining for utrophin A indicating high level expression of (green), laminin A (red), and nuclei (blue). (B) Adjacent sections of μUtrn treated *mdx*$^{4cv}$ muscles with corresponding fiber typing. Symbols provide examples of 1a, 2a and 2d/x fibers expressing high levels of μUtrn. The white squares, "x's", triangles, and diamonds indicate type 2b, 2d/x, 2a, 1a fibers respectively. Scale bar = 50 μm. (C.) Quantification of the proportion of fiber types expressing μUtrn (Mean +/- S.D.). (D.) Myofiber area as indicated by fiber type. Box and whiskers plots displaying median +/- 75% fiber area in wild-type, *mdx*$^{4cv}$ and *mdx*$^{4cv}$ treated skeletal muscles. μUtrn expression leads to myofiber hypertrophy in all muscle fiber types. Bars show the mean +/- S.D., (N = 4). $^{*}P < 0.05$ and $^{**}P < 0.01$ relative to wt $^{\#}P < 0.05$, $^{\#\#}P < 0.01$, $^{\#\#\#}P < 0.001$ relative to untreated *mdx*$^{4cv}$.

https://doi.org/10.1371/journal.pgen.1009179.g004

the number of myofibers expressing μUtrn at 3 months of age was significantly reduced from the earlier time points demonstrating the uUtrn was less able to protect type 1a, 2a and 2d fibers from dystrophy when compared to the type 2b fibers (S2D–S2F Fig).

As a further control, *mdx*$^{4cv}$ mice were intravenously injected with rAAV6-CK8e-μDys and analyzed 8 months later. In contrast with the μUtrn studies, expression of μDys was maintained in the vast majority of myofiber types even at 8 months, leading to a significant functional improvement of the muscles (S3 Fig). We also note that our original hinge2-μDys[75, 76] displayed stable expression for up to one year in DMD patients[77], and that a different μDys vector, rAAV6-CK8e-μDys5, showed stable expression in all striated muscles for more than 27 months in *mdx*$^{4cv}$ mice [78].

Considering uUtrn co-exists on the sarcolemma with the full-length utrophin and that full-length utrophin is found at higher levels in type Ia, 2a, and 2d fibers (Fig 5 for example, and [71]) that are less protected by uUtrn, these results raised the possibility that endogenous utrophin expression could adversely impact the therapeutic potential of μUtrn. To evaluate μUtrn expression in the absence of endogenous utrophin we examined the gastrocnemius muscles of

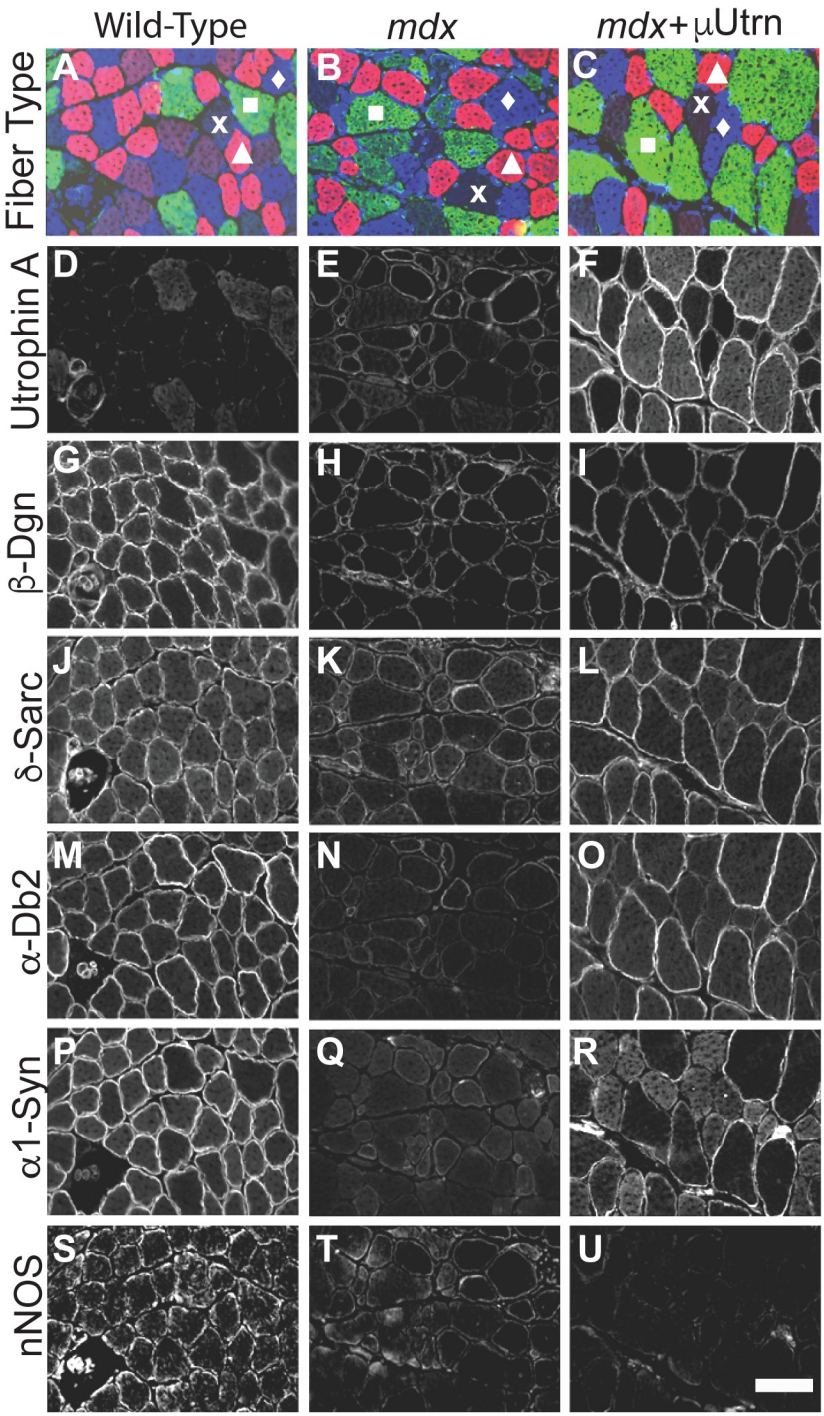


**Fig 5. Restoration of DGC components α-dystrobrevin-2 and $\alpha_1$-syntrophin localization to the dystrophin-glycoprotein complex by μUtrn expression is fiber type selective.** Scale bar = 100 μm.

https://doi.org/10.1371/journal.pgen.1009179.g005

*mdx*:*utrn*$^{-/-}$ (*dko*) mice from a previous study [47]. These mice had received an intravenous injection of 2.5x10$^{14}$ vg/kg of rAAV6-CMV-μUtrn, at 3 weeks of age and were analyzed at 4 months of age. We found no preference toward μUtrn expression in the fast 2b fibers when compared with the 2a or 2d fiber types (S2J–S2L Fig). The status of type 1a fibers in this study

is uncertain because there were very few type 1a myofibers in the *dko* gastrocnemius and only ~6% of these had detectable μUtrn (S2J–S2L Fig).

## μUtrn expression in mdx$^{4cv}$ muscle fibers affects costamere structure

Costameres are rib-like sarcolemmal structures juxtaposed over the Z and M lines of myofibers, and are the primary sites where cytoskeletal proteins link elements of the contractile apparatus to integral and peripheral membrane protein complexes [79, 80]. Costameres can also be oriented parallel to the myofiber longitudinal axis, resulting in a rectilinear structural lattice. Historically, dystrophin represents the first costameric protein found to be associated with muscular dystrophy, displaying periodic association with costameres running transversal to the long axis of the myofiber [79, 81]. Interestingly, in *mdx* myofibers, the up-regulated FL-Utrn only partially compensates for the absence of dystrophin, leading to a weakened linkage between the contractile apparatus and the sarcolemma [79, 82–84]. To examine the effects of μUtrn on *mdx$^{4cv}$* costameres, gastrocnemius muscles were removed from 3-month old FLAG-μUtrn-treated and control *mdx$^{4cv}$* mice and cryosections were immunostained for endogenous utrophin A (using a utrophin C-terminal antibody), or for μUtrn (using a FLAG antibody). In longitudinal cryosections endogenous utrophin A was found within a standard ~2.2 μm costameric lattice, as well as between the costameric striations (S4A Fig, panel #1) in both untreated and μUtrn treated *mdx$^{4cv}$* mice (S4A Fig, panel #3 *vs*_panel #6). We next examined the location of FLAG-μUtrn and found that it localized in a costameric pattern with striations that were only ~0.8 μm apart (S4B and S4C Fig ($P < 0.001$)). However, μUtrn localizes in normal, 2.2 μm striations in the absence of full-length Utrn, as seen in treated *mdx:utrn$^{-/-}$* muscles (S4D Fig). Thus, high-level expression of FLAG-μUtrn in *mdx$^{4cv}$* mice leads to the localization of μUtrn in closely spaced striations that co-exist with the normal, FL-Utrn containing costameres.

## Assembly of the dystrophin-glycoprotein complex following μUtrn treatment

Expression of μDys has been shown to restore assembly and sarcolemmal localization of the dystrophin-glycoprotein complex (DGC) [9, 32, 85–87], so we asked whether μUtrn expression also restores DGC components in *mdx$^{4cv}$* muscles. This was tested utilizing the same mice described for the rAAV6-CMV-μUtrn IM injection study from Fig 2. Serial cryosections from injected gastrocnemius muscles were immunostained to detect myosin heavy chain isoforms associated with different muscle fiber types (Fig 5A–5C), utrophin (Fig 5D–5F), and the representative DGC components β-dystroglycan (β-Dgn) (Fig 5G–5I), δ-sarcoglycan (δ-Sarc) (Fig 5J–5L), α-dystrobrevin-2 (α-Db2) (Fig 5M–5O), α-1-syntrophin (α1-Syn) (Fig 5P–5R) and neuronal nitric oxide synthase (nNOS) (Fig 5S–5U).

As expected, endogenous FL-Utrn was only expressed at low levels in wild-type muscles (Fig 5D), but was up-regulated in *mdx$^{4cv}$* muscle fibers (Fig 5E)[88–91]. However, the relative sarcolemmal intensity of endogenous utrophin A immunostaining was highly variable between and within different fiber types (e.g., Fig 5B and 5E). In contrast, numerous myofibers within rAAV6-CMV-μUtrn IM injected *mdx$^{4cv}$* muscles exhibited intense utrophin immunostaining, with type 2b fibers displaying the highest relative intensities (e.g., Fig 5F). The DGC components, β-Dgn, δ-Sarc were broadly restored in myofiber types (Fig 5, 5I vs. 5H, and 5L vs. 5K), while α-Dbn-2, and α1-Syn were most strongly re-localized in 2b fibers (Fig 5, 5O vs. 5N, and 5R vs. 5Q), which displayed the highest expression of μUtrn. In contrast, nNOS remained relatively absent from the sarcolemma (Fig 4U vs 4S), even though α1-Syn, a DGC component with which nNOS and endogenous utrophin are known to interact [92, 93], was re-localized to the sarcolemma. This observation has been confirmed in previous work where

it was shown that the α-Syn binding motif within dystrophin spectrin-like repeat-17 enables recruitment of nNOS to the sarcolemma[32, 33, 52]. These results show that μUtrn, like utrophin A, does not localize nNOS to the sarcolemma [87]. The ability of μUtrn to localize α1-Syn is presumably due to additional components of the DGC, such as α-Db isoforms that are known to interact with α1-Syn, and potentially the sarcoglycans [94]. These results thus indicate that delivery of AAV6-CMV-μUtrn to *mdx*$^{4cv}$ mouse muscles localizes most, but not all, dystrophin glycoprotein-complex proteins to the sarcolemma.

## Influence of μUtrn on the structure of neuromuscular junctions

The acetylcholine receptor (AChR) clusters on the postsynaptic membranes of neuromuscular junctions (NMJs) in wild-type mice mature into pretzel-like profiles that exhibit generally continuous junctions (defined here as a NMJ that has three or less continuous segments) when viewed *en face* (Fig 6A, panel 1). These profiles are known to further fragment upon skeletal muscle necrosis in *mdx*$^{4cv}$ and *mdx*:*utrn*$^{-/-}$ mice [18–20, 74]. We found that μUtrn expression in gastrocnemius muscles of *mdx*$^{4cv}$ and *mdx*:*utrn*$^{-/-}$ mice prevented the formation of fragmented synapses (Fig 6A, panel #3 vs #2, and panel #5 vs #4). Importantly, the overall continuity of junctional membranes was significantly improved in μUtrn-treated muscles (Fig 6B). We also examined electron micrographs of NMJs in these mice and found, as in normal muscle fibers, that the presynaptic motor nerve terminal directly abuts the postsynaptic apparatus and that the presynaptic terminal contains folds [black arrow head, (wt) vs black arrow, (mdx +μUtrn)] that invaginate into the muscle (Fig 6A, compare panel #'s 6–10).

In wild type muscles utrophin is primarily restricted to the crests of folds whereas dystrophin is found in the troughs of folds [95, 96]. Utrophin is also restricted to the crests of folds in NMJs of *mdx* skeletal muscles (S5 Fig, panel #5). We found that the NMJs in *mdx*$^{4cv}$ postsynaptic membranes have a small, but significant reduction in the length and number of folds (Fig 6C & 6D), and that μUtrn is mis-localized to the troughs of the synaptic folds in treated *mdx*$^{4cv}$ muscles (S5 Fig, panel #6). μUtrn delivery restored the length of synaptic folds in *mdx*$^{4cv}$ muscles to depths similar to those in wild-type muscles (Fig 6A, panels #6–8, and 6C). Interestingly however, while μUtrn did not restore the number of post-synaptic folds in *mdx*$^{4cv}$ mice (Fig 6D), the folds in μUtrn-treated mice became highly branched (Fig 6A, panel #8). Expression of μUtrn did restore the number of folds in the NMJs of *mdx*:*utrn*$^{-/-}$ muscles to the levels found in *mdx*$^{4cv}$ muscles (Fig 6A panels #5 & 10, 6D).

## Influence of μUtrn on the structure of myotendinous junctions

Treatment of *mdx*$^{4cv}$ mice with a first-generation μDys$^{(\Delta R4\text{-}R23/\Delta CT)}$ leads to myotendinous strain injury and "ringbinden" or ringed fiber formation in gastrocnemius muscles [19, 26, 39]. This is associated with the presence of a polyproline motif within the 'Hinge-2' domain of this particular μDys [19, 26, 39]. We therefore asked whether expression of the analogous μUtrn would lead to similar deleterious effects (Fig 7). Electron micrographic analysis of transverse gastrocnemius muscle sections from untreated wt, *mdx*$^{4cv}$, *mdx*:*utrn*$^{-/-}$, as well as in *mdx*$^{4cv}$ or *mdx*:*utrn*$^{-/-}$ mice treated with μUtrn revealed no ringed fibers in any of the muscles (Fig 7A, panels #3 and #5). Thus, the polyproline motif from utrophin hinge 2 does not adversely affect muscle ultrastructure.

To assess the presence of endogenous utrophin and μUtrn within MTJs we immunostained cryosections with a C-terminal antibody (to detect endogenous utrophin) and with the FLAG antibody (to detect FLAG-μUtrn). Both types of utrophin colocalized within folds in the Achilles myotendinous junctions [S6 Fig, where each panel shows the myofiber(s) integrated into the tendon at the base of the image(s)]. Since the folds in MTJs play critical roles in reducing

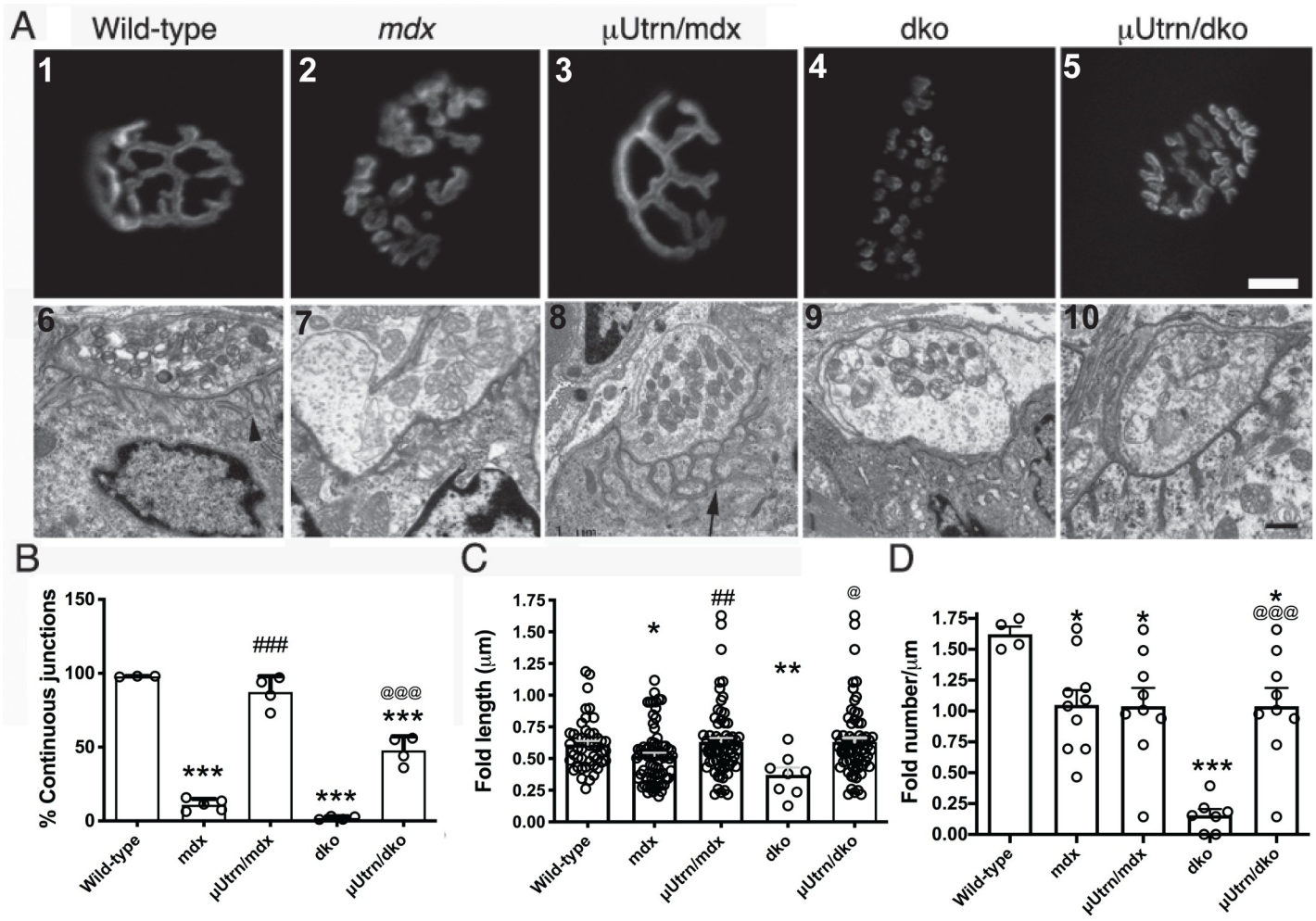


**Fig 6. µUtrn expression partially restores the structure of neuromuscular junctions.** (A) Top panel: AChR cluster visualization in the postsynaptic apparatus reveals that µUtrn expression prevents the fragmentation of synapses seen in *mdx*$^{4cv}$ and *dko* muscles. Scale bar = 10 µm. Lower panel: Electron microscopic images of neuromuscular synapses reveals that the synaptic folds in wild-type mice (arrow head) are shallower and less in number in muscles from *mdx*$^{4cv}$ mice and dko mice. µUtrn restores the depth, but not the number of synaptic folds. However, the synaptic folds are highly branched in the *mdx*$^{4cv}$ mice treated with rAAV-µUtrn. Scale bar = 0.5 µm. (B) Mean +/- S.D. of continuous synapses. (C) Mean +/- S.D. of fold lengths in the postsynaptic apparatus. (D) Mean +/- S.D. of the number of postsynaptic folds/µm. $^{*}P < 0.05$, $^{**}P < 0.001$, and $^{***}P < 0.001$ compared to wild-type. $^{\#\#}P < 0.01$ and $^{\#\#\#}P < 0.001$ compared to *mdx*$^{4cv}$. $^{@}P < 0.05$ and $^{@@@}P < 0.001$ compared to dko.

https://doi.org/10.1371/journal.pgen.1009179.g006

membrane shear stress during muscle contraction [22], we also analyzed electron micrograph sections to determine the lengths of the MTJ folds. The MTJ folds were shorter in muscles from *mdx*$^{4cv}$ mice than in wild type controls, as indicated by the white arrows (Fig 7A; compare panel #6 vs #7, and Fig 7B). However, the folds were also more numerous than in controls (Fig 7C), resulting in a reduction in the total length of membrane provided by the junctional folds when compared to wild-type muscles (Fig 7D). µUtrn treatment partially restored the MTJ fold length and number in *mdx*$^{4cv}$ muscles (Fig 7B and 7C); thereby essentially restoring the total length of membrane provided by the folds (Fig 7D).

## Discussion

Here we demonstrate that µUtrn improves the dystrophic pathophysiology of *mdx*$^{4cv}$ muscles, as well as the maturation and maintenance of the neuromuscular and myotendinous junctions.

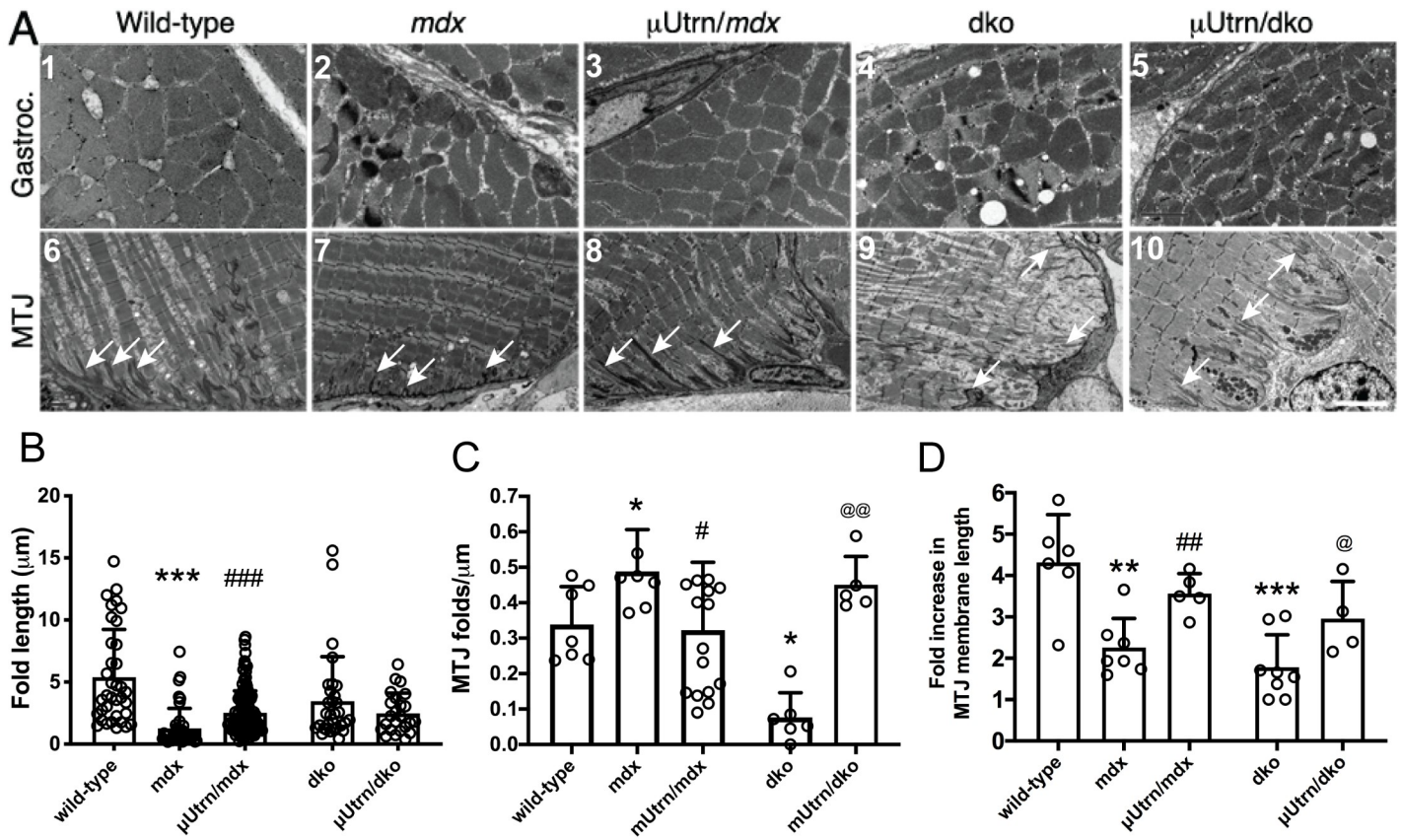


**Fig 7. µUtrn expression partially restores the structure of myotendinous junctions without leading to ringed fiber formation.** (A) Top panel: Electron microscopy of transverse sections of gastrocnemius muscles. Scale bar = 2 µm. Lower panel: Longitudinal sections of Achilles myotendinous junctions. Note the loss of folds in *mdx*$^{4cv}$ and *dko* mice is partially restored by µUtrn expression. Scale bar = 5 µm. (B) Mean +/- S.D. length of folds. (C) Mean +/- S.D. fold per µm of MTJ. (D) Mean +/- S.D. increase in membrane length brought about by the MTJ folds.

https://doi.org/10.1371/journal.pgen.1009179.g007

Histologically, following µUtrn treatment there was an abrupt reduction in the number of myofibers undergoing regeneration as indicated by central nucleation. We also observed the restoration of DGC components β–Dgn and δ-Sgn, however the localization of α-Db2 and α1-Syn was skewed toward fast 2b fiber expression. Indeed, at longer time-points within our study the improvement in pathophysiology appears to primarily stem from the stable expression of µUtrn within fast 2b fibers rather than the 1a, 2a and 2d/x fiber types irrespective of the transcriptional regulatory cassette used to drive expression. These observations have potentially important implications for the treatment of DMD skeletal muscles with AAV-delivered µUtrn.

## Does steric hindrance between µUtrn and endogenous utrophin impact efficacy?

A fundamental question of this study is not only could uUtrn compensate for the lack of dystrophin, but whether uUtrn could function optimally when co-existing with the endogenous full-length utrophin. More specifically, is there potential for steric hindrance between the full-length utrophin and the smaller µUtrn that could impact the function and survival of muscle cells? Slower fiber types have long been known to have slightly higher levels of endogenous utrophin expression and this correlates with a slightly milder dystrophic phenotype in

untreated *mdx* mice[67–69]. Consistent with this, in *mdx* mice, we previously found there is more endogenous utrophin in Type 1a, 2a and 2d fiber types, when compared to fast Type 2b [71]. Strikingly, we found that uUtrn is better able to prevent the dystrophic pathology in Type 2a and 2d fibers in *mdx/utrn*$^{-/-}$ mice lacking both dystrophin and utrophin when compared to the same muscle fiber types in *mdx* mice (Compare S2J–S2L to S2D–S2I Fig). This phenotype was likely unique to μUtrn treatment as delivery of second-generation uDys[39] with the same vector and promoter was able to prevent the dystrophic pathology of *mdx*$^{4cv}$ mice, independent of fiber-type. Furthermore, uUtrn profoundly reduced the spacing of costameres in *mdx*$^{4cv}$ mice (S4 Fig) providing a unique environment for steric hindrance with full-length utrophin within the sarcolemma.

Importantly, steric hindrance requires that both the full-length utrophin and uUtrn are on the sarcolemma at the same time. Our time-course study demonstrates we targeted the majority of muscle fibers (88%) with the therapeutic at the early age when endogenous utrophin is present on the sarcolemma. We originally anticipated that the expression of μUtrn would prevent the dystrophic pathology and allow the endogenous utrophin to follow its natural time course, and dissipate from the sarcolemma as it would with dystrophin. However, Fig 2A, panels 2 & 4 shows this wasn't the case, as low levels of the endogenous utrophin can be found on the same fibers as the μUtrn at 3 months of age. The greater levels of full-length utrophin in type 1a, 2a and 2d sarcolemma could sterically hinder the μUtrn more than in fast 2b fibers where full-length utrophin is minimal[71]. Steric hindrance between full-length utrophin and μUtrn leave the skeletal muscles more susceptible to contraction-induced injury, leading to the death of the muscle fibers and regeneration of the myotubes without the uUtrn therapeutic. This would explain why we see broad μUtrn expression and prevention of dystrophy in fast 2b fibers, but less so in other fiber types. Together, our results support an *in vivo* condition where the stoichiometry of full-length utrophin and μUtrn at the sarcolemma of skeletal muscle fibers could impact the efficacy of the therapeutic.

We also note that in a recent study with *mdx* mice and cxmd canines treated with AAV-mediated micro-utrophin demonstrated impressive efficacy at early timepoints (~2 weeks post-delivery)[46], which was also seen in dko mice[47], and to a large degree here as well. However, in the recent[46] and the present studies the functional benefit seen in *mdx*$^{4cv}$ mice waned over time in fiber types 2A, 1A, & 2D, possibly due to competition with fl utrn. The sustained uUtrn expression in fast 2B fibers in the present study suggests the *mdx* mice did not outgrow expression as previously postulated[46], a conclusion further supported by the sustained uDystrophin expression observed for at least 8 months and up to 2 years in all fiber types in *mdx* mice, and for >1 year in DMD patients [77, 78]. The relative expression levels of fl utrn in various fiber-types and between species such as mice, dogs and humans is not well established and detailed biodistribution and time course studies will be required to understand the longevity of the therapy. Further, the canine studies were followed only for a relatively short time period, such that fiber-type expression levels might potentially wane over time.

## Neuromuscular synapse

The neuromuscular junction contains distinct structural features that ensure nerve evoked stimulation of the muscle exceeds that needed to generate an action potential in the postsynaptic membrane [97]. The presynaptic nerve terminal contains active zones where quanta of acetylcholine are released onto AChR clusters on the crests of the postsynaptic folds [95, 96]. The postsynaptic folds contain a high concentration of voltage gated sodium channels that reduce the threshold required to generate endplate currents [98]. The number of quanta reduces with repeat stimulation of the nerve during normal muscle activity [99], but the sodium channels in

the folds ensure the safety of transmission is maintained [98–100]. The depth and number of folds determines the concentration of voltage gated sodium channels [19, 101]. Thus, the reduction in depth and number of folds could contribute to the functional deficits in synaptic transmission in *mdx*$^{4cv}$ mice [98, 102]. Here we found that μUtrn was able to restore the depth, but not the number of fold openings in *mdx*$^{4cv}$ mice. However, μUtrn expression did lead to a profound increase in fold branching. Utrophin is normally localized to the crests of folds, and dystrophin is primarily localized with the troughs of folds along with voltage gated sodium channels. Therefore, it is possible that the mislocalization of μUtrn increased the branching. In support of this hypothesis, utrophin is required to maintain the fold openings at the neuromuscular junction [103]. We previously found that miniaturized dystrophins can restore the depth and number of folds [19, 39]. Therefore, dystrophin and utrophin are both required for normal development of the synaptic folds. The neuromuscular junctions in humans are smaller than mice and the folds are deeper, suggesting the safety-factor of synaptic transmission relies more on the voltage gated sodium channels [97]. Therefore, a loss of synaptic folds and inclusive sodium channels resulting in decreased synaptic currents within the neuromuscular junctions of DMD patients could potentially reduce the neuromuscular transmission contributing to fatigue. An increase in fold branching could potentially compensate for the lack of fold openings in DMD to restore the safety of neuromuscular synaptic transmission.

### Myotendinous junction

The myotendinous junction is a major site of force transfer in skeletal muscles [22]. The folds within the MTJ reduce membrane stress under shear [22]. The depth of the folds is reduced within the Achilles MTJ in *mdx*$^{4cv}$ mice and in some DMD patients [21, 23, 24, 26]. Further, the MTJ is a primary site of contraction-induced injury in *mdx*$^{4cv}$ mice and some DMD patients [21, 23, 24, 26]. Treatment with μUtrn partially increased the MTJ folds in *mdx*$^{4cv}$ mice and restored the sarcomere attachments in the *dko* mice. Importantly, μUtrn did not lead to chronic myotendinous strain injury or ringed fibers despite containing a polyproline site in hinge 2 [39]. Therefore, the structure and function of μUtrn likely differs from that of an analogous μDys$^{(\Delta R4\text{-}R23/\Delta CT)}$ that did lead to myotendinous strain injury and ringed fiber formation when expressed in *mdx*$^{4cv}$ muscles.

In conclusion, μUtrn was able to replace most functions of dystrophin at the sarcolemma, neuromuscular junctions, and myotendinous junctions of dystrophin-deficient *mdx*$^{4cv}$ mice. However, we also present several lines of *in vivo* evidence consistent with steric hindrance between the full-length endogenous utrophin and uUtrn, which could impact the dystrophic pathophysiology in a myofiber type selective manner. Further studies are needed to better understand the stoichiometry of steric hindrance to predict its relevance in large animal models and humans.

## Materials and methods

### Mice and ethics statement

C57Bl/6 mice and *mdx*$^{4cv}$ mice were utilized in this study. The *mdx*$^{4cv}$ mice were genotyped by sequencing as previously described [104]. All Animal experiments were performed in accordance with and approval by the Institutional Animal Care and Use Committee of the University of Washington under protocol 3333–01. The UW guidelines are at least as protective as those of the National Institutes of Health, they conform to all applicable laws and regulations, they meet prevailing community standards for responsible scientific research and were applied throughout the project to ensure the humane treatment of all animals involved in the project.

## Viral vector production and injection

The μUtrn cDNA sequence was codon-optimized using GenScript (Piscataway, NJ). The rAAV6-CK8-codon optimized μUtrn and rAAV6-CMV-μUtrn (not codon optimized) expression vectors were sequenced and co-transfected with the pDGM6 packaging plasmid into HEK293 cells to generate recombinant AAV vectors comprising serotype 6 capsids. Vectors were harvested, purified, and quantitated as described previously [73]. The rAAV6-μUtrns were formulated in Hanks' balanced salt solution and injected either directly into the gastrocnemius muscles or intravenously by retro-orbital injection at two weeks of age while the mice were anaesthetized with isofluorane.

## Histology

Muscles were frozen directly in OCT cooled in 2-methylbutane in liquid $N_2$. Ten micrometer transverse sections of skeletal muscles were immunostained as previously described [71]. Briefly adjacent sections were immunostained with conjugated monoclonal antibodies to myosin heavy chain to identify fiber-types as previously described [105], N terminal utrophin antibody, C-terminal utrophin antibody (both 1:800; and kindly provided by Stanley Froehner, University of Washington, Seattle, USA), α2-laminin (1:800; SIGMA, St. Louis MO), and hematoxylin and eosin using manufacturer protocols (Electron Microscopy Sciences; Hatfeild, PA). For detecting DGC components, adjacent frozen sections were immunostained with α-dystrobrevin 2 (1:1000), α1-syntrophin (1:500; the latter two antibodies were kind gifts from Stanley Froehner), β-dystroglycan (1:100; BD Biosciences, San Jose, CA), δ-sarcoglycan (1:40; Leica Biosystems, Buffalo Grove, IL), or nNOS (1,100; Invitrogen, Carlsbad, CA). For detecting AChRs, cryosections we incubated in α-bungarotoxin conjugated to TRITC (1,800; Invitrogen, Carlsbad, CA). All fluorescent immunostained sections were coverslipped with ProLong Gold mounting medium containing DAPI (Invitrogen, Carlsbad, CA). Sections were imaged with either a Leica SP5 confocal or an Olympus SZX16 dissection fluorescent microscope.

## Immunoblotting

Western blots were performed on whole muscle lysates as previously described [26]. Briefly, the gastrocnemius muscles treated *mdx*$^{4cv}$ muscles and contralateral controls (n = 4) were ground in liquid $N_2$ and homogenized in extract buffer (50 mM Tris-HCl, 150 mM NaCl, 0.2% SDS, 24 mM Na deoxycholate, 1% NP40, 47.6 mM Na Fluoride, 200 mM Na Orthovanadate, Roche, Basel, CH). Protein concentration of whole muscle was determined by Coomassie Plus Bradford Assay (Thermoscientific, Rockford, IL). Equal amounts of protein (20 μg) were resolved on a 4–12% SDS polyacrylamide gel. The blots were incubated in N-terminal anti-utrophin (1:1000; kind gift from Stanley C. Froehner) overnight at 4˚C. The GAPDH antibody (1:50,000; Sigma, St. Louis, MO) was used as a loading control as its expression was unchanged when comparing the treated and untreated *mdx*$^{4cv}$ muscles. The primary antibodies were detected with IgG HRP secondary antibodies (1:25,000; Jackson ImmunoResearch Labs). The blots were developed with ECL plus (Thermoscientific, Rockford, IL) and scanned with the Storm 860 imaging system (GE Healthcare Lifesciences, Piscataway, NJ). The band intensity was measured using Image J software (NIH).

## Real time PCR

To isolate the RNA, approximately 20μg of gastrocnemius muscle previously ground by mortar and pestle in liquid $N_2$ was used to extract total RNA following manufacturer's instructions (TRI Reagent, Molecular Research Center, Inc. Cincinnati, OH). The pelleted RNA was

suspended in 50 μl nuclease free elution solution (Ambion Inc., Austin, TX). Five μg of total RNA was treated with Turbo DNA-free (Ambion Inc., Austin, TX) in order to remove trace amounts of contaminating DNA. The DNAase Treated RNA (0.5μg) was diluted to 8μl with nuclease free water followed by use of the SuperScript III First-Strand Synthesis kit (Invitrogen, Carlsbad, CA) to generate cDNA. Subsequently 2μl of the cDNA was used for qPCR with utrophin primer-probe sets. The mouse utrophin oligonucleotide sequences were: Forward 5'-ACCAGCTGGACCGATGGA-3', Reverse 5'- CTCGTCCCAGTCGAAGAGATCT-3', Probe 5'-6FAM- CGTTCAACGCCGTGCTCCACC-3'-BHQa1-Q. The primer sequences for the μUtrn H2-R22 unique junction were Forward 5'-GCGATAACCTGGAGACCTGAAG-3', reverse 5'-TTTATTACTAGCCACCGGTATCGAT-3', probe 6FAM-ATTCATCCGGCCA ACCAATGTTCTCG. As a reference gene the oligonucleotide set was used to target the mouse Ywhaz gene sequence (Tyrosine 3-monooxygenase; [106]): Forward 5'- GCTGGTGATGAC AAGAAAGGAAT-3', Reverse 5'- GGTGTGTCGGCTGCATCTC-3', Probe 5'-6FAM-TGG ACCAGTCACAGCAAGCATACCAAGA-3'-BHQa1-Q.

### Muscle fiber areas

The muscle fiber areas were quantitated for each fiber-type using the FIJI Open Source image processing software package based on ImageJ, as previously described [71].

### Skeletal muscle physiology

The tibialis anterior muscle physiology was performed as previously described [37, 39, 47, 73, 107].

### Electron microscopy

The electron microscopy was performed on transverse and longitudinal sections of the gastrocnemius muscles as previously described [26]. The junctional fold number and lengths were measured from N = 4 mice at 3 months of age in mdx mice treated with the rAAV6-CK8-μUtrn and the contralateral control using FIJI computer program. The counts represent the fold numbers and lengths from all fibers.

### Quantitation of neuromuscular synapses

Neuromuscular synapses were analyzed in wholemount immunostained teased muscle fibers and quantitated as previously described [19, 39]. Synapses were quantitated from N = 4 $mdx^{4cv}$ or dko muscles treated with rAAV6-CK8-mUtrn or rAAV6-CMV-μUtrn respectively.

### Statistics

The data were compared using a one-way ANOVA with a Tukey post-test that compares all data sets with a Student's t-test. All data analyses were performed using the PRISM software.

## Supporting information

**S1 Fig.** (A.) μUtrn expression reduces the number of fibers undergoing regeneration. The number of developmental myosin heavy chain positive fibers in the gastrocnemius muscles are displayed at 4 months of age. Data are shown as mean +/- S.D. $^{**}P < 0.01$ compared to wild-type. $^{\#\#}P < 0.01$.
(TIF)

**S2 Fig. Fiber-type expression of μUtrn expression is influenced by expression of endogenous full-length utrophin.** A) μUtrn is present in all fiber-types 2 weeks after vector administration at similar levels each approaching ~90%; B) corresponding myofiber typing for the 2 week time point; and C) Quantification of the proportion of fiber types expressing μUtrn (Mean +/- S.D.). D) μUtrn is unable to prevent necrosis in most 1a, 2a and 2d/x fiber types at 3 months of age. E) Representative fiber typing; F) Mean +/- S.D. proportion of μUtrn-positive fiber types. $^{***}P < 0.001$ compared to the fast 2b fibers at 3 months of age. G) μUtrn is predominantly expressed in the fast 2b fibers when driven by the CMV promoter. H) Representative fiber typing; I) Mean +/- S.D. proportion of μUtrn positive fiber types. $^{***}P < 0.001$ compared to the fast 2b fibers at 4 months of age. J) μUtrn was not selective for the fast 2b fibers in *mdx*$^{4cv}$:utrophin double knockout (*dko*) mice. K) Representative fiber typing; & L) Mean +/- S.D. proportion of μUtrn positive fiber types. $^{*}P < 0.05$ compared to the 2a, 2b and 2d fiber types at 4 months of age. Scale bar = 100 μm.
(TIF)

**S3 Fig. Intravenous administration of rAAV6-CK8-microdystrophin$^{(\Delta H2\text{-}21/\Delta CT+H3)}$ vectors to *mdx*$^{4cv}$ mice results widespread expression & increased muscle function at 9 months post-administration.** In comparison to untreated *mdx*$^{4cv}$, the gastrocnemius muscles of μDys treated *mdx*$^{4cv}$ mice exhibited (A) increased force generating capacity; (B) increased specific force (sPo); (C) decreased susceptibility to eccentric contraction-induced injury; (D) increased recovery force generation; and (E) Display of broad immunostaining for dystrophin and (F.) corresponding adjacent H&E. Data are shown as mean +/- S.D. $^{**}P < 0.01$ compared to wild-type. $^{\#\#}P < 0.01$, $^{\#\#\#}P < 0.001$, compared to *mdx*$^{4cv}$. sPo, specific force; WT, wild type; hematoxylin & eosin, H&E. Scale bar = 50 μm.
(TIF)

**S4 Fig. Influence of μUtrn localization on the costameres.** (A) Utrophin localizes in a rectilinear pattern with α-sarcomeric actin in *mdx*$^{4cv}$ and rAAV-μUtrn treated muscles (S4 Fig, panels 3 & 6). Note however, the prominent utrophin localization between the large costameric striations. Scale bar = 10 μm. (B) Localization of μUtrn with the FLAG antibody revealed the costameric striations to be very close together. Scale bar = 10 μm. C) Immunostaining of μUtrn with the utrophin A antibody reveals the costameric striations in *dko* mice treated with AAV6-CMV-μUtrn. Scale bar = 10 μm. Mean +/- S.D. distance between the costameric striations in *mdx*$^{4cv}$ controls and the FLAG-μUtrn expressing muscles. $^{\#\#\#}P < 0.001$.
(TIF)

**S5 Fig. μUtrn localization within neuromuscular synapses of *mdx* mouse muscles.** Note that utrophin (green) localizes on the crests of the folds in *mdx* mice (arrow in top panel inset). However, FLAG-μUtrn was found within the folds (arrow in lower panel inset). Note also the lack of subsynaptic nuclei (blue, DAPI) in the *mdx* myofiber, but not the μUtrn/mdx myofiber. This *mdx* myofiber (top panel) has regenerated as revealed by the centrally-located nucleus. α-bungaratoxin (αBTX) staining is shown in red. Scale bar = 10 μm.
(TIF)

**S6 Fig. μUtrn within the *mdx* myotendinous junctions.** Note that utrophin and FLAG-μUtrn (green) were found in the folds (merged panel, arrows). α2-laminin is shown in red, while DAPI is shown in blue. Scale bar = 20 μm.
(TIF)

## Acknowledgments

We would like to thank Eric Finn and James Allen for assistance with vector production, and Bobbie Schneider at the Fred Hutchinson Cancer Research Centre for assistance with electron microscopy.

## Author Contributions

**Conceptualization:** Glen B. Banks, Jeffrey S. Chamberlain, Guy L. Odom.

**Data curation:** Glen B. Banks, Guy L. Odom.

**Formal analysis:** Glen B. Banks, Guy L. Odom.

**Funding acquisition:** Guy L. Odom.

**Investigation:** Glen B. Banks, Guy L. Odom.

**Methodology:** Glen B. Banks, Guy L. Odom.

**Resources:** Jeffrey S. Chamberlain, Guy L. Odom.

**Supervision:** Guy L. Odom.

**Visualization:** Glen B. Banks, Guy L. Odom.

**Writing – original draft:** Glen B. Banks, Guy L. Odom.

**Writing – review & editing:** Glen B. Banks, Guy L. Odom.

## References

1. Hoffman EP, Brown RH Jr., Kunkel LM. Dystrophin: the protein product of the Duchenne muscular dystrophy locus. Cell. 1987; 51(6):919–28. Epub 1987/12/24. https://doi.org/10.1016/0092-8674(87)90579-4 PMID: 3319190.
2. Koenig M, Hoffman EP, Bertelson CJ, Monaco AP, Feener C, Kunkel LM. Complete cloning of the Duchenne muscular dystrophy (DMD) cDNA and preliminary genomic organization of the DMD gene in normal and affected individuals. Cell. 1987; 50(3):509–17. Epub 1987/07/31. https://doi.org/10.1016/0092-8674(87)90504-6 PMID: 3607877.
3. Bhasin N, Law R, Liao G, Safer D, Ellmer J, Discher BM, et al. Molecular extensibility of mini-dystrophins and a dystrophin rod construct. Journal of molecular biology. 2005; 352(4):795–806. Epub 2005/09/06. https://doi.org/10.1016/j.jmb.2005.07.064 PMID: 16139300.
4. Mirza A, Sagathevan M, Sahni N, Choi L, Menhart N. A biophysical map of the dystrophin rod. Biochimica et biophysica acta. 2010; 1804(9):1796–809. Epub 2010/04/13. https://doi.org/10.1016/j.bbapap.2010.03.009 PMID: 20382276.
5. Henderson DM, Lee A, Ervasti JM. Disease-causing missense mutations in actin binding domain 1 of dystrophin induce thermodynamic instability and protein aggregation. Proceedings of the National Academy of Sciences of the United States of America. 2010; 107(21):9632–7. Epub 2010/05/12. https://doi.org/10.1073/pnas.1001517107 PMID: 20457930; PubMed Central PMCID: PMC2906886.
6. Ervasti JM, Sonnemann KJ. Biology of the striated muscle dystrophin-glycoprotein complex. Int Rev Cytol. 2008; 265:191–225. https://doi.org/10.1016/S0074-7696(07)65005-0 PMID: 18275889.
7. Ervasti JM, Campbell KP. Membrane organization of the dystrophin-glycoprotein complex. Cell. 1991; 66(6):1121–31. https://doi.org/10.1016/0092-8674(91)90035-w PMID: 1913804.
8. Koenig M, Kunkel LM. Detailed analysis of the repeat domain of dystrophin reveals four potential hinge segments that may confer flexibility. The Journal of biological chemistry. 1990; 265(8):4560–6. Epub 1990/03/15. PMID: 2407739.
9. Ervasti JM, Ohlendieck K, Kahl SD, Gaver MG, Campbell KP. Deficiency of a glycoprotein component of the dystrophin complex in dystrophic muscle. Nature. 1990; 345(6273):315–9. https://doi.org/10.1038/345315a0 PMID: 2188135.
10. Ervasti JM. Dystrophin, its interactions with other proteins, and implications for muscular dystrophy. Biochim Biophys Acta. 2007; 1772(2):108–17. https://doi.org/10.1016/j.bbadis.2006.05.010 PMID: 16829057.

11. Kobayashi YM, Rader EP, Crawford RW, Iyengar NK, Thedens DR, Faulkner JA, et al. Sarcolemma-localized nNOS is required to maintain activity after mild exercise. Nature. 2008; 456(7221):511–5. Epub 2008/10/28. nature07414 [pii] https://doi.org/10.1038/nature07414 PMID: 18953332; PubMed Central PMCID: PMC2588643.

12. Grady RM, Grange RW, Lau KS, Maimone MM, Nichol MC, Stull JT, et al. Role for alpha-dystrobrevin in the pathogenesis of dystrophin-dependent muscular dystrophies. Nat Cell Biol. 1999; 1(4):215–20. https://doi.org/10.1038/12034 PMID: 10559919

13. Brooks SV. Rapid recovery following contraction-induced injury to in situ skeletal muscles in mdx mice. Journal of muscle research and cell motility. 1998; 19(2):179–87. Epub 1998/04/16. https://doi.org/10.1023/a:1005364713451 PMID: 9536444.

14. Dellorusso C, Crawford RW, Chamberlain JS, Brooks SV. Tibialis anterior muscles in mdx mice are highly susceptible to contraction-induced injury. Journal of muscle research and cell motility. 2001; 22 (5):467–75. Epub 2002/04/20. https://doi.org/10.1023/a:1014587918367 PMID: 11964072.

15. Faulkner JA, Ng R, Davis CS, Li S, Chamberlain JS. Diaphragm muscle strip preparation for evaluation of gene therapies in mdx mice. Clinical and experimental pharmacology & physiology. 2008; 35 (7):725–9. Epub 2008/01/25. https://doi.org/10.1111/j.1440-1681.2007.04865.x PMID: 18215182.

16. Moens P, Baatsen PH, Marechal G. Increased susceptibility of EDL muscles from mdx mice to damage induced by contractions with stretch. J Muscle Res Cell Motil. 1993; 14(4):446–51. https://doi.org/10.1007/BF00121296 PMID: 7693747.

17. Petrof BJ, Shrager JB, Stedman HH, Kelly AM, Sweeney HL. Dystrophin protects the sarcolemma from stresses developed during muscle contraction. Proceedings of the National Academy of Sciences of the United States of America. 1993; 90(8):3710–4. Epub 1993/04/15. https://doi.org/10.1073/pnas.90.8.3710 PMID: 8475120; PubMed Central PMCID: PMC46371.

18. Lyons PR, Slater CR. Structure and function of the neuromuscular junction in young adult mdx mice. Journal of neurocytology. 1991; 20(12):969–81. Epub 1991/12/01. https://doi.org/10.1007/BF01187915 PMID: 1686056.

19. Banks GB, Chamberlain JS, Froehner SC. Truncated dystrophins can influence neuromuscular synapse structure. Mol Cell Neurosci. 2009; 40(4):433–41. Epub 2009/01/28. S1044-7431(08)00317-5 [pii] https://doi.org/10.1016/j.mcn.2008.12.011 PMID: 19171194; PubMed Central PMCID: PMC2826111.

20. Faber RM, Hall JK, Chamberlain JS, Banks GB. Myofiber branching rather than myofiber hyperplasia contributes to muscle hypertrophy in mdx mice. Skeletal Muscle. 2014; 4(10). https://doi.org/10.1186/2044-5040-4-10 PMID: 24910770

21. Nagao H, Morimoto T, Sano N, Takahashi M, Nagai H, Tawa R, et al. [Magnetic resonance imaging of skeletal muscle in patients with Duchenne muscular dystrophy—serial axial and sagittal section studies]. No to hattatsu Brain and development. 1991; 23(1):39–43. Epub 1991/01/01. PMID: 1994993.

22. Tidball JG. Force transmission across muscle cell membranes. Journal of biomechanics. 1991; 24 Suppl 1:43–52. Epub 1991/01/01. https://doi.org/10.1016/0021-9290(91)90376-x PMID: 1791181.

23. Hasegawa T, Matsumura K, Hashimoto T, Ikehira H, Fukuda H, Tateno Y. [Intramuscular degeneration process in Duchenne muscular dystrophy—investigation by longitudinal MR imaging of the skeletal muscles]. Rinsho shinkeigaku = Clinical neurology. 1992; 32(3):333–5. Epub 1992/03/01. PMID: 1628461.

24. Law DJ, Caputo A, Tidball JG. Site and mechanics of failure in normal and dystrophin-deficient skeletal muscle. Muscle & nerve. 1995; 18(2):216–23. Epub 1995/02/01. https://doi.org/10.1002/mus.880180211 PMID: 7823981.

25. Law DJ, Tidball JG. Dystrophin deficiency is associated with myotendinous junction defects in prenecrotic and fully regenerated skeletal muscle. The American journal of pathology. 1993; 142(5):1513–23. Epub 1993/05/01. PMID: 8494050; PubMed Central PMCID: PMC1886922.

26. Banks GB, Combs AC, Chamberlain JR, Chamberlain JS. Molecular and cellular adaptations to chronic myotendinous strain injury in mdx mice expressing a truncated dystrophin. Human molecular genetics. 2008; 17(24):3975–86. Epub 2008/09/19. ddn301 [pii] https://doi.org/10.1093/hmg/ddn301 PMID: 18799475; PubMed Central PMCID: PMC2638580.

27. Jung D, Yang B, Meyer J, Chamberlain JS, Campbell KP. Identification and characterization of the dystrophin anchoring site on beta-dystroglycan. J Biol Chem. 1995; 270(45):27305–10. https://doi.org/10.1074/jbc.270.45.27305 PMID: 7592992.

28. Winder SJ, Gibson TJ, Kendrick-Jones J. Dystrophin and utrophin: the missing links! FEBS letters. 1995; 369(1):27–33. Epub 1995/08/01. https://doi.org/10.1016/0014-5793(95)00398-s PMID: 7641878.

29. Banks GB, Chamberlain JS. The value of mammalian models for duchenne muscular dystrophy in developing therapeutic strategies. Curr Top Dev Biol. 2008; 84:431–53. Epub 2009/02/03. S0070-2153(08)00609-1 [pii] https://doi.org/10.1016/S0070-2153(08)00609-1 PMID: 19186250.

30. Legardinier S, Raguenes-Nicol C, Tascon C, Rocher C, Hardy S, Hubert JF, et al. Mapping of the lipid-binding and stability properties of the central rod domain of human dystrophin. Journal of molecular biology. 2009; 389(3):546–58. Epub 2009/04/22. https://doi.org/10.1016/j.jmb.2009.04.025 PMID: 19379759.

31. Amann KJ, Renley BA, Ervasti JM. A cluster of basic repeats in the dystrophin rod domain binds F-actin through an electrostatic interaction. The Journal of biological chemistry. 1998; 273(43):28419–23. Epub 1998/10/17. https://doi.org/10.1074/jbc.273.43.28419 PMID: 9774469.

32. Lai Y, Thomas GD, Yue Y, Yang HT, Li D, Long C, et al. Dystrophins carrying spectrin-like repeats 16 and 17 anchor nNOS to the sarcolemma and enhance exercise performance in a mouse model of muscular dystrophy. J Clin Invest. 2009; 119(3):624–35. Epub 2009/02/21. 36612 [pii] https://doi.org/10.1172/JCI36612 PMID: 19229108; PubMed Central PMCID: PMC2648692.

33. Adams ME, Odom GL, Kim MJ, Chamberlain JS, Froehner SC. Syntrophin binds directly to multiple spectrin-like repeats in dystrophin and mediates binding of nNOS to repeats 16–17. Hum Mol Genet. 2018; 27(17):2978–85. Epub 2018/05/24. https://doi.org/10.1093/hmg/ddy197 PMID: 29790927; PubMed Central PMCID: PMC6097012.

34. Belanto JJ, Mader TL, Eckhoff MD, Strandjord DM, Banks GB, Gardner MK, et al. Microtubule binding distinguishes dystrophin from utrophin. Proc Natl Acad Sci U S A. 2014; 111(15):5723–8. Epub 2014/04/08. https://doi.org/10.1073/pnas.1323842111 [pii]. PMID: 24706788; PubMed Central PMCID: PMC3992671.

35. Odom GL, Banks GB, Schultz BR, Gregorevic P, Chamberlain JS. Preclinical studies for gene therapy of Duchenne muscular dystrophy. J Child Neurol. 2010; 25(9):1149–57. https://doi.org/10.1177/0883073810371006 PMID: 20498332.

36. Goyenvalle A, Seto JT, Davies KE, Chamberlain J. Therapeutic approaches to muscular dystrophy. Human molecular genetics. 2011; 20(R1):R69–78. Epub 2011/03/26. https://doi.org/10.1093/hmg/ddr105 PMID: 21436158; PubMed Central PMCID: PMC3095062.

37. Gregorevic P, Allen JM, Minami E, Blankinship MJ, Haraguchi M, Meuse L, et al. rAAV6-microdystrophin preserves muscle function and extends lifespan in severely dystrophic mice. Nat Med. 2006; 12(7):787–9. https://doi.org/10.1038/nm1439 PMID: 16819550.

38. Wang B, Li J, Fu FH, Xiao X. Systemic human minidystrophin gene transfer improves functions and life span of dystrophin and dystrophin/utrophin-deficient mice. Journal of orthopaedic research: official publication of the Orthopaedic Research Society. 2009; 27(4):421–6. Epub 2008/11/01. https://doi.org/10.1002/jor.20781 PMID: 18973234.

39. Banks GB, Judge LM, Allen JM, Chamberlain JS. The polyproline site in hinge 2 influences the functional capacity of truncated dystrophins. PLoS Genet. 2010; 6(5):e1000958. Epub 2010/05/27. https://doi.org/10.1371/journal.pgen.1000958 PMID: 20502633; PubMed Central PMCID: PMC2873924.

40. Wang Z, Storb R, Halbert CL, Banks GB, Butts TM, Finn EE, et al. Successful regional delivery and long-term expression of a dystrophin gene in canine muscular dystrophy: a preclinical model for human therapies. Mol Ther. 2012; 20(8):1501–7. https://doi.org/10.1038/mt.2012.111 PMID: 22692496; PubMed Central PMCID: PMC3412492.

41. Shin JH, Pan X, Hakim CH, Yang HT, Yue Y, Zhang K, et al. Microdystrophin ameliorates muscular dystrophy in the canine model of duchenne muscular dystrophy. Mol Ther. 2013; 21(4):750–7. Epub 2013/01/16. https://doi.org/10.1038/mt.2012.283 [pii]. PMID: 23319056; PubMed Central PMCID: PMC3616540.

42. Crudele JM, Chamberlain JS. AAV-based gene therapies for the muscular dystrophies. Hum Mol Genet. 2019; 28(R1):R102–R7. Epub 2019/06/27. https://doi.org/10.1093/hmg/ddz128 PMID: 31238336; PubMed Central PMCID: PMC6796995.

43. Flanigan KM, Campbell K, Viollet L, Wang W, Gomez AM, Walker CM, et al. Anti-dystrophin T cell responses in Duchenne muscular dystrophy: prevalence and a glucocorticoid treatment effect. Hum Gene Ther. 2013; 24(9):797–806. Epub 2013/09/10. https://doi.org/10.1089/hum.2013.092 PMID: 24010700; PubMed Central PMCID: PMC3768239.

44. Fairclough RJ, Wood MJ, Davies KE. Therapy for Duchenne muscular dystrophy: renewed optimism from genetic approaches. Nature reviews Genetics. 2013; 14(6):373–8. Epub 2013/04/24. https://doi.org/10.1038/nrg3460 PMID: 23609411.

45. Mueller C, Chulay JD, Trapnell BC, Humphries M, Carey B, Sandhaus RA, et al. Human Treg responses allow sustained recombinant adeno-associated virus-mediated transgene expression. J Clin Invest. 2013; 123(12):5310–8. Epub 2013/11/16. https://doi.org/10.1172/JCI70314 PMID: 24231351; PubMed Central PMCID: PMC3859421.

46. Song Y, Morales L, Malik AS, Mead AF, Greer CD, Mitchell MA, et al. Non-immunogenic utrophin gene therapy for the treatment of muscular dystrophy animal models. Nat Med. 2019; 25(10):1505–11. https://doi.org/10.1038/s41591-019-0594-0 PMID: 31591596.

47. Odom GL, Gregorevic P, Allen JM, Finn E, Chamberlain JS. Microutrophin delivery through rAAV6 increases lifespan and improves muscle function in dystrophic dystrophin/utrophin-deficient mice. Mol Ther. 2008; 16(9):1539–45. https://doi.org/10.1038/mt.2008.149 PMID: 18665159; PubMed Central PMCID: PMC2643133.

48. Rybakova IN, Ervasti JM. Identification of spectrin-like repeats required for high affinity utrophin-actin interaction. The Journal of biological chemistry. 2005; 280(24):23018–23. Epub 2005/04/14. https://doi.org/10.1074/jbc.M502530200 PMID: 15826935.

49. Prochniewicz E, Henderson D, Ervasti JM, Thomas DD. Dystrophin and utrophin have distinct effects on the structural dynamics of actin. Proceedings of the National Academy of Sciences of the United States of America. 2009; 106(19):7822–7. https://doi.org/10.1073/pnas.0812007106 PMID: 19416869; PubMed Central PMCID: PMC2683112.

50. Rybakova IN, Humston JL, Sonnemann KJ, Ervasti JM. Dystrophin and utrophin bind actin through distinct modes of contact. The Journal of biological chemistry. 2006; 281(15):9996–10001. https://doi.org/10.1074/jbc.M513121200 PMID: 16478721.

51. Lin AY, Prochniewicz E, Henderson DM, Li B, Ervasti JM, Thomas DD. Impacts of dystrophin and utrophin domains on actin structural dynamics: implications for therapeutic design. J Mol Biol. 2012; 420 (1–2):87–98. Epub 2012/04/17. https://doi.org/10.1016/j.jmb.2012.04.005 [pii]. PMID: 22504225; PubMed Central PMCID: PMC3367031.

52. Li D, Bareja A, Judge L, Yue Y, Lai Y, Fairclough R, et al. Sarcolemmal nNOS anchoring reveals a qualitative difference between dystrophin and utrophin. Journal of cell science. 2010; 123(Pt 12):2008–13. Epub 2010/05/21. https://doi.org/10.1242/jcs.064808 PMID: 20483958; PubMed Central PMCID: PMC2880012.

53. Tinsley J, Deconinck N, Fisher R, Kahn D, Phelps S, Gillis JM, et al. Expression of full-length utrophin prevents muscular dystrophy in mdx mice. Nat Med. 1998; 4(12):1441–4. https://doi.org/10.1038/4033 PMID: 9846586.

54. Ervasti JM, Kahl SD, Campbell KP. Purification of dystrophin from skeletal muscle. The Journal of biological chemistry. 1991; 266(14):9161–5. PMID: 2026615.

55. Ohlendieck K, Ervasti JM, Snook JB, Campbell KP. Dystrophin-glycoprotein complex is highly enriched in isolated skeletal muscle sarcolemma. The Journal of cell biology. 1991; 112(1):135–48. https://doi.org/10.1083/jcb.112.1.135 PMID: 1986002; PubMed Central PMCID: PMC2288808.

56. Yoshida M, Ozawa E. Glycoprotein complex anchoring dystrophin to sarcolemma. Journal of biochemistry. 1990; 108(5):748–52. https://doi.org/10.1093/oxfordjournals.jbchem.a123276 PMID: 2081733.

57. Sonnemann KJ, Heun-Johnson H, Turner AJ, Baltgalvis KA, Lowe DA, Ervasti JM. Functional substitution by TAT-utrophin in dystrophin-deficient mice. PLoS Med. 2009; 6(5):e1000083. Epub 2009/05/30. https://doi.org/10.1371/journal.pmed.1000083 PMID: 19478831; PubMed Central PMCID: PMC2680620.

58. Call JA, Ervasti JM, Lowe DA. TAT-muUtrophin mitigates the pathophysiology of dystrophin and utrophin double-knockout mice. J Appl Physiol (1985). 2011; 111(1):200–5. Epub 2011/05/14. https://doi.org/10.1152/japplphysiol.00248.2011 PMID: 21565990; PubMed Central PMCID: PMC3137527.

59. Kennedy TL, Guiraud S, Edwards B, Squire S, Moir L, Babbs A, et al. Micro-utrophin Improves Cardiac and Skeletal Muscle Function of Severely Affected D2/mdx Mice. Mol Ther Methods Clin Dev. 2018; 11:92–105. Epub 2018/11/13. https://doi.org/10.1016/j.omtm.2018.10.005 PMID: 30417024; PubMed Central PMCID: PMC6216100.

60. Khurana TS, Watkins SC, Chafey P, Chelly J, Tome FM, Fardeau M, et al. Immunolocalization and developmental expression of dystrophin related protein in skeletal muscle. Neuromuscular disorders: NMD. 1991; 1(3):185–94. Epub 1991/01/01. https://doi.org/10.1016/0960-8966(91)90023-l PMID: 1822793.

61. Pons F, Nicholson LV, Robert A, Voit T, Leger JJ. Dystrophin and dystrophin-related protein (utrophin) distribution in normal and dystrophin-deficient skeletal muscles. Neuromuscular disorders: NMD. 1993; 3(5–6):507–14. Epub 1993/09/01. https://doi.org/10.1016/0960-8966(93)90106-t PMID: 8186702.

62. Helliwell TR, Man NT, Morris GE, Davies KE. The dystrophin-related protein, utrophin, is expressed on the sarcolemma of regenerating human skeletal muscle fibres in dystrophies and inflammatory myopathies. Neuromuscular disorders: NMD. 1992; 2(3):177–84. Epub 1992/01/01. https://doi.org/10.1016/0960-8966(92)90004-p PMID: 1483043.

63. Harper SQ, Hauser MA, DelloRusso C, Duan D, Crawford RW, Phelps SF, et al. Modular flexibility of dystrophin: implications for gene therapy of Duchenne muscular dystrophy. Nat Med. 2002; 8(3):253–61. https://doi.org/10.1038/nm0302-253 PMID: 11875496.

64. Lai Y, Zhao J, Yue Y, Wasala NB, Duan D. Partial restoration of cardiac function with DeltaPDZ nNOS in aged mdx model of Duchenne cardiomyopathy. Hum Mol Genet. 2014; 23(12):3189–99. Epub 2014/01/28. https://doi.org/10.1093/hmg/ddu029 [pii]. PMID: 24463882; PubMed Central PMCID: PMC4030774.

65. Crawford GE, Faulkner JA, Crosbie RH, Campbell KP, Froehner SC, Chamberlain JS. Assembly of the dystrophin-associated protein complex does not require the dystrophin COOH-terminal domain. The Journal of cell biology. 2000; 150(6):1399–410. https://doi.org/10.1083/jcb.150.6.1399 PMID: 10995444; PubMed Central PMCID: PMC2150715.

66. Gregorevic P, Blankinship MJ, Chamberlain JS. Viral vectors for gene transfer to striated muscle. Curr Opin Mol Ther. 2004; 6(5):491–8. PMID: 15537050.

67. Chakkalakal JV, Stocksley MA, Harrison MA, Angus LM, Deschenes-Furry J, St-Pierre S, et al. Expression of utrophin A mRNA correlates with the oxidative capacity of skeletal muscle fiber types and is regulated by calcineurin/NFAT signaling. Proc Natl Acad Sci U S A. 2003; 100(13):7791–6. https://doi.org/10.1073/pnas.0932671100 PMID: 12808150.

68. Ljubicic V, Miura P, Burt M, Boudreault L, Khogali S, Lunde JA, et al. Chronic AMPK activation evokes the slow, oxidative myogenic program and triggers beneficial adaptations in mdx mouse skeletal muscle. Human molecular genetics. 2011; 20(17):3478–93. https://doi.org/10.1093/hmg/ddr265 PMID: 21659335.

69. Selsby JT, Morine KJ, Pendrak K, Barton ER, Sweeney HL. Rescue of dystrophic skeletal muscle by PGC-1alpha involves a fast to slow fiber type shift in the mdx mouse. PLoS One. 2012; 7(1):e30063. https://doi.org/10.1371/journal.pone.0030063 PMID: 22253880; PubMed Central PMCID: PMC3256197.

70. Weir AP, Morgan JE, Davies KE. A-utrophin up-regulation in mdx skeletal muscle is independent of regeneration. Neuromuscul Disord. 2004; 14(1):19–23. https://doi.org/10.1016/j.nmd.2003.09.004 PMID: 14659408.

71. Banks GB, Combs AC, Odom GL, Bloch RJ, Chamberlain JS. Muscle structure influences utrophin expression in mdx mice. PLoS Genet. 2014; 10(6):e1004431. Epub 2014/06/13. https://doi.org/10.1371/journal.pgen.1004431 [pii]. PMID: 24922526; PubMed Central PMCID: PMC4055409.

72. Lynch GS, Hinkle RT, Chamberlain JS, Brooks SV, Faulkner JA. Force and power output of fast and slow skeletal muscles from mdx mice 6–28 months old. J Physiol. 2001; 535(Pt 2):591–600. https://doi.org/10.1111/j.1469-7793.2001.00591.x PMID: 11533147.

73. Banks GB, Gregorevic P, Allen JM, Finn EE, Chamberlain JS. Functional capacity of dystrophins carrying deletions in the N-terminal actin-binding domain. Human molecular genetics. 2007; 16 (17):2105–13. Epub 2007/06/26. ddm158 [pii] https://doi.org/10.1093/hmg/ddm158 PMID: 17588958.

74. Faber RM, Hall JK, Chamberlain JS, Banks GB. Myofiber branching rather than myofiber hyperplasia contributes to muscle hypertrophy in mdx mice. Skelet Muscle. 2014; 4:10. Epub 2014/06/10. https://doi.org/10.1186/2044-5040-4-10 [pii]. PMID: 24910770; PubMed Central PMCID: PMC4047439.

75. Salva MZ, Himeda CL, Tai PW, Nishiuchi E, Gregorevic P, Allen JM, et al. Design of tissue-specific regulatory cassettes for high-level rAAV-mediated expression in skeletal and cardiac muscle. Mol Ther. 2007; 15(2):320–9. https://doi.org/10.1038/sj.mt.6300027 PMID: 17235310.

76. Harper SQ, Hauser MA, DelloRusso C, Duan D, Crawford RW, Phelps SF, et al. Modular flexibility of dystrophin: Implications for gene therapy of Duchenne muscular dystrophy. Nat Med. 2002; 8(3):253–61. https://doi.org/10.1038/nm0302-253 PMID: 11875496.

77. Mendell JR, Sahenk Z, Lehman K, Nease C, Lowes LP, Miller NF, et al. Assessment of Systemic Delivery of rAAVrh74.MHCK7.micro-dystrophin in Children With Duchenne Muscular Dystrophy: A Nonrandomized Controlled Trial. JAMA Neurol. 2020. Epub 2020/06/17. https://doi.org/10.1001/jamaneurol.2020.1484 PMID: 32539076; PubMed Central PMCID: PMC7296461.

78. Ramos JN, Hollinger K, Bengtsson NE, Allen JM, Hauschka SD, Chamberlain JS. Development of Novel Micro-dystrophins with Enhanced Functionality. Mol Ther. 2019; 27(3):623–35. Epub 2019/02/06. https://doi.org/10.1016/j.ymthe.2019.01.002 PMID: 30718090; PubMed Central PMCID: PMC6403485.

79. Porter GA, Dmytrenko GM, Winkelmann JC, Bloch RJ. Dystrophin colocalizes with beta-spectrin in distinct subsarcolemmal domains in mammalian skeletal muscle. The Journal of cell biology. 1992; 117(5):997–1005. https://doi.org/10.1083/jcb.117.5.997 PMID: 1577872; PubMed Central PMCID: PMC2289490.

80. Williams MW, Resneck WG, Bloch RJ. Membrane skeleton of innervated and denervated fast- and slow-twitch muscle. Muscle & nerve. 2000; 23(4):590–9. https://doi.org/10.1002/(sici)1097-4598(200004)23:4<590::aid-mus19>3.0.co;2-z PMID: 10716771.

81. Straub V, Bittner RE, Leger JJ, Voit T. Direct visualization of the dystrophin network on skeletal muscle fiber membrane. J Cell Biol. 1992; 119(5):1183–91. https://doi.org/10.1083/jcb.119.5.1183 PMID: 1447296.

82. Ehmer S, Herrmann R, Bittner R, Voit T. Spatial distribution of beta-spectrin in normal and dystrophic human skeletal muscle. Acta neuropathologica. 1997; 94(3):240–6. https://doi.org/10.1007/s004010050699 PMID: 9292693.

83. Rybakova IN, Patel JR, Ervasti JM. The dystrophin complex forms a mechanically strong link between the sarcolemma and costameric actin. J Cell Biol. 2000; 150(5):1209–14. https://doi.org/10.1083/jcb.150.5.1209 PMID: 10974007.

84. Williams MW, Bloch RJ. Extensive but coordinated reorganization of the membrane skeleton in myofibers of dystrophic (mdx) mice. The Journal of cell biology. 1999; 144(6):1259–70. https://doi.org/10.1083/jcb.144.6.1259 PMID: 10087268; PubMed Central PMCID: PMC2150591.

85. Gregorevic P, Blankinship MJ, Allen JM, Chamberlain JS. Systemic microdystrophin gene delivery improves skeletal muscle structure and function in old dystrophic mdx mice. Mol Ther. 2008; 16(4):657–64. https://doi.org/10.1038/mt.2008.28 PMID: 18334986; PubMed Central PMCID: PMC2650831.

86. Harper SQ, Crawford RW, DelloRusso C, Chamberlain JS. Spectrin-like repeats from dystrophin and alpha-actinin-2 are not functionally interchangeable. Hum Mol Genet. 2002; 11(16):1807–15. https://doi.org/10.1093/hmg/11.16.1807 PMID: 12140183.

87. Lai Y, Zhao J, Yue Y, Duan D. alpha2 and alpha3 helices of dystrophin R16 and R17 frame a microdomain in the alpha1 helix of dystrophin R17 for neuronal NOS binding. Proceedings of the National Academy of Sciences of the United States of America. 2013; 110(2):525–30. https://doi.org/10.1073/pnas.1211431109 PMID: 23185009; PubMed Central PMCID: PMC3545791.

88. Infante JP, Huszagh VA. Mechanisms of resistance to pathogenesis in muscular dystrophies. Molecular and cellular biochemistry. 1999; 195(1–2):155–67. https://doi.org/10.1023/a:1006972315739 PMID: 10395079.

89. Blake DJ, Weir A, Newey SE, Davies KE. Function and genetics of dystrophin and dystrophin-related proteins in muscle. Physiol Rev. 2002; 82(2):291–329. https://doi.org/10.1152/physrev.00028.2001 PMID: 11917091.

90. Gramolini AO, Karpati G, Jasmin BJ. Discordant expression of utrophin and its transcript in human and mouse skeletal muscles. Journal of neuropathology and experimental neurology. 1999; 58(3):235–44. https://doi.org/10.1097/00005072-199903000-00003 PMID: 10197815.

91. Weir AP, Burton EA, Harrod G, Davies KE. A- and B-utrophin have different expression patterns and are differentially up-regulated in mdx muscle. The Journal of biological chemistry. 2002; 277(47):45285–90. https://doi.org/10.1074/jbc.M205177200 PMID: 12235137.

92. Adams ME, Anderson KN, Froehner SC. The alpha-syntrophin PH and PDZ domains scaffold acetylcholine receptors, utrophin, and neuronal nitric oxide synthase at the neuromuscular junction. The Journal of neuroscience: the official journal of the Society for Neuroscience. 2010; 30(33):11004–10. https://doi.org/10.1523/JNEUROSCI.1930-10.2010 PMID: 20720107; PubMed Central PMCID: PMC2936458.

93. Miyagoe-Suzuki Y, Takeda SI. Association of neuronal nitric oxide synthase (nNOS) with alpha1-syntrophin at the sarcolemma. Microscopy research and technique. 2001; 55(3):164–70. https://doi.org/10.1002/jemt.1167 PMID: 11747091.

94. Yoshida M, Hama H, Ishikawa-Sakurai M, Imamura M, Mizuno Y, Araishi K, et al. Biochemical evidence for association of dystrobrevin with the sarcoglycan-sarcospan complex as a basis for understanding sarcoglycanopathy. Human molecular genetics. 2000; 9(7):1033–40. https://doi.org/10.1093/hmg/9.7.1033 PMID: 10767327.

95. Sanes JR, Lichtman JW. Development of the vertebrate neuromuscular junction. Annual review of neuroscience. 1999; 22:389–442. Epub 1999/04/15. https://doi.org/10.1146/annurev.neuro.22.1.389 PMID: 10202544.

96. Banks GB, Fuhrer C, Adams ME, Froehner SC. The postsynaptic submembrane machinery at the neuromuscular junction: requirement for rapsyn and the utrophin/dystrophin-associated complex. J Neurocytol. 2003; 32(5–8):709–26. https://doi.org/10.1023/B:NEUR.0000020619.24681.2b PMID: 15034263.

97. Slater CR. Structural determinants of the reliability of synaptic transmission at the vertebrate neuromuscular junction. Journal of neurocytology. 2003; 32(5–8):505–22. Epub 2004/03/23. https://doi.org/10.1023/B:NEUR.0000020607.17881.9b PMID: 15034250.

98. Wood SJ, Slater CR. The contribution of postsynaptic folds to the safety factor for neuromuscular transmission in rat fast- and slow-twitch muscles. The Journal of physiology. 1997; 500 (Pt 1):165–76. Epub 1997/04/01. https://doi.org/10.1113/jphysiol.1997.sp022007 PMID: 9097941; PubMed Central PMCID: PMC1159367.

99. Hennig R, Lomo T. Firing patterns of motor units in normal rats. Nature. 1985; 314(6007):164–6. Epub 1985/03/14. https://doi.org/10.1038/314164a0 PMID: 3974720.

100. Sealock R, Butler MH, Kramarcy NR, Gao KX, Murnane AA, Douville K, et al. Localization of dystrophin relative to acetylcholine receptor domains in electric tissue and adult and cultured skeletal muscle. The Journal of cell biology. 1991; 113(5):1133–44. Epub 1991/06/01. https://doi.org/10.1083/jcb.113.5.1133 PMID: 2040646; PubMed Central PMCID: PMC2289019.

101. Bailey SJ, Stocksley MA, Buckel A, Young C, Slater CR. Voltage-gated sodium channels and ankyrinG occupy a different postsynaptic domain from acetylcholine receptors from an early stage of neuromuscular junction maturation in rats. The Journal of neuroscience: the official journal of the Society for Neuroscience. 2003; 23(6):2102–11. Epub 2003/03/27. https://doi.org/10.1523/JNEUROSCI.23-06-02102.2003 PMID: 12657669.

102. Carlson CG, Roshek DM. Adult dystrophic (mdx) endplates exhibit reduced quantal size and enhanced quantal variation. Pflugers Archiv: European journal of physiology. 2001; 442(3):369–75. Epub 2001/08/04. https://doi.org/10.1007/s004240100561 PMID: 11484767.

103. Deconinck AE, Potter AC, Tinsley JM, Wood SJ, Vater R, Young C, et al. Postsynaptic abnormalities at the neuromuscular junctions of utrophin-deficient mice. The Journal of cell biology. 1997; 136 (4):883–94. Epub 1997/02/24. https://doi.org/10.1083/jcb.136.4.883 PMID: 9049253; PubMed Central PMCID: PMC2132499.

104. Banks GB, Combs AC, Chamberlain JS. Sequencing protocols to genotype mdx, mdx(4cv), and mdx (5cv) mice. Muscle & nerve. 2010; 42(2):268–70. Epub 2010/06/15. https://doi.org/10.1002/mus.21700 PMID: 20544945.

105. Gregorevic P, Meznarich NA, Blankinship MJ, Crawford RW, Chamberlain JS. Fluorophore-labeled myosin-specific antibodies simplify muscle-fiber phenotyping. Muscle & nerve. 2008; 37(1):104–6. Epub 2007/08/11. https://doi.org/10.1002/mus.20877 PMID: 17691104; PubMed Central PMCID: PMC2788960.

106. Gubern C, Hurtado O, Rodriguez R, Morales JR, Romera VG, Moro MA, et al. Validation of housekeeping genes for quantitative real-time PCR in in-vivo and in-vitro models of cerebral ischaemia. BMC molecular biology. 2009; 10:57. Epub 2009/06/18. https://doi.org/10.1186/1471-2199-10-57 PMID: 19531214; PubMed Central PMCID: PMC2706836.

107. Odom GL, Gregorevic P, Allen JM, Chamberlain JS. Gene therapy of mdx mice with large truncated dystrophins generated by recombination using rAAV6. Mol Ther. 2011; 19(1):36–45. https://doi.org/10.1038/mt.2010.205 PMID: 20859263; PubMed Central PMCID: PMC3017440.